INFLUENCE OF AU NANOPARTICLES ON THE PROPERTIES OF TIO2 FILMS FOR USE IN DYE-SENSITIZED SOLAR CELL

HU XIAOPING

(M. Eng. CISRI)

THESIS SUBMITTED FOR THE DEGREE OF

DOCTOR OF PHILOSOPHY

DEPARTMENT OF MATERIALS SCIENCE AND ENGINEERING

NATIONAL UNIVERSITY OF SINGAPORE

2008

Acknowledgement

First and foremost, I would like to thank my advisor, Associate Professor Daniel John Blackwood, for his excellent guidance, encouragement, and support throughout my entire graduate career. I really learned a lot, especially the essential elements to launch scientific undertaking, such as critical thinking and writing. I am also very grateful for many research, professional, and career-related experiences that he has given to me.

I wish to record my deep appreciation to Assistant Professor Xue Junming and Mr. Wang Changhai, who have given me beneficial discussions and suggestions for my research project. I wish to thank all the group members Miss Liu Minghui, Dr. Sudesh, and Miss Viji for their continuous support and helpful discussions. Thank all the lab officers Dr. Yin Hong, Mr. Chen Qun, Miss Agnes, and Mr. Chan Yuwen from the Department of Materials Science, for their technique support. I would like to thank Miss. Chow Xueying and Mr. Sue Chiwen from Institute Materials Research & Engineering (IMRE) for their selfless help on transmission electron microscopy.

Thanks to Materials Science Department of NUS for giving me kinds of support.

I also would like thank my friends from Department of Materials Science and Tropical Marine Science Institute; their friendship gave me strong emotional support to help me finish my study and writing. Last but not least, the thesis is dedicated to my lovely son and my beloved family for their constant moral support.

Table of Contents

Summary

Gold nanoparticle composite materials are attractive due to its unique optical properties, such as surface plasmon resonance (SPR) in the visible light region, which has potential application in photocatalysis and photon-electron conversion. In this work, Au/TiO_2 composite films were investigated to ascertain the influence of Au particle concentration (1%, 5%, 10%, 15%, 25% and 50%), along with composite structure on the optical absorption and photocurrent properties of TiO_2 films. Experimental techniques used included: UV/visible spectroscopy, photocurrent spectroscopy (both dc and intensity modulation techniques), electrochemical impedance spectroscopy, and photoluminescence measurements, whilst the structure of the composites was probed by TEM and XRD.

Results indicate that SPR performance was directly related to the structure of Au particles and TiO_2 films and crystallization of the TiO_2 matrix was influenced by the introduction of Au particles. Although above 1% Au concentrations the Au/TiO_2 composites exhibited strong SPR performance, this SPR did not directly transfer into visible region photocurrents. On the contrary, increasing the Au particle level decreased the photocurrent of TiO_2 film in UV region.

From Raman and photoelectron spectroscopy data, it was concluded that the insertion of Au nanoparticles increased the concentrations of Ti^{3+} and Ti^{2+} species (as opposed to Ti^{4+}), which are believed to influence the density of surface states as well as the level of oxygen vacancies at the film's surface. Oxygen vacancies are thought to be effective pathways for electron injection in TiO_2, but these are also the positions occupied first by Au atoms inserted into the composite films. The loss of the injection

pathways contributes to the lowering of the photocurrents. Furthermore, for the high Au concentration composite films, the large size of the Au particles physically blocking the light from reaching the TiO_2 film was also an important reason for the dampened photocurrent in the UV region.

It was clear that the "hoped for" improved photocurrent efficiency on introducing Au nanoparticles was not achieved. In view of this, a modification was carried out on the structure of composite films by forming a sandwich structure of Au/TiO_2-TiO_2 film. For this modified structure it was found that the influence of the Au particle was dependent on both its own concentration and of the presence of a dye-sensitizer.

Overall it was found in this study that the SPR effect did not show any noticeable improvement in the photocurrent efficiency and that the influence of Au nanoparticle concentration is not simply to improve or depressed the photocurrent of the TiO_2 film. Rather its influence is dependent on the size distribution of the Au particles and how it alters the structure of composite film. Future work should concentrate on understanding the mechanism of charge transfer between the Au nanoparticles and TiO_2 matrix.

List of Figures

List of Tables

List of Symbols

hv	Photon energy
h	Planck's Constant 6.62×10^{-34} W·s
C	The speed of light 3×10^{8} m/s
E	Charge constant of an electron 1.6021×10^{-19}C
V_{oc}	Open-circuit photovoltage
I_{sc}	Short-circuit current
F_f	Fill factor
E_f	Fermi level
I_s	Intensity of light
η_{globle}	Overall the whit light-to-electricity conversion efficiency
A	Absorption coefficient
E_g	Band gap of semiconductor
D_n	Diffusion coefficient
τ_n	Electron lifetime
CBM	Minimum of conduction band
VBM	Maximum of valance band
IPCE	Incident photon-to-current conversion efficiency for monochromatic irradiation
IMVS	Intensity modified photovoltage spectroscopy
HOMO	High occupied molecular orbital
LUMO	Low unoccupied molecular orbital
MLCT	Metal ligand charge transfer

Chapter 1 Introduction

Solar cells are attracting increasing interest for utilizing nature's energy flow to produce electricity. Basically, a solar cell converts sunlight to electricity through the photovoltaic effect, in which a photon excites an electron from a semiconductor's valence band into its conduction band, leaving a hole behind. After generation of the electron-hole pair, light-electricity conversion is achieved by the processes of separating the electron from the hole and transporting it through external circuit. Although all these processes (photon generation, electron-hole separation and electron transport) are important, electron-hole separation is the most crucial because of the fact that the excited electron-hole pair recombines spontaneously as the system wants to be electrically neutral.

In a conventional silicon solar cell, the excited electron is successfully separated from the hole by a p-n junction. The junction region is depleted of both electrons (on one side) and holes (on the other side), so it always presents a barrier to majority carriers and a low resistance path to minority carriers. It drives the collection of minority carriers, which are photogenerated throughout the p and n layers, reaching the junction by diffusion[1]. However, since electron-hole separation and electron transport all take place in a single semiconductor, electrons can still be captured by defects before being transported to an external circuit; consequently the light-electricity conversion efficiency is reduced[2,3]. To prevent recombination of electron at defects, a silicon solar cell relies on a high quality single crystal wafer; this dramatically increases the manufacturing costs.

With the development of materials science and engineering, various materials as replacement for single crystal silicon wafer, as well as new types of solar cell have been developed. Among these contributions, the most well known solar cell is the low cost, high efficiency, dye-sensitized TiO_2 nanoparticle solar cell (DSSC) developed by O'Regan and Grätzel in 1991[4]. The unique character of the DSSC is that photogeneration and electron transport take place in different materials. Photons generate electrons and holes in the dye, after which the electrons are injected into the conduction band of a TiO_2 particle. Hence there is no hole in the TiO_2's valence band so no direct recombination can occur within the semiconductor. This electron generation and injection process is known as dye-sensitization. Most of the sunlight in the visible region can be absorbed by dyes due to a variety of low-lying electronically excited states in the dye. Therefore, dye-sensitization plays an important role in the light-electron conversion. However, the electron injection takes place only when dye molecules are in direct contact with the TiO_2 surface, that is restricted to the first monolayer.

Although the concept behind the DSSC was developed in the 1970's, the light-electricity conversion of DSSC was too low to be of practical interest. Then in 1991, Grätzel *et al*. invented high conversion efficiency (~10%) DSSC (now termed the Grätzel cell), which attributed its high photon-electron conversion from: the highly efficient dye; the large surface area of the porous nanostructured TiO_2; and the wide band gap, non-toxic, TiO_2 semiconductor[4]. However, the efficiency of Grätzel cell is still lower than that of crystalline silicon based solar cells. Efficient operation of DSSC relies on minimization of the possible recombination occurring at the TiO_2/dye/electrolyte interface. Therefore, studies aimed at improving the conversion

efficiency of the Grätzel cell are highly desirable.

Throughout the development of the Grätzel cell, many alternative wide bandgap semiconductors such as SnO_2[5], ZnO [6] and Nb_2O_5[7] have been tested. However, the best choice remains TiO_2 (anatase) because of its low cost, stability and high photon-electron yield. The majority of modifications on the Grätzel cell have paid attention to how to reduce the electron loss caused by recombination at the TiO_2/dye/electrolyte the interface[8]. In this interface, the surface morphology and structure of the TiO_2 film is decisive to the chemical absorption of dye, the electron injection step and the recombination pathways.

Although a porous nanocrystal structure TiO_2 film provides large surface area for dye absorption, it also causes some unexpected problems. The first is that as the nanocrystalline TiO_2 is extremely small, it could be smaller than the space charge layer in semiconductor, thus there may be no band bending in the TiO_2 surface, so the electron will not be rapidly removed from the interface, leaving it vulnerable to recombination with a hole or a redox species in the electrolyte[5]. Secondly, the porous structure could increase the dark reaction if part of the back contact electrode comes into contact with the electrolyte, i.e. its surface coverage is not complete[9]. Likewise if the dye does not penetrate all the pores of the TiO_2 matrix electron injection will be reduced, as this only occurs when dye molecules are in direct contact with the TiO_2, that is restricted to a monolayer[10]. Thirdly, since there are so many interfaces in a DSSC, energy levels between different phases may be mismatched, thus increasing energy loss[10]. Finally, unlike the totally solid p-n junction silicon solar cells the DSSC

has several phases, including solids (semiconductor, dye and back electrode) and liquid (electrolyte), which may cause electron energy loss at the interfaces[9].

To date, modifications of the TiO_2 film have mainly been reported on the following four aspects:

1) Increase of the dye-sensitization area. TiO_2 films synthesized with controlled structure and desired morphology have been applied to improve monolayer dye absorption, e.g. nanocrystalline, nanotubes[11] and nanowires[12]. Referring to nanotube and nanowire structures, although both have been synthesized and exhibited large surface area in the laboratory, their opaque nanostructures have limited their optical applications.

2) Suppression of the recombination process at the TiO_2/dye/electrolyte interfaces. The most common approach is to block the excited electron from recombining with a hole in the dye (i.e. the oxidized dye) by adding another metal oxide semiconductor with a different band structure between the dye and TiO_2 film. This metal oxide semiconductor will create a depletion layer at the surface of TiO_2 particle to direct the electrons toward the back contact electrode. Zaban *et al*. and Durrant *et al*. reported that composite semiconductors, such as SnO_2-TiO_2[5], $SrTiO_3$-TiO_2[13], ZnO-TiO_2[6], Nb_2O_5-TiO_2[7] and Al_2O_3-TiO_2[14] retarded the interfacial charge recombination rate by several orders of magnitude.

3) Control of the back reaction between the photoinjected electrons and the oxidized half of the redox electrolyte. Besides recombination, back reactions in DSSC have also been recognized as another major cause for the low light-

electricity conversion[9,15,16]. Attempts to reduce the dark current caused by the back reaction included post treatment with titanium tetrachloride[17] on the surface of TiO_2 film or the deposition of a dense TiO_2 layer between the porous TiO_2 film and the back contact electrode[9]. Both methods suppress the back reaction effectively.

4) Improvement of the photon-electron conversion in the visible region. The dye, as sensitizer, plays an important role in the light harvesting. However, because the area occupied by one molecule is much larger than its optical cross section for light capture[18], a monolayer of dye absorbs only a part of the surface irradiation light, thus light absorption is not efficient. Two solutions to this problem have been proposed: synthesis of higher efficiency dyes[19] and improvement of light absorption by using a photocatalytic noble metal nanoparticle/TiO_2 composite film. Composites of noble metal nanoparticles and semiconductors have been widely employed in photocatalysis[19-21]. For instance, Au nanoparticles, as a promoter, enhanced the room temperature photocatalysis of CO oxidation at TiO_2 particles[22]. Likewise, due to their property of surface plasmon resonance (SPR) in the visible region, Au metal nanoparticles have also been reported as promoters in dye-sensitization[23]. Because of these advantages, Au nanoparticles have been targeted for use in DSSC's with the aim of improving dye-sensitization and photon-electron conversion in the visible region. However, due to a lack of understanding of the properties of the nanoscale materials used, previous experiments in this field were not as successful as anticipated[24]. Consequently, less work has been focused on the influence of noble metal nanocomposite films for the photon-

electron conversion than for photocatalytic applications.

The focus of the research reported in this present thesis was based on the last of the above mentioned techniques to improve the DSSC, i.e. to improve the photon-electron conversion in the visible region, in particular by the incorporation of noble metal nanoparticles into the TiO_2 films.

The objectives of this study were to:

1. investigate the causes of low photon-electron conversion efficiency in the DSSC;
2. investigate possible techniques to improve the photon-electron conversion efficiency in the DSSC, with emphasis on the visible region;
3. characterize Au/TiO_2 composite films that may be suitable for use in DSSC's;
4. study the influence of Au nanoparticle on the photoelectrochemistry of TiO_2 films;
5. evaluate the application of the proposed Au/TiO_2 films and suggest possible improvements for further study.

Although some reports indicated that noble metals improved dye-sensitization[23], Zhao *et al*.'s research on Au/TiO_2 nanocomposite[24] showed that the photocurrent of TiO_2 in the UV region was damped by the addition of noble metal nanoparticles. This was explained as being due to the noble metals forming Schottky barriers with the semiconductor and thereby retarding electron transport in the TiO_2 film. However, this explanation was not conclusive, since it neglected the fact that the photocurrent is an integrated parameter of both photon absorption and electron transport. To investigate

the cause of this loss of photocurrent was the one of the motivations for the present study.

Regarding the advantage of Au nanoparticles improving the photocatalytic performance of TiO_2[22,25,26] and Au thin films improving the electron transport and separation of electron-hole in DSSC[27], the inspiration for this study was that the properties of Au particles may vary with size and distribution. For example, dispersed small Au particles support the photocatalytic property of TiO_2 films due to quantum confinement inducing a high active surface, whilst a continuous distribution of gold particles (e.g. gold film) could play an important role in separating photo-induced electron-hole pairs. In present study, experiments were carried out to investigate the influence of Au particles size and distribution on the photoelectrochemical properties. Furthermore, although the small TiO_2 particle size increases the absorption of dye molecules, the large band gap of TiO_2 still limited the light absorption in the visible region. Therefore, in this study, another aim was to test if the addition of gold particles could be helpful by red-shifting light absorption into the visible region, thereby increasing the light-electricity conversion efficiency.

In addition, an investigation on why noble metal nanoparticles dampen the photocurrent obtained from DSSC's in the UV region has also been conducted. This included an exploration of the influence of Au particles on the crystalline structure and light absorbance of TiO_2 particles, as well as experiments to examine the influence of Au particles on the photoelectrochemistry. In present study, Au particle size was controlled by the Au concentration in the TiO_2 film; that is through aggregation. In addition, the influence of Au particles on the surface states of a TiO_2 film was also

investigated. In an attempt to improve the performance of Au/TiO_2 composite films, a modification was made by adding a compact TiO_2 layer between the Au/TiO_2 film and the ITO conductive transparent glass back contact electrode.

Results from the present study showed that in Au/TiO_2 composite films the SPR absorption peak of the Au particles red-shifts with increasing Au particle size, whilst the SPR peak intensity increases with higher Au concentration. These results suggested that the SPR peak position is related to the particle size and distribution, whilst its intensity is related to the concentration of active Au nanoparticles. An investigation into the cause of the damping of the photocurrent of Au/TiO_2 composite films in the UV region showed that poor crystallization of TiO_2 in composite film may be responsible. That is bulk recombination of excited electrons with defects in the amorphous structure may reduce the photocurrent of Au/TiO_2 composite films.

An investigation on the recombination of excited electrons and holes in the Au/TiO_2 composite films, by measuring photoluminescence, showed its efficiency decreased with increasing Au concentration. This result suggests that more excited electrons are localized and more TiO_2 structure contains more defects as the Au concentration increases. Although Au composite films showed SPR absorption in the visible region, this did not transfer to an improvement in the photocurrent of the composite films in the visible region; this may be due to the low SPR intensity, as well as some photoexcited electrons being lost in unexpected processes. Therefore, in present study, the composite film structure was modified by inserting a TiO_2 layer between the Au/TiO_2 composite film and the back electrode. The photocurrent of these Au/TiO_2-TiO_2 films showed a red-shift toward the visible region. This modification demonstrates a potential to improve the photocurrent of composite films, even to

improve the photon-electron conversion of porous TiO_2 film. In this study, in order to investigate the SPR performance of Au/TiO_2 composites films, the films were prepared in a compact film, rather than the porous structure used in most of DSSC studies. The porous structure films, useful for absorbing dye, would induce more scattering and thus decrease the SPR performance. Therefore, the work on dye-sensitization of the Au/TiO_2 composites was only an additional study on samples already made.

This thesis is organized into six chapters. The first chapter is a general introduction covering the background, objectives of the study and some of the highlights of the results obtained. A comprehensive literature review on the subject is given in Chapter 2. It includes the development of the dye-sensitized solar cell, research on dyes and electrolytes, as well as on modification methods for the TiO_2 film. The chapter finishes with a theoretical presentation of the principals of the DSSC cell, the process of photon-electron conversion and modifications of TiO_2, e.g., Au/TiO_2 films.

Chapter 3 introduces the materials and methods applied in this present study. This includes synthesis of the composite film and techniques to characterize its physical properties as well as to investigate its photoelectrochemistry and photon-electron conversion efficiency.

Chapter 4 documents the characterization of the Au/TiO_2 films produced in the current work. It includes results and a discussion on the influences of Au particle size and concentration on the crystallization of TiO_2 particles in the composite films. Discussions on the influence of Au particles on the surface state of composite films

and the effect of these surface states on the photon-electron conversion are also provided.

Chapter 5 describes the influence of Au particles on the photoelectrochemistry of TiO_2 films, such as open-circuit potential shifts and changes in polarization resistance and double layer capacitance. Chapter 5 also gives the results and discussion on the photocurrent of modified composite films, including the photon-electron conversion of Au/TiO_2 composite films and the difference in response of Au/TiO_2 composite films with and without modification.

In chapter 6, conclusions are drawn and directions for future work suggested. Based on the results and discussion in the previous chapters, the conclusions focus on the explanation of photocurrent damping seen for Au/TiO_2 composite films in the UV region and on the role of Au particles in the photon-electron conversion process. In addition, the photocurrent improvement in the Au/TiO_2-TiO_2 modified film is also explained. The potential applications of this modified film structure are also discussed.

Reference

(1) Nelson, J. *The physics of solar cells*; Imperial College Press: London, **2003**.

(2) Chapin, D. M.; Fuller, C. S.; Pearson, G. L. *J. Appl. Phys.* **1954**, *25*, 676-677.

(3) Goetzberger, A.; Hebling, C. *Sol. Energy Mater. Sol. Cells* **2000**, *62*, 1-19.

(4) O'Regan, B.; Grätzel, M. *Nature* **1991**, *353*, 737-740.

(5) Chappel, S.; Chen, S.-G.; Zaban, A. *Langmuir* **2002**, *18*, 3336-3342.

(6) Wang, Z. S.; Huang, C.-H.; Huang, Y.-Y.; Hou, Y.-J.; Xie, P.-H.; Zhang, B.-W.; Cheng, H.-M. *Chem. Mater.* **2001**, *13*, 678-682.

(7) Chen, S. G.; Chappel, S.; Diamant, Y.; Zaban, A. *Chem. Mater.* **2001**, *13*, 4629-4634.

(8) Hagfeldt, A.; Grätzel, M. *Chem. Rev.* **1995**, *95*, 49-68.

(9) Cameron, P. J.; Peter, L. M.; Hore, S. *J. Phys. Chem. B* **2005**, *109*, 930-936.

(10) Kalyanasundaram, K.; Grätzel, M. *Coord. Chem. Rev.***1998**, *177*, 347-414.

(11) Mor, G. K.; Shankar, K.; Varghese, O. K.; Grimes, C. A. *J. Mater. Res.* **2004**, *19*, 2989-2996.

(12) Longo, C.; De Paoli, M. A. *J. Braz. Chem. Soc.* **2003**, *14*, 889-901.

(13) Diamant, Y.; Chen, S. G.; Melamed, O.; Zaban, A. *J. Phys. Chem. B* **2003**, *107*, 1977-1981.

(14) Palomares, E., Clifford, J. N., Haque, S.A., Lutz, T., Durrant, J.R. *Chem. Commun.* **2002**, 1464-1465.

(15) Cameron, P. J.; Peter, L. M. *J. Phys. Chem. B* **2005**, *109*, 7392-7398.

(16) Ito, S.; Liska, P.; Comte, P.; Charvet, R.; Bach, U.; Schmidt-Mende, L.; Zakeeruddin, S. M.; Kay, A.; Nazeeruddin, M. K.; Grätzel, M. *Chem. Commun.* **2005**, 4351-4353.

(17) Zeng, L. Y.; Dai, S. Y.; Wang, K. J.; Pan, X.; Shi, C. W.; Guo, L. *Chin. Phys. Lett.* **2004**, *21*, 1835-1837.

(18) Grätzel, M. *Inorg. Chem.* **2005**, *44*, 6841-6851.

(19) Nazeeruddin, M. K.; Klein, C.; Liska, P.; Grätzel, M. *Coord. Chem. Rev. 15th International Symposium on the Photochemistry and Photophysics of Coordination Compounds. Hong Kong, July '04.* **2005**, *249*, 1460-1467.

(20) Subramanian, V.; Wolf, E.; Kamat, P. V. *J. Phys. Chem. B* **2001**, *105*, 11439-11446.

(21) Radecka, M.; Gorzkowska-sobas, A.; Zakrzewska, K.; Sobas, P. *Opto-electron. Rev.* **2004**, *12*, 53-56.

(22) Yang, J. H.; Henao, J. D.; Raphulu, M. C.; Wang, Y.; Caputo, T.; Groszek, A. J.; Kung, M. C.; Scurrell, M. S.; Miller, J. T.; Kung, H. H. *J. Phys. Chem. B* **2005**, *109*, 10319-10326.

(23) Tian, Y.; Tatsuma, T. *Chem. Commun.* **2004**, 1779-1883.

(24) Zhao, G.; Kozuka, H.; Yoko, T. *Sol. Energy Mater. Sol. Cells* **1997**, *46*, 219-231.

(25) Lee, S.; Fan, C.; Wu, T.; Anderson, S. L. *J. Am. Chem. Soc.* **2004**, *126*, 5682-5683.

(26) Zakrzewska, K.; Radecka, M.; Kruk, A.; Osuch, W. *Solid State Ionics* **2003**, *157*, 349-356.

(27) McFarland, E. W.; Tang, J. *Nature* **2003**, *421*, 616-618.

Chapter 2 Literature Review

Since the dye-sensitized mesoporous TiO_2 film solar cell (DSSC) was invented by Grätzel in 1991, there have been a great number of works that focused on the DSSC[1]. In this chapter, the review is focused on three aspects. The first aspect is the operational principle of DSSC and the mechanisms of the processes which influence the light-electricity conversion in the DSSC, such as: the mechanism of light absorption and electron-hole separation on the dye[2,3]; the mechanism of electron transport in the semiconductor[4-6]; the energy loss processes by electron-hole recombination in the DSSC[7-9]; and the back-reaction[10-12]. The second aspect is on the improvement of light-electricity conversion efficiency, such as selecting an efficient dye[3,13] or modifying the semiconductor structure to reduce the energy or electron losses [14-16]. The third aspect in this review is the development of new types of solar cells, such as modification of the structure of the DSSC to improve its potential for practical applications and avoiding the use of "wet chemistry"[17-20].

2.1 Operational principle of DSSC

Light-electricity conversion in DSSC, as with solid silicon solar cells, has three basic processes: photon absorption, electron-hole separation and electron transport. The operation principle of DSSC is well understood and summarized in Figure2-1[3].

The structure of DSSC includes three key components: porous semiconductor, sensitizer (S) and redox mediator (A/A-). This solar cell operates as follows: at first the dye, as sensitizer, absorbs a photon that excites an electron to jump from HOMO (high occupied molecular orbital) to LUMO (low unoccupied molecular orbital); next

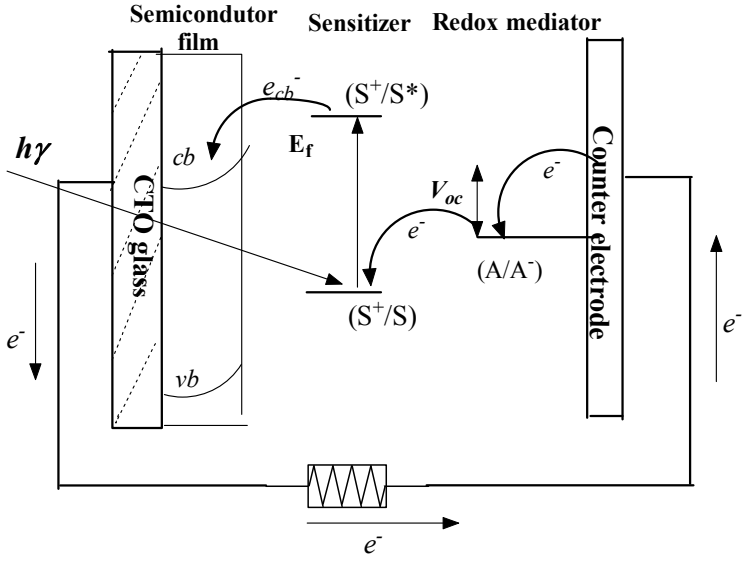

Figure 2-1 Schematic diagram of operation principle of dye-sensitized thin film solar cell adapted from reference [3]. (E_f: Fermi level, S: dye, CTO: conductive transparent oxide, V_{oc}: photovoltage)

the excited electron is injected into the conduction band of the semiconductor (Eq. 2.1); subsequently, electron transport occurs through the semiconductor film to the back electrode (conduction transparent oxide, CTO, glass) then through the external circuit to the counter electrode; finally, the circuit is closed by recovering the excited dye with an electron donor (A) from the redox mediator (Eq. 2.2), which itself is recovered by accepting an electron from the counter electrode to keep the equilibrium of the system (Eq. 2.3). The key reactions are[3]:

$$S^* \rightarrow S^+ + e_{cb}^- \qquad (2.1)$$

$$S^+ + A^- \rightarrow S + A \qquad (2.2)$$

$$A + e^- \rightarrow A^- \qquad (2.3)$$

In the DSSC, the energy level at the dye-semiconductor interface drives the electron's injection into the semiconductor and its transport to back electrode (CTO). This requires that both the LOMO of dye is higher than the conduction band of the semiconductor and the HOMO of dye is lower than the redox potential of the

electrolyte. These energy level differences present the driving force for electron injection into the semiconductor and hole injection into the electrolyte. If there were no loss causing processes, i.e. no recombination reactions, the obtained photocurrent would only be dependent on the intensity and spectrum of the illuminating sunlight, the redox properties of the dye and the efficiencies of the charge injection process and collection of the electron in the semiconductor electrode. Likewise, the maximum photovoltage would be determined by the difference between the Fermi level (conduction band) of the semiconductor under illumination and the redox potential of the mediating redox couple.

Quantitative assessment of the solar cell performance is given by two key parameters, i.e. incident photon-to-current conversion efficiency (IPCE) for monochromatic radiation and overall the white light-to-electricity conversion efficiency η_{globle}[3].

The IPCE value is the ratio of the observed photocurrent divided by the incident photon flux, uncorrected for reflective losses during optical excitation through the conducting glass back electrode:

$$\text{IPCE}=\frac{\text{no. of electrons flowing through the exteral circuit}}{\text{no. of photons incident}} \qquad (2.4)$$

or

$$\text{IPCE}=\frac{hc}{e}\times\frac{\left[I_{sc}(A/cm^2)\right]}{\left[\lambda(\text{nm})\times I_s(W/cm^2)\right]}\times 100 = 1240\times\frac{\left[I_{sc}(A/cm^2)\right]}{\left[\lambda(\text{nm})\times I_s(W/cm^2)\right]} \qquad (2.5)$$

where, I_{sc} is the short circuit current density, λ in the wavelength of the incident light and I_s is the incident light power. The constant 1240 is derived from the constants *hc/e* (*h*: Planck's constant 6.62 $\times 10^{-34}$ W·s; *e*: charge constant of an electron 1.6021 $\times 10^{-19}$ C;

c: the speed of light 3 $\times 10^8$ m/s). The IPCE value can be considered as the effective quantum yield of the device [3].

The overall efficiency (η_{global}) of the photovoltaic cell can be obtained as a product of the integral photocurrent density (i_{ph}), the open-circuit photovoltage (V_{oc}), the fill factor (*ff*) and the intensity of the incident light (I_s) [3]:

$$\eta_{global} = \left(i_{ph} \cdot V_{oc} \cdot ff \right) / I_S \qquad (2.6)$$

$$ff = \frac{V_m \cdot I_m}{V_{oc} \cdot I_{sc}} \qquad (2.7)$$

where, V_m is the maximum output voltage and I_m is the maximum output current. The fill factor *ff* is derived from the *I-V* curve as shown in Figure2-2[21].

The limitation of these assessment methods is the difficulty to get a comparable intensity of incident light, as this varies with location on the earth and the mass of the air (e.g. height above sea level). Therefore, it is necessary to have a standard for the intensity of incident light. It has been defined that AM 0 (air-mass zero) corresponds to the absence of any atmosphere between the sun and the device (e.g. outer space), more practical standards are AM 1.0 which is defined as the sunlight irradiation at the angle of 0 ^{o} on the device and AM 1.5 which is defined as the sunlight irradiation at an angle of 48.19^o to the device normal[3]. Although these definitions avoid the influence of geographic location, scattering and absorption of the photons by suspended particles in the air still take place. To solve this, solar simulators are now commercially available for indoor experiments with simulated sunlight[3]. Regarding to the study of efficiency of the DSSC, O'Regan *et al*. found a DSSC composed of porous TiO_2 nanoparticles on conductive transparent metal oxide (SnO_2: F) coated glass (CTO

glass), Ru complex (N3) as sensitizer and an iodine/iodide containing electrolyte, shows a high light-electricity conversion of ~10% [1].

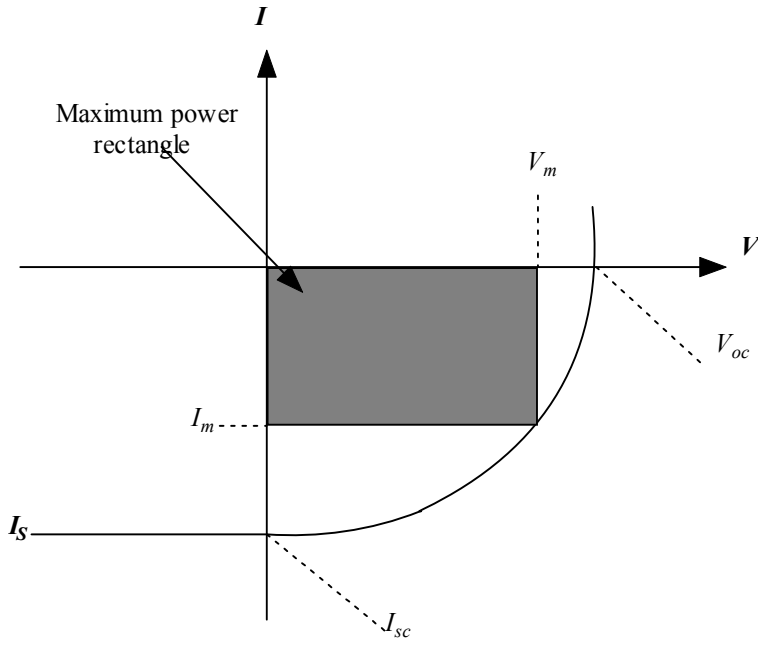

$$FF = I_m V_m / I_{sc} V_{oc}$$

I_s= *photon flux level*

Figure 2-2 I-V Characteristic of illuminated solar cell adapted from reference [21]

2.2 Main processes in DSSC

2.2.1Dye-sensitization

As a photosensitizer, the dye needs to meet certain requirements. At first, the dye needs to have the property of light absorption in the visible, IR and near-IR regions, where the intensity of sunlight is strong[3]. This requirement means the dye must possess multiple excited states to absorb as much sunlight as possible. Secondly, the dye needs to match the energy levels with the semiconductor and redox-mediator in the DSSC. As mentioned above, the LUMO of the dye needs to be higher than the conduction band of the semiconductor and the HOMO of the dye lower than the Fermi level of the redox mediator as shown in Figure2-1. Thirdly, the redox properties or reversibility and stability of dye are also important[3]. It is required to satisfy the

condition that the rate of recovering dye is slower than the electron injection into the conduction band of the semiconductor.

From Grätzel *et al.*'s studies, transition metal (Ru) complexes derived from polypyridines, porphine or phthalocyanine as ligands are the preferred choice for the dyes[1,3,22]. These complexes exhibit a variety of low-lying electronically excited states (π-π^*, d-d* and d-π^*/CT) which supply many energy states for accepting photon excitation. This character allows the dye to exhibit tunable absorption especially in the visible, near IR and IR regions.

The most important feature of the transition metal complex is the metal-ligand charge transfer (MLCT), as shown in Figure2-3, which results in long-lived luminescent excited states[2,23]. The excited electron is quenched by the charge injection into the empty conduction band of the semiconductor, moreover, this injection is a fast process compared to the recombination between the hole in the dye and the electron donor from the redox mediator[24]. However, in DSSC, this electron injection, i.e. the efficiency of dye sensitization, depends on whether the dye is absorbed on the supporting semiconductor surface's in a monolayer; dye molecules in an second monolayer would be too far away from the semiconductor to allow electron injection[2]. This monolayer attachment directly influences the efficiency of electron injection from ligands to the conduction band of semiconductor. Although the dye spontaneously attaches on the surface of semiconductor via covalent anchoring groups[3], the area of dye optical absorption is smaller than the area occupied by the molecular. This limits the effective area of dye attachment. Therefore, to increase the attachment area of the

dye to achieve efficient dye sensitization, a porous and nanostructure film of very high surface area is the preferred choice[2].

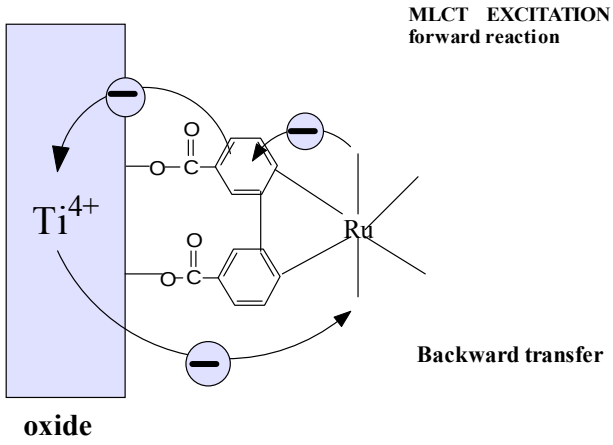

Figure 2-3 Schematic of the interfacial electron transfer involving a ruthenium complex bound to the surface of TiO_2 via a carboxylated bipyridyl ligand, adapted from reference [2]

So far, the best performance of a DSSC was achieved with a mesoporous TiO_2 film sensitized with the ruthenium complex cis-dithiocyanato bis(2,2'-bipyridyl-4,4'-dicarboxylate) Ru(II), (N_3 dye), and this has achieved an efficiency of 11.2%[13]. However, the ideal sensitizer would absorb nearly all the sunlight incident on the earth, like a black-body absorber[3]. Recently, Nazeeruddin *et al.*[25] synthesized a new ruthenium(II) complex tri(thiocyanato)-2,2',2"-terpyridyl-4,4',4"-tricarboxylate) Ru (II), the so called black dye, which exhibited an increasing optical extinction coefficient and very efficient sensitization yielding IPCE of 10.4%. Although black dye absorbs more sunlight, it does not adsorb efficiently on the TiO_2 surface, hence it has not yielded the large increase in conversion efficiency hoped for. So far, N3 dye has emerged as the standard dye to compare and select other new sensitizer for DSSC, because of its high photo- and chemical-stability[26,27]. More information on the history of dye-sensitization and the application of dye on solar cell can be found from a review by Kalyanasundaram and Grätzel[3].

2.2.2 Electron transport and recombination

After being injected from the dye into the conduction band of the semiconductor, the electron is transported to the back contact electrode, i.e. processes 2 and 3 in Figure2-4, with the excited dye being recovered by the electrolyte as shown by the process 4. If only these reactions took place, the solar cell would be stable and efficient. However, the electrons could take place recombination with the electrolyte and surface traps, as shown by the dashed lines in Figure2-4, i.e. by processes 7 and 8[7]. These unwanted processes cause a deactivation of photoexcited electrons and reduce the electron density in the conduction band of the semiconductor. Note that because light absorption is by the dye at no time is there a hole created in the TiO_2's valence band so the conventional electron-hole pair recombination across the band gap does not occur.

Besides two these unwanted processes, a back reaction between the conductive substrate (CTO glass) and the electrolyte can be another source of energy loss. The back reaction of photoinjected electrons with electrolyte has three routes, i.e the electron is transferred from a TiO_2 nanoparticle via conduction band (process 7 in Figure2-4), via surface states to the redox electrolyte or directly transferred from the highly conducting back electrode to redox species in the electrolyte[2,11]. By investigating the incident photon to current conversion efficiencies (IPCE) under short circuit conditions, Cameron *et al.* found a high IPCE of 90%, which they concluded suggests that the back reaction with the redox electrolyte would greatly decrease the conversion efficiency in a practical circuit, particularly at lower light intensities[11]. To prevent these back reactions, some researches have found that using a extra TiO_2 film as a blocking layer deposited on the top of back contact electrode[11] or post treatment

by immersing the TiO_2 film into $TiCl_4$ solution forming top layer[20,28] are efficient ways to prevent the back reaction between redox couples and the substrate.

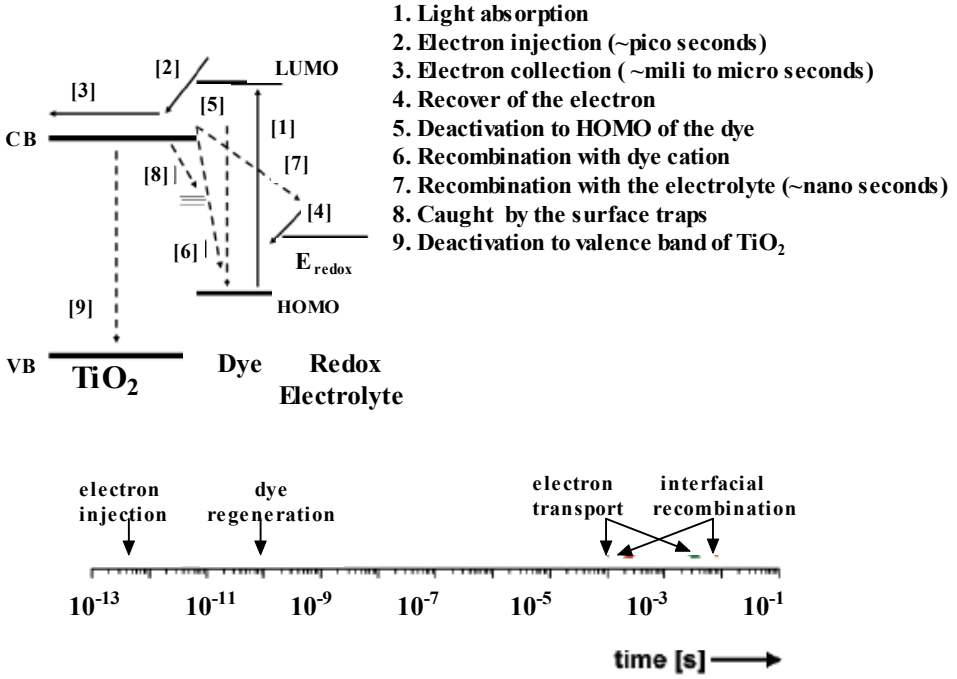

Figure 2-4 Illustration of electron transport and possible recombination in dye-sensitized solar cell, dot line marks the undesirable recombination, solid line marks electron transport. The time scales of different processes also are illustrated. Adapted from reference [2, 7]

The mechanism of electron transport in the semiconductor depends on its morphology and structure. In DSSC, the recombination of the photoexcited electron-hole pair needs to be retarded for an efficient charger transfer process to occur on the semiconductor surface. Charge carrier trapping would suppress recombination and increase the lifetime of the separated electron and hole[29]. For colloidal and polycrystalline structures, surface and bulk irregularities naturally occur during the preparation processes. These irregularities are associated with surface electron states, which serve as charge carrier traps and help suppress the recombination of electrons and holes. Differing from the electron transport forced by electric field in silicon solar cell[30], electron transport in the nanostructured semiconductor films of DSSC is assumed to proceed primarily via diffusion[31], because of the absence of a significant electrical

potential gradient in the film. As shown in Figure2-5, on the microscopic (or local) level, an electrical potential decrease occurs only across the Helmholtz layer at the semiconductor particle/electrolyte interface. On the macroscopic level, no significant electrical potential decrease exists within the porous semiconductor film when it is in contact with an electrolyte[5]. A driving force for the electron flow, through the porous structure toward the conducting substrate, is the equilibration of the electron density through the film, i.e. diffusion. The diffusion length (L_n) of electrons can be estimated from:

$$L_n = (D_n \tau_n)^{1/2} \qquad (2.8)$$

The properties of charge transport are often explained by considering the involvement of electron trapping in surface states. This mechanism is most often discussed in terms of a trapping/detrapping model, where electrons move between mid-band gap states via the conduction band. Alternatively, a hopping model can be used, where the electron moves between localized mid-band gap states [32].

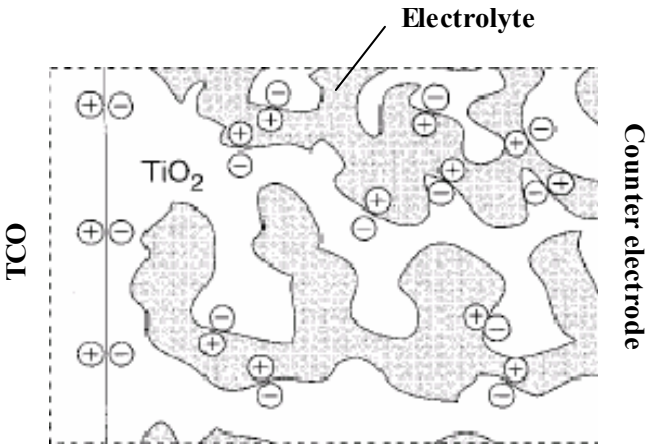

Figure 2-5 Electron distribution at the electrode/electrolyte interface in DSSC. (adapted from [31])

Many publications in this field suggest the presence of electronic states with energies located below the conduction band[33-36], suggesting that the electron transport in

nanostructured TiO_2 is a thermally activated process with activation energies. Within a trapping/detrapping model, this activation energy would imply that the effective trap depth is 0.1-0.15 eV[37]. The nanostructured film consists of separate TiO_2 nanoparticles, usually single crystals that are connected together in a random way. The particle-particle connection is most likely to be a distinct grain boundary, where the material properties differ from those in the bulk of the nanocrystal. Electrons can probably move freely in a nanocrystal but experience some kind of barrier to move to an adjacent nanocrystal. The limiting step for electron transport could be the jump from one nanoparticle to another. For the trap sites in a TiO_2 film, a number of surface science studies on rutile single crystals have shown that reduction of the TiO_2 (110) surface leads to oxygen vacancy formation at the surface. In the near-surface region of the crystal there are not only oxygen vacancies but also Ti^{3+} sites. A Ti^{3+} species may be considered as a trapped electron in the band gap region[38]. With direct band gap semiconductors, such as TiO_2, the electron or hole traps and impurity states (defect sites) are the predominant sites for recombination. When these traps become filled by photoexcitation, a sudden increase in the rate of the photoelectrochemical process should be observed[38]. In the trapping/detrapping mechanism, as shown in Figure2-6, electron transport occurs between adjacent redox centers at the surface of the nanostructure semiconductor electrode[2,39]. These redox centers are surface Ti atoms that have a valence of 4+ when they are empty or 3+ when they are occupied by an electron[2,5].

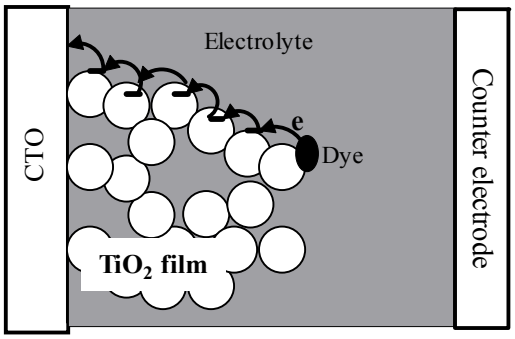

Figure 2-6 Schematic diagram of electron trapping/detrapping transport in TiO_2 film to back contact electrode.

2.3 Semiconductor films in DSSC

Since the surface area of the semiconductor is crucial for the efficiency of dye sensitization, the structure and morphology of the semiconductor are important features for high light-electricity conversion. As the heart of the system, the semiconductor needs to possess the following properties: first a large band gap, which makes the semiconductor transparent to most of the sunlight shining on the dye; second electrochemically stable, to ensure the integrity of semiconductor during light-electricity conversion; third energy levels in the semiconductor that matches with dye sensitization and the Fermi level of dye recovery via the redox mediator[3].

The most popular choice of semiconductor has been TiO_2 (anatase), although some other large band gap semiconductors also have been investigated, such as ZnO[40,41], Nb_2O_5[42], and SnO_2[43,44]. The band structure of some of these semiconductors is illustrated in Figure2-7[29]. These other oxide semiconductors exhibited lower performance in comparison to cells prepared with TiO_2[3,23]. A possible explanation could be that the different band structure in the other semiconductors influences the electron density and electron injection, even though these semiconductors have large band gaps. For instance, the band structure of Nb_2O_5 has the same band gap energy as

TiO_2 (3.2 eV) but has its conduction band located 0.2-0.3eV more negative, such that it is below the LUMO of the dye[3] as shown in Figure2-7. Thus, under visible light, electron injection from dye occurs on TiO_2 but not on Nb_2O_5. Another instance is ZnO, it has a similar band gap and band structure to TiO_2, however, although according to the research on the conductivity of TiO_2[5] and ZnO[45] films permeated with electrolyte, the electron mobility in ZnO is higher than in TiO_2, the effective mobility of TiO_2 was found to increase strongly with increasing carrier concentration[45]. This is coherent with the trapping/detrapping mechanism of electron transport in DSSC, i.e. movable electron concentration increases when traps are filled or the barrier height decreases as the Fermi level is raised. This may be one of the reasons for why TiO_2 is the best choice for DSSC as electron injection by dye-sensitization increases the electron concentration. An alternative, the possible reason for why the ZnO film is not as effective as TiO_2 could be due to the surface chemistry of ZnO film and lack of variable valence of the metal ion[45], i.e. Ti is variable as Ti^{3+}, Ti^{4+}, but Zn is always in the state of Zn^{2+}.

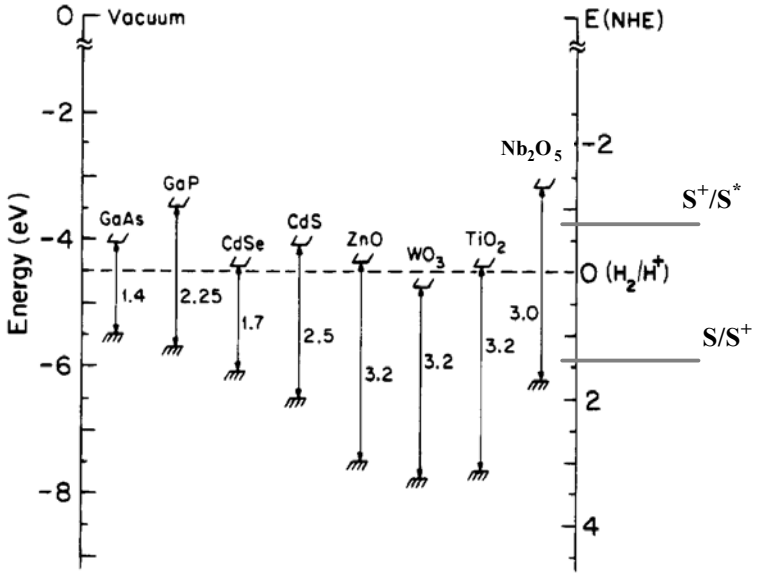

Figure 2-7 Energies for various semiconductors in aqueous electrolytes at pH=1. The electric structure position of dye and Nb_2O_5 are schematiclly illustrated in the this diagram. (Adapted from reference [29])

Two different crystal structures of TiO_2 are commonly used in the photocatalysis, i.e anatase and rutile (brookite is also a crystal structures of TiO_2, but it is hard to be obtained)[3]. On the material stability, rutile (needle-like) is formed by high temperature preparation, and it is more stable than anatase (pyramid-like), formed at low temperature. The anatase to rutile transformation occurs in the temperature region 700-1000 ^oC [3]. The structures of both anatase and rutile can be described in terms of TiO_6 octahedra, each Ti^{4+} ion being surrounded by six O^{2-} ions[29]. The difference between the two structures is the different distortion of each octahedron and the assembly pattern of the octahedral chains. The distortion of the octahedron in rutile is less than in anatase. The Ti-Ti distances in anatase are greater (3.04 and 3.79Å) than in rutile (2.96 and 3.57 Å), where as the Ti-O distances are shorter in anatase (1.934 and 1.980 Å in anatase vs. 1.949and 1.980 Å in rutile)[46-48]. In the rutile structure each octahedron is in contact with 10 neighbor octahedrons (two sharing edge oxygen pairs and eight sharing corner oxygen atoms) while in the anatase structure each octahedron is in contact with eight neighbors (four sharing an edge and four sharing a corner). These differences in lattice structure cause different mass densities and electric band structures (E_g=3.1eV ρ=4.250g/cm^3 in rutile, E_g=3.3eV ρ=3.894g/cm^3 in anatase)[29]. The surface structures of rutile and anatase have been extensively investigated, it being found that the (110) facets are the most thermodynamically stable and the lowest energy surface[2,29]. Other faces will reconstruct upon heating to high temperature and transfer to (110) facets[49,50]. These structure differences directly influence the electron transport in DSSC.

Park *et. al.* compared the performance of dye-sensitized rutile- and anatase-based TiO_2 solar cells and concluded that electron transport in a rutile layer is slower than in an

anatase layer[51]. As a consequence, the short-circuit photocurrent of the rutile based cell is lower than that of anatase based cell. This result suggests that rutile or other impurities in TiO_2 photoelectrode would result in a lower performance of the DSSC. So the anatase structure is favorable for solar energy conversion[3].

In addition, DSSC performance also depends on the morphology and porosity of the TiO_2 film. For instance, on one hand, the high the surface area of a TiO_2 nanoparticle film is necessary to meet the requirement of absorbing a large amount of dyes in the monolayer. On the other hand, it was found that large size particles cause light scattering and that the multi-reflection of light results in increased light absorption, enhancing the photoresponse of film, especially in the low light energy region[3]. Obviously, it is impossible to meet the requirements for increasing surface area with small particle size and employing light scattering with large porosity simultaneously.

In order to improve electron transport, nanowires were partly or fully introduced into the nanoparticle structure TiO_2 film[52]. The results showed that electron transport was effectively improved, and the nanowire also can increase scattering light and thus enhance the light harvesting in the low energy region, but at the expense of a smaller surface area for dye adsorption. In Tan and Wu's work[52], cells made with TiO_2 films containing different percentages of nanowires and nanoparticles exhibited higher short-cuicuit current densities than that of cells containing only TiO_2 nanoparticles. The best light-electricity conversion efficiency of 8.6% was exhibited in a 20%/80% nanowire/nanopartile cell; this was higher than that of the pure nanoparticle cell made in their study. Law *et al.*'s[53] study showed that the performance of a pure nanowire cell is primarily limited by the surface area of the nanowire array; i.e. the amount of absorbed dye. Also, Wang *et al.* [26] did a similar experiment in an attempt to balance

the conflict between the surface area and the light scattering by making a multilayer film with different nanoparticle sizes and obtained an improved energy conversion efficiency. Ohsaki *et al.*[54] looked at using nanotube morphology and revealed that a high efficiency resulted from an increase in the electron density, resulting from a much longer electron lifetime in the nanotube than in the nanoparticle. Their work also was benefited from a $TiCl_4$ post-treatment forming a blocking layer to reduce the back-reaction.

Methods for modification of the TiO_2 film have been widely investigated, such as print screening, sputtering and sol-gel methods. The sol-gel method is used widely, because of its advantages on low-cost and particle size control[55]. In these methods, sintering of the particles is a necessary step. This step is not only to crystallize the film into the target lattice structure, but also can produce low ohmic resistance contacts between the particles. Hence, the electrons injected in the network of particles can hop through several particles and reach the back contact[3].

2.4 Recent study on DSSC

2.4.1Modification on DSSC structure

Recent research on modifying the DSSC structure has focused on two aspects, replacing the liquid electrolyte by a solid-state inorganic or an organic electrolyte and using a multi-layer structure to increase the number of photoexcited electrons.

Solar cells composed of dye-sensitized nanostructure of TiO_2 with an I^-/I_3^- electrolyte have exhibited >10% light-electricity conversion efficiency, however, the use of a liquid electrolyte in this solar cell may limit device stability. For example, the liquid

may evaporate if the cell is imperfectly sealed or diffusion and reaction of water or oxygen molecules may worsen cell performance[56]. Furthermore, the liquid electrolyte also makes the manufacture of multi-cell modules difficult because cells must be connected electrically yet separated chemically, preferably on a single substrate. One way to solve these problems is to replace the liquid electrolyte by a solid state conducting materials[20]. Recent studies utilized alternative "hole transport media", including cobalt redox complexes[57] and solid-state organic hole conductors[58].

However, employing solid state electrolyte still cannot avoid the influence of the dark current, which occurs when photoexcited electrons react with the redox electrolyte. In order to prevent the recapture of photoexcited electron, a multilayer structure DSSC has emerged by the introduction of an additional thin compact TiO_2 underlayer between the porous TiO_2 film and the back contact conductive substrate[11,28]. This additional layer acts as a blocking layer to stop the photoelectron transferring back to redox electrolyte. This modification brought about both an increase in the photovoltage and reduced the dark current. It was also found by Hart *et al.*[59] that photocurrent was further improved by increasing the number of blocking layers. Similar to this underlayer, another blocking layer method is the post treatment by $TiCl_4$ on the top of TiO_2 film[60]. After deposition of porous TiO_2 film, the electrode is immersed into $TiCl_4$ solution at 70^{o}C for 30 min. It was found that the solar cell modified by both underlayer and $TiCl_4$ post treatment showed the better performance compared with those modified only by one method[28].

Among the various types of modified solar cells, a new device developed by McFarland and Tang[17] is worth mentioning. This solar cell took the TiO_2 DSSC as its

prototype, but innovating the cell structure into a multilayer structure, consisting of a Ti sheet on top of which is a compact TiO_2 film, followed by an ultra thin Au layer and lastly the dye layer; i.e. the dye is in contact with the Au not the TiO_2. Upon photoexcitation of the dye, electrons are injected into the TiO_2 layer by ballistic transport through gold film. In such a way, a photovoltage is generated between the Au and Ti electrode. This solar cell shows several advantages: i) it avoids the problem of the liquid electrolyte; ii) it has a multilayered structure that physically separates the processes of light absorption and charge-carrier transport; iii) it simplifies the solar cell structure; iv) it shows a strikingly high internal quantum efficiency for electric-current generation[61]. However, the overall quantum efficiency is presently low due to the small active surface area, i.e. it is a flat film rather than a porous nanoparticle one.

2.4.2 Modification on TiO_2 semiconductor film

Modifications on the TiO_2 film in DSSC aim to reduce the loss of the photoexcited electrons and thereby increase their lifetime, thus increasing the overall performance. Although the porous nanostructured TiO_2 film can increase the dye uptake, the small particle size causes the absence of space charge layer at the surface of TiO_2 particles[2], thus increasing the probability of recombination between the photoexcited electron and the redox electrolyte (Figure2-4). If this recombination is faster than the recovery of the photoexcited dye[2], it reduces the conversion efficiency. Attempts to reduce the loss of photoexcited electron in the back reaction include modifying the TiO_2 film to either a metal-TiO_2 composite[62,63] or a semiconductor-TiO_2 composite[64] or by transition metal doping[65,66]. The feature of these composite materials is that the particles of metal or semiconductor are in the nano-size regime so that these cover only a small area of the TiO_2 surface leaving a large surface area available to adsorb the dye[29].

These modifications were first successfully applied in the field of photocatalysis. For metal-TiO_2 composites, a noble metal is attractive because of its own photocatlytic properties. Although the chemistry of bulk noble metals is stable, nano-size noble metal particles exhibited extraordinary activity, due to the size effect of metal nanoparticles that have a high surface atoms to bulk atoms ratio. Furthermore, when a noble metal and TiO_2 come in contact, the Fermi levels of the two species align causing electrons to flow to the metal from the semiconductor. The electron is trapped in the metal particle at the surface of the TiO_2 [66]， so the holes are free to diffuse to the semiconductor surface where oxidation of organic species can occur. This feature is effective in the photocatalysis of TiO_2 in which the decrease in electron density within the TiO_2 leads to an increase in the oxidation reaction of the hole (Figure2-8 a))[29]. The metal actually modifies the photocatalytic properties of the semiconductor by changing the distribution of the electrons.

In the semiconductor-TiO_2 composite, the combination of different energy gap semiconductors increases the charge separation, extending the energy range of photoexcitation for the system. Figure2-8 b) illustrates geometrically and energetically the photoexcitation process for a composite photocatalyst CdS-TiO_2[67,68]. The energy of the excitation light is too small to directly excite the TiO_2, but it is large enough to excite an electron from the valence band across the band gap of CdS to its conduction band. According to this energetic model, the hole produced in the CdS valence band from the excitation process remains in the CdS particle while the electron transfers to the conduction band of the TiO_2 particle. The electron transfer from CdS to TiO_2 increases the charge separation and efficiency of the photocatalytic process. The

separated electron and hole are then free to undergo electron transfer with adsorbates on the surface.

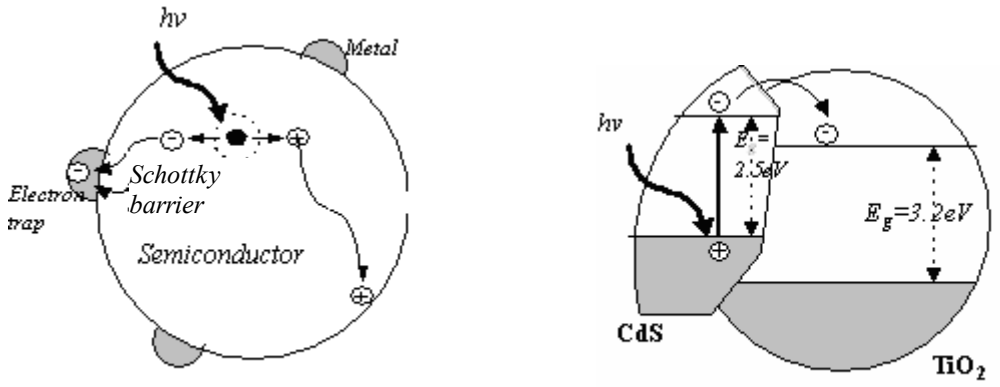

a) b)

Figure 2-8 Illustration of the photocatalysis of surface modified TiO_2 particle, a) metal composite forms at the TiO_2 particle surface, and affecting electron attribution; b) semiconductor-semiconductor composite is helpful to absorb the low energy light and inject electrons into TiO_2 particles. Both surface modifications increase the charge separation and efficiency of the photocatalytic process. Adapted from reference [28].

The improvements that these composite materials bring to the DSSC are mostly to increase the open-circuit voltage, short-circuit current or fill factor. For example, Chen *et al*.[16] investigated the photovoltaic performance of a TiO_2/Nb_2O_5 thin film in which an inner nanoporous TiO_2 matrix was covered with a thin layer of Nb_2O_5 and formed a core-shell structure. This new electrode has an inherent energy barrier set at its surface, due to the conduction band of Nb_2O_5 being about 100mV more negative than that of the TiO_2. This potential difference forms an energy barrier at the electrode-electrolyte interface, which can block the injected electrons recombining with the oxidized species in the electrolyte. It was thought that the oxidation potential of the dye (1.09V vs. NHE in acetonitrile) would be sufficient to allow excited electrons to be injected through both the TiO_2 and Nb_2O_5, via a ballistic mechanism. In Chen's cell, compared to a device without Nb_2O_5 layer, short-circuit photocurrent of composite film was increased from 10.2 to 11.4mA/cm^2, the open-circuit photovoltage from 659 to 732 mV and the fill factor from 51.1 to 56.4%. Similarly, other researchers obtained the

improvements of performance of DSSC by adding metal oxide semiconductor. Yang *et al*.[65] reported their improved results on a SrO-TiO_2 film: I_{sc} from 18.38 to 20.12 mA/cm^2; V_{oc} from 633 to 702 mV and the conversion efficiency η also increased from 7.3% to 9.3%. Palomare *et al.*[69] found that an Al_2O_3 coating can also improve the performance of a TiO_2 based solar cell: the I_{sc} improved from 8.1 to 10.9 mA/cm^2; V_{oc} from 705 to 750mV; and the conversion efficiency from 3.8% to 5%. Wang *et al*.[15] found that a ZnO additive layer improved the property of electron transport for colloidal TiO_2 films: I_{sc} improved from 18.2 to 21.3 mA/cm^2; V_{oc} from 663 to 712 mV; and the conversion efficiency from 7.7% to 9.8%. The ZnO covering led to a positive shift in the flat band potential and an increase in the free electron concentration in the conduction band with respect to a pure TiO_2 film. This increase in free electron concentration after ZnO covering may have resulted from a blockade of surface states; this favors charge transport and prevents loss of photogenerated electrons due to the presence of electron acceptors. Although the insulating shell layer covering on TiO_2 film can suppress the recombination of electron and hole, the thickness of shell layer is crucial parameter. It was reported that the thickness of the insulating layer above 0.5nm will deteriorate the effectiveness of solar cell performance. To prepare this thin insulating layer, one of successful methods is microwave heating technology[70]. However, the insulating layer still could impede electron flow between the particles. Therefore, it was suggested that applying coating on the TiO_2 film is better than making the film with core-shell particles[59,71].

The different effects of composite materials in photocatalysis and DSSC is due to the fact that in the former, the TiO_2's role is to separate the electron and hole, but in the latter the TiO_2 particles act as electron acceptor and transporter. Moreover, the

performance of a composite in DSSC also depends on the environment surrounding the TiO_2, such as the influence of the redox electrolyte, dye and back contact electrode.

A recent new application of these composite materials is to replace the dyes as the light-harvesting units in DSSC[72]. This takes advantage of the quantum effect of these nanosize composite particles. Light absorption produces excitons or electron-hole pairs in the semiconductor quantum dots, that can be formed from for example PbS[72]. The electron is subsequently injected in the TiO_2 film, while the hole is transferred to the redox electrolyte. Furthermore, by controlling the particle size, the quantum dots have higher optical cross sections than dye moleculars. However, the challenge is how to collect the excitons before they recombine. If this problem is solved, this finding looks as a promising strategy to make photoconverters reach high IPCE values[2].

2.5 Researches on the influence of Au on DSSC performance

The application of Au in the DSSC has been used for three reasons. The first application is that the Au nanoparticles dispersed into TiO_2 porous film can scavenge the photoexcited electron and retard the electron-hole recombination[73]. This is similar to the application in the photocatalysis mentioned in the previous section. Au nanoparticle (around 5~10nm) acting as sinks to facilitate charge rectification and improve the open-circuit voltage. However, this improvement is still not enough to increase the final photon-electron efficiency.

The second application is the cooperation of Au enhances the dye-sensitization. Dye sensitizers chemisorbed on the gold acts as an antenna layer. The Schottky barrier at the TiO_2/Au interface is essential for irreversible electron injection into the TiO_2 layer.

An example of this is the design of McFarland and Tang, previously described towards the end of Section 2.3.1, in which the outer Au layer not only acts as the antenna layer, but also acts as the counter electrode to recovery the dye to form a close circuit[17]. This feature is different with the Au nanoparticle modified DSSC, in which Au nanoparticles only act as photoelectron scavenger and the dye is recovered by a redox electrolyte. Other research conducted on TiO_2/Au systems, has suggested that it is the chemistry at the TiO_2 surface that determines the electrical characteristics of the interface[74].

The third application is to make use of the surface plasmon resonance of Au nanoparticle to extend the optical absorption of the TiO_2 film into the visible region[75]. The optical absorption of a metal nanoparticle is derived from the size effect, as the particle size approaches the size of the Bohr's radius of the exciton, energy bands split into different energy levels. Under the influence of an electromagnetic wave, an excitation of the collective oscillations of conduction electrons takes place in metal particles. This is presented as a strong absorption peak in the absorption spectrum, named surface plasmon resonance (SPR). It is known that the optical absorption band of Au nanoparticle in the visible region is dependent on the Au nanoparticle size[76]. SPR is also applied to enhance signals in surface Raman scattering spectroscopy[77]. The Raman signal from molecules adsorbed on certain metal surfaces (Au, Ag, and Cu) can be five-to-six orders of magnitude stronger than the Raman signal from the same molecules in bulk volume. The exact reason for such dramatic improvement is still under discussion. However, because the intensity of the Raman signal is proportional to the square of electric dipole moment $\mathbf{P} = \mathbf{aE}$, two possible reasons can be considered: the enhancement of polarizability **a** and the enhancement of electrical field **E**. The first

enhancement of polarizability **a** may occur because of a charge-transfer effect or chemical bond formation between the metal surface and molecules under observation, which is called chemical enhancement. The field enhancement takes into account the interaction of the laser beam with irregularities on metal surfaces, such as metal micro-particles, or roughness profile. It is believed that laser light excites conduction electrons at the metal surface leading to a surface plasmon resonance and a strong enhancement of the electric field **E**, known as electromagnetic enhancement. However, the application of SPR to DSSC also has a disadvantage, as report by Zhao' *et al.*, the photoresponse of Au/TiO_2 composite in the visible region does not matched with the SPR spectra of Au nanoparticles, moreover, the UV photoresponse was decreased as the Au amount increased[78]. A possible reason is that the Schottky barriers at the TiO_2/Au interface retard the electron transport. Alternatively, Subramanian *et al.* suggested the decreases was due to the photogenerated holes in the TiO_2 inducing the oxidation of the gold deposit at the interface (Reaction 2.12)[66]:

$$TiO_2\ (h) + Au^0 \rightarrow TiO_2 + Au^+ \qquad (2.12)$$

Recently, Tian *et al.* developed a system which obtained complete matching between the plasmon absorption spectra of the metal nanoparticles and the photopotential and photocurrent action spectra obtained without bias voltage[79]. However, the mechanism of this finding is still under discussion.

Recent research on the influence of Au in a DSSC has focused on: the surface states on the TiO_2 film (such as oxygen vacancies)[80]; electron transfer[79]; and plasmon induced energy transfer[81]. A study on the effect of surface oxygen vacancies by Wang *et al.* suggested that the binding of Au to an oxygen vacancy site is substantially stronger than to the stoichiometric surface[80]. These authors also noticed that the re-structuring

of the TiO_2 surface after doping or composite formation with metal nanoparticles may lead to an activity loss of metal nanoparticles, which is indeed a drawback found with oxide supported metal catalysts[82]. He *et al.* also found that metal particles disrupted the crystal structure of TiO_2 and this could be the explanation for the decreased photoresponse of Au/TiO_2 composite in the UV region[82]. With respect to research on electron transport, in terms of trapping/detrapping mechanism, the photo-generated electron can more easily flow through surface defects toward the back contact electrode rather than via the bulk, because the trap/detrapping transfer mechanism and diffusion can be more effectively operated at the surface[83]. Among defect trap sites, the TiO_2 surface Ti^{3+} site is thought to play an important injected electron-transfer role. However, according to mechanism of the dye-sensitization, the dye mostly attaches on the TiO_2 surface at Ti^{4+} sites[2]. An increase of Ti^{3+} at the surface of TiO_2 film could decrease the chemisorptions of dye. These conflicts in the system may contribute to the low photon-electron conversion efficiencies determined to date for Au modified DSSC.

2.6 Summary

Low cost is a very important advantage of dye-sensitized solar cells compared to the widely used Si-solar cells. However, the best TiO_2 dye sensitized solar cell efficiency is only of the order of 10%, as obtained by Grätzel *et al.*[1]. The photo-generated charge recombination is an important reason for low photon-electron conversion efficiency. In order to reduce the loss by this recombination, most efforts have been directed at modification of the TiO_2 film. Noble metals, such as Au nanoparticle composites are one of these modifications. Although this modification successfully improves photocatalysis of TiO_2 film, the performance in DSSC to date was disappointing.

However, it is not impossible to change this situation. In terms of the performance of ultra-thin gold film in the cell studied by MacFarland and Tang, Au benefits the electron-hole separation by the Schottky barrier ballistically transporting the electron to TiO_2 film and allows fast recovery dye. Also, in terms of the performance of Au nanoparticles in the enhancement of dye-sensitization, an optimize particle size could benefit to the conversion efficiency. From previous work on nanosize porous TiO_2 films and ultra-thin Au films on compact TiO_2, it appears that the Au could be beneficial the photon-electron conversion efficiency. However, to design high photo-electron conversion efficiency DSSC, it is necessary to understand the reason of depressed performance of the Au/TiO_2 composite formed to date.

From this review of the previous works, it was decided that research on the influence of Au nanoparticles in this study should focused on:

1. How and Why the Au nanoparticles decreased the TiO_2 photocurrent in the UV region, but increased it in the visible region? (i.e. the influence of Au particle size, crystal structure and surface states on the photocurrent.) .
2. Why the performances of Au nanoparticles in the visible region do not match with SPR spectra?
3. How to improve the performance of Au nanoparticles in the photocurrent spectrum?

Attempts to answer these questions initiated the experimental plan shown schematically in Figure2-9, which formed the experimental part of this thesis.

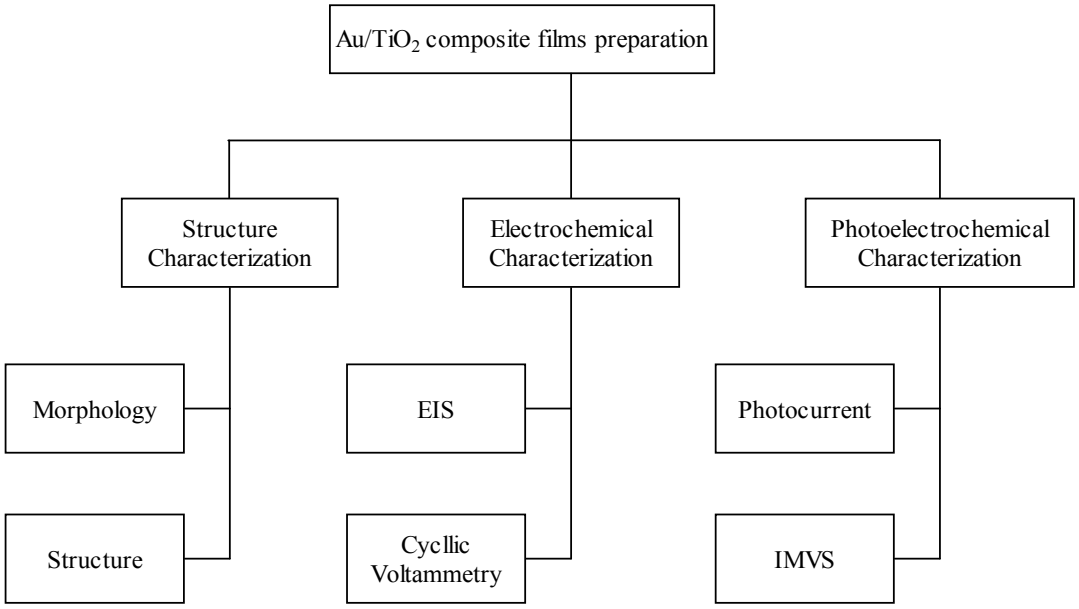

Figure 2-9 Illustration of the experimental procedures used in this study. EIS: Electrochemistry Impedance Spectroscopy; EC-STM: electrochemistry Scan Tunneling Spectroscopy; IMVS: Intensity Modulated Photovoltage Spectroscopy.

Reference

(1) O'Regan, B.; Grätzel, M. *Nature* **1991**, *353*, 737-740.

(2) Grätzel, M. *Inorg. Chem.* **2005**, *44*, 6841-6851.

(3) Kalyanasundaram, K.; Grätzel, M. *Coord. Chem. Rev.* **1998**, *177*, 347-414.

(4) Pichot, F.; Gregg, B. A. *J. Phys. Chem. B* **2000**, *104*, 6-10.

(5) Agrell, H. G.; Boschloo, G.; Hagfeldt, A. *J. Phys. Chem.B* **2004**, *108*, 12388-12396.

(6) Montanari, I.; Nelson, J.; Durrant, J. R. *J. Phys. Chem. B* **2002**, *106*, 12203-12210.

(7) Nonomura, K. Ph.D Dissertation, Justus-Liebig University, **2006**.

(8) Gregg, B. A.; Pichot, F.; Ferrere, S.; Fields, C. L. *J. Phys. Chem. B* **2001**, *105*, 1422-1429.

(9) Mora-Sero, I.; Dittrich, T.; Belaidi, A.; Garcia-Belmonte, G.; Bisquert, J. *J. Phys. Chem. B* **2005**, *109*, 14932-14938.

(10) Cameron, P. J.; Peter, L. M. *J. Phys. Chem. B* **2005**, *109*, 7392-7398.

(11) Cameron, P. J.; Peter, L. M.; Hore, S. *J. Phys. Chem. B* **2005**, *109*, 930-936.

(12) Cameron, P. J.; Peter, L. M. *J. Phys. Chem. B* **2003**, *107*, 14394-14400.

(13) Liska, P.; Vlachopoulos, N.; Nazeeruddin, M. K.; Comte, P.; Grätzel, M. *J. Am. Chem. Soc.* **1988**, *110*, 3686-3687.

(14) Diamant, Y.; Chen, S. G.; Melamed, O.; Zaban, A. *J. Phys. Chem. B* **2003**, *107*, 1977-1981.

(15) Wang, Z. S.; Huang, C.-H.; Huang, Y.-Y.; Hou, Y.-J.; Xie, P.-H.; Zhang, B.-W.; Cheng, H.-M. *Chem. Mater.* **2001**, *13*, 678-682.

(16) Chen, S. G.; Chappel, S.; Diamant, Y.; Zaban, A. *Chem. Mater.* **2001**, *13*, 4629-4634.

(17) McFarland, E. W.; Tang, J. *Nature* **2003**, *421*, 616-618.

(18) Tennakone, K.; Kumara, G. R. R. A.; Kumarasinhe, A. R.; Wijayantha, K. G. U.; Sirimanne, P. M. *Semicond. Sci. Technol.* **1995**, *10*, 1689-1693.

(19) O'Regan, B.; Schwarz, D. T. *Chem. Mater.* **1998**, *10*, 1501-1509.

(20) Bach, U.; Lupo, D.; Comte, P.; Moser, J. E.; Weissortel, F.; Salbeck, J.; Spreitzer, H.; Grätzel, M. *Nature* **1998**, *395*, 583-585.

(21) Parker, G. J. *Introductory Semiconductor Device Physics*; Prentic Hall International (UK) Limited: Hemel Hempstead, **1994**.

(22) Milgrom, L. R. *The Colors of Life: an Introduction to the Chemistry of Porphyrins and Related Compounds*; Oxford University Press: New York, **1997**.

(23) Longo, C.; De Paoli, M. A. *J. Braz. Chem. Soc.* **2003**, *14*, 889-901.

(24) Tachibana, Y.; Moser, J. E.; Grätzel, M.; Klug, D. R.; Durrant, J. R. *J. Phys. Chem.* **1996**, *100*, 20056-20062.

(25) Nazeeruddin, M. K.; Pechy, P.; Renouard, T.; Zakeeruddin, S. M.; Humphry-Baker, R.; Comte, P.; Liska, P.; Cevey, L.; Costa, E.; Shklover, V.; Spiccia, L.; Deacon, G. B.; Bignozzi, C. A.; Grätzel, M. *J. Am. Chem. Soc.* **2001**, *123*, 1613-1624.

(26) Wang, Z.-S.; Kawauchi, H.; Kashima, T.; Arakawa, H. *Coordination Chemistry Reviews Michael Grätzel Festschrift, a tribute for his 60th Birthday, Dye Sensitized Solar Cells* **2004**, *248*, 1381-1389.

(27) Renouard, T.; Fallahpour, R.-A.; Nazeeruddin, M. K.; Humphry-Baker, R.; Gorelsky, S. I.; Lever, A. B. P.; Grätzel, M. *Inorg. Chem.* **2002**, *41*, 367-378.

(28) Ito, S.; Liska, P.; Comte, P.; Charvet, R.; Bach, U.; Schmidt-Mende, L.; Zakeeruddin, S. M.; Kay, A.; Nazeeruddin, M. K.; Grätzel, M. *Chem. Commun.* **2005**, 4351-4353.

(29) Linsebigler, A. L.; Lu, G.; Yates, J. T. *Chem. Rev.* **1995**, *95*, 735-758.

(30) Nelson, J. *The physics of solar cells*; Imperial college Press: London, **2003**.

(31) Peter, L. M.; Wijayantha, K. G. U. *Electrochem. Commun.* **1999**, *1*, 576-580.

(32) Bisquert, J.; Cahen, D.; Hodes, G.; Ruhle, S.; Zaban, A. *J. Phys. Chem. B* **2004**, *108*, 8106-8118.

(33) Solbrand, A.; Henningsson, A.; Sodergren, S.; Lindstrom, H.; Hagfeldt, A.; Lindquist, S. E. *J. Phys. Chem. B* **1999**, *103*, 1078-1083.

(34) Zaban, A.; Meier, A.; Gregg, B. A. *J. Phys. Chem. B* **1997**, *101*, 7985-7990.

(35) Dloczik, L.; Ileperuma, O.; Lauermann, I.; Peter, L. M.; Ponomarev, E. A.; Redmond, G.; Shaw, N. J.; Uhlendorf, I. *J. Phys. Chem. B* **1997**, *101*, 10281-10289.

(36) Nelson, J. *Phys. Rev. B* **1999**, *59*, 15374 LP - 15380.

(37) Boschloo, G.; Hagfeldt, A. *J. Phys. Chem. B* **2005**, *109*, 12093-12098.

(38) Thompson, T. L.; Yates, J. T. *J. Phys. Chem. B* **2005**, *109*, 18230-18236.

(39) Bisquert, J. *J. Phys. Chem. B* **2002**, *106*, 325-333.

(40) Bahadur, L.; Srivastava, P. *J. Electrochem. Soc.* **2004**, *151*, G740-G745.

(41) Zeng, L. Y.; Dai, S. Y.; Wang, K. J.; Shi, C. W.; Kong, F. T.; Hu, L. H.; Pan, X. *Acta Phys. Sin.* **2005**, *54*, 53-57.

(42) Guo, P.; Aegerter, M. A. *Thin Solid Films* **1999**, *351*, 290-294.

(43) Bergeron, B. V.; Marton, A.; Oskam, G.; Meyer, G. J. *J. Phys. Chem. B* **2005**, *109*, 937-943.

(44) Dinh, N. N.; Bernard, M. C.; Hugot-Le Gof, A.; Stergiopoulos, T.; Falaras, P. *C. R. Chim.* **2006**, *9*, 676-683.

(45) Meulenkamp, E. A. *J. Phys. Chem. B* **1999**, *103*, 7831-7838.

(46) Burdett, J. K. *Inorg. Chem.* **1985**, *24*, 2244-2253.

(47) Burdett, J. K.; Hughbanks, T.; Miller, G. J.; Richardson, J. W.; Smith, J. V. *J. Am. Chem. Soc.* **1987**, *109*, 3639-3646.

(48) Fahmi, A.; Minot, C.; Silvi, B.; Causá M. *Phys. Rev. B* **1993**, *47,* 11717 LP - 11724.

(49) Poirier, G. E.; Hance, B. K.; White, J. M. *J. Phys. Chem.* **1993**, *97,* 5965-5972.

(50) Poirier, G. E.; Hance, B. K.; White, J. M. *J. Phys. Chem.* **1993**, *97,* 6500-6503.

(51) Park, N. G.; van de Lagemaat, J.; Frank, A. J. *J. Phys. Chem. B* **2000**, *104,* 8989-8994.

(52) Tan, B.; Wu, Y. *J. Phys. Chem. B* **2006**, *110,* 15932-15938.

(53) Law, M.; Greene, L. E.; Johnson, J. C.; Saykally, R.; Yang, P. *Nat. Mater.* **2005**, *4,* 455-459.

(54) Ohsaki, Y.; Masaki, N.; Kitamura, T.; Wada, Y.; Okamoto, T.; Sekino, T.; Niihara, K.; Yanagida, S. *Phys. Chem. Chem. Phys.* **2005**, *7,* 4157-4163.

(55) Karthikeyan, C. S.; Thelakkat, M.; Willert-Porada, M. T*hin Solid Films* **2006**, *511,* 187-194.

(56) Sinke, W. C.; Wienk, M. M. *Nature* **1998**, *395,* 544-545.

(57) Nusbaumer, H.; Moser, J. E.; Zakeeruddin, S. M.; Nazeeruddin, M. K.; Grätzel, M. *J. Phys. Chem. B* **2001**, *105,* 10461-10464.

(58) Kruger, J.; Plass, R.; Grätzel, M.; Cameron, P. J.; Peter, L. M. *J. Phys. Chem. B* **2003**, *107,* 7536-7539.

(59) Hart, J. N.; Menzies, D.; Cheng, Y.-B.; Simon, G. P.; Spiccia, L. *C. R. Chim.* **2006**, *9,* 622-626.

(60) Song, M. Y.; Kim, D. K.; Jo, S. M.; Kim, D. Y. *Synth. Met.* **2005**, *155,* 635-638.

(61) Grätzel, M. N*ature* **2003**, *421,* 586-587.

(62) Subramanian, V.; Wolf, E.; Kamat, P. V. *J. Phys. Chem. B* **2001**, *105,* 11439-11446.

(63) Sclafani, A.; Mozzanega, M. N.; Pichat, P. *Photochem. Photobiol. A* **1991**, *59,* 181-189.

(64) Palomares, E.; Clifford, J. N.; Haque, S.A.; Lutz, T.; Durrant, J.R. C*hem. Commun.* **2002**, 1464-1465.

(65) Yang, S.; Huang, Y.; Huang, C.; Zhao, X. C*hem. Mater.* **2002**, *14,* 1500-1504.

(66) Subramanian, V.; Wolf, E. E.; Kamat, P. V. L*angmuir* **2003**, *19,* 469-474.

(67) Gopidas, K. R.; Bohorquez, M.; Kamat, P. V. *J. Phys. Chem.* **1990**, *94,* 6435-6440.

(68) Spanhel, L.; Weller, H.; Henglein, A. *J. Am. Chem. Soc.* **1987**, *109,* 6632-6635.

(69) Palomares, E.; Clifford, J. N.; Haque, S. A.; Lutz, T.; Durrant, J. R. *J. Am. Chem. Soc.* **2003**, *125,* 475-482.

(70) Menzies, D. B.; Dai, Q.; Bourgeois, L.; Caruso, R. A.; Cheng, Y. B.; Simon, G. P.; Spiccia, L. N*anotechnology* **2007**, *18,* 125608.

(71) Hart, J. N.; Menzies, D.; Cheng, Y. B.; Simon, G. P.; Spiccia, L. *Sol. Energy Mater. Sol. Cells* **2007***, 91,* 6-16.

(72) Plass, R.; Pelet, S.; Krueger, J.; Grätzel, M.; Bach, U. *J. Phys. Chem. B* **2002**, *106,* 7578-7580.

(73) Kamat, P. V. *Pure Appl. Chem.* **2002**, *74,* 1693-1706.

(74) Koole, R.; Liljeroth, P.; Oosterhout, S.; Vanmaekelbergh, D. *J. Phys. Chem. B* **2005**, *109,* 9205-9208.

(75) Creighton, J. A.; Eadon, D. G. *J. Chem. Soc., Faraday Trans.* **1991**, *87,* 3881-3891.

(76) Ung, T.; Liz-Marzan, L. M.; Mulvaney, P. *J. Phys. Chem. B* **2001**, *105,* 3441-3452.

(77) Fleischmann, M.; Tian, Z. Q.; Li, L. J. *J. Electroanal. Chem.* **1987**, *217,* 397-410.

(78) Zhao, G.; Kozuka, H.; Yoko, T. S*ol. Energy Mater. Sol. Cells* **1997**, *46,* 219-231.

(79) Tian, Y.; Tatsuma, T. *J. Am. Chem. Soc.* **2005**, *127,* 7632-7637.

(80) Wang, Y.; Hwang, G. S. S*urf. Sci.* **2003**, 5*42,* 72-80.

(81) Standridge, S. D.; Schatz, G. C.; Hupp, J. T. 233rd ACS National Meeting, Chicago, IL, United States, **2007**; 862.

(82) He, C.; Yu, Y.; Hu, X.; Larbot, A. *Appl. Surf. Sci.* **2002**, *200,* 239-247.

(83) Ko, K. H.; Lee, Y. C.; Jung, Y. J. *J. Colloid Interface Sci.* **2005**, *283,* 482-487.

Chapter 3 Experimental

In this study, TiO_2 and Au/TiO_2 composite films were prepared by the sol-gel method. Different Au concentrations were used in order to control the Au particle size in the composite films. Investigations were conducted in to the influence of Au particles on the TiO_2 films':

- physical properties, such as it morphology and crystal structure;
- optical properties, including absorption and surface states;
- and electrochemical properties, such as impedance and ability to generate a photocurrent.

The sample preparation and experimental methods are illustrated in the following sections.

3.1 Chemicals and Reagents

The chemicals used in this study included: a) for substrate cleaning; acetone (99.9%, Merck), and methanol (99.9%, Merck). b) for preparation of the sol-gel precursor; Titanium (IV) isopropoxide (>98%, Acros), nitric acid (69.0-70.0%, J.T.Baker), absolute alcohol (>99.8%, Merck) and de-ionized water. c) for preparation of the Au nanocomposite; hydrogen tetrachloroaurate (III) trihydrate ($HAuCl_4 \cdot 3H_2O$, 99.9%, Aldrich). d) for preparing the electrolyte solution used in; (i) photoresponse and electrochemical experiments 0.5M $NaSO_4$ aqueous solution (anhydrous sodium sulfate >99%, Fluka) in de-ionized water) and (ii) Intensity Modulated Photovoltage Spectroscopy 0.5M LiI/0.05M I_2 in acetonitrile (LiI, 99%, Fluka; I_2 , 99.5% Fluka)[1];. e) for dye-sensitization, Ruthium 505 (Solaronix) [cis-bis(cyanido) bis(2,2'-bipyridyl-

4,4' dicarboxylato) ruthenium (II) （$RuL_2(CN)_2$ (L = 2,2'-bipyridyl-4,4'-dicarboxylic acid)].

The substrates used in this study were either fused quartz glass (cut into 1×1cm squares) or ITO conductive glass (10 ohm/cm^2, Sanyo, cut into1×3cm rectangles) clean ultrasonically in acetone for 30 minutes, followed by methanol for 30 minutes and finally distilled water for 30 minutes. Lastly, the substrates were blown dried under nitrogen. Quartz substrates were used to deposited composite films for UV/visible absorption characterization investigations. ITO conductive substrates were used to prepare samples for measuring photoresponse and electrochemical properties. For the photoresponse and electrochemical experiments electrical connections were made to the samples by copper wires attached via silver epoxy resin (RS Company).

3.2 Sample preparation

The films were synthesised by the sol-gel method which included preparing precursor solutions, gelling the solution, depositing the film and sintering.[2, 3] A flowchart of the film sample preparation procedure is illustrated in Figure 3-1.

The ratio of components in the precursor solutions used for the present work followed those proposed by Takahashi' *et al*.[4], i.e. $Ti(OC_3H_7)4^i:C_2H_5OH:H_2O:HNO_3$ = 1:20:1: 0.2. The precursor solution was mixed in a dry glove box in order to delay the hydrolysis process, after that the precursor solution was put into a closed bottle and left overnight to obtain a stable solution. To prepare the range of Au/TiO_2 films, different quantities of hydrogen tetrachloroaurate (III) trihydrate were introduced into

the stable precursor solution. The molar ratio of Au:TiO_2 was varied as 1%, 5%, 10%, 25%, and 50%. The films were deposited by dropping precursor solution onto the substrates, followed by spin-coating at 1500 rpm for 30s and then continuously at 3000 rpm for a further 60s. For structural characterization studies, the films were deposited on fused quartz glass, whereas ITO glass was used for electrochemical and photoelectrochemical investigations. After film deposition, samples were pre-treatment in an 80^{o}C oven and on a 200 ^{o}C hot-plate to evaporate the leftover solvent in the film. Finally, the film samples were sintered for 30 minutes in a 500 ^{o}C oven with the using of heating and cooling rates of 10 ^{o}C /min.

In this study, all of the films were deposited by spin-coating onto a smooth compact structure, rather the than porous structure synthesized by doctor blade technique used in previous literature studies[5]. The reason for using smooth surfaces was to reduce the influence of structure on the properties of films, since the aim of this research was to focus on the effects of the Au nanoparticles. For example, the porous structure of a film can affect its density of surface states; the electron transfer kinetics at its interface as well as the electron transport rates within the film (see Chapter 2, Section 2.2).

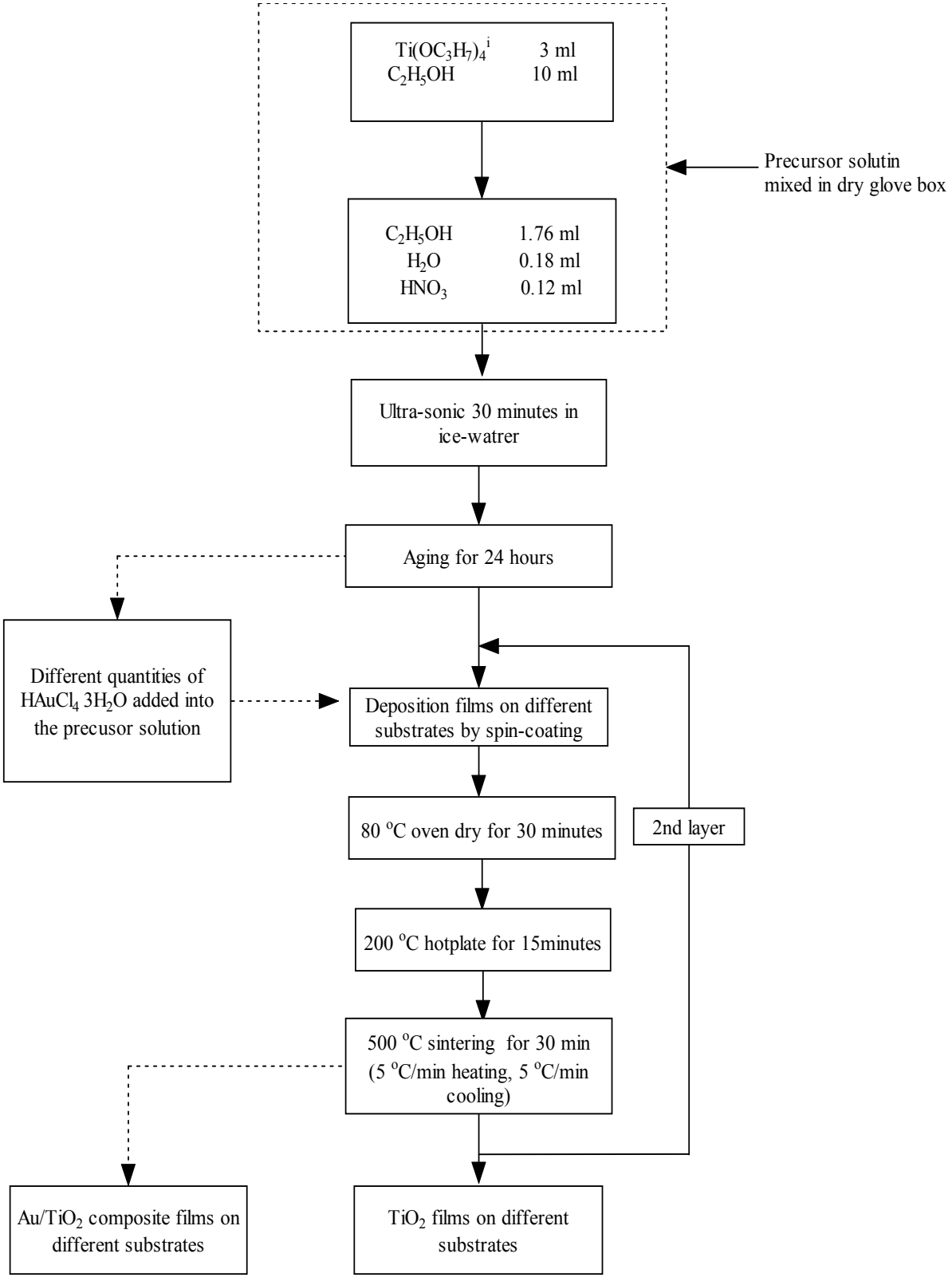

Figure 3-1 Flowchart of sample preparation procedure

3.3 Dye-sensitization

For investigations into the influence of Au particles on the dye-sensitization composite films deposited on ITO glass were immersed into 0.001M Ruthenium 505 (the chemical structure of Ruthenium 505 is shown in Figure 3-2) absolute alcohol solutions for overnight. After immersion, films were flushed with absolute alcohol until the color of dye faded. Finally, samples were blown dry by N_2 gas.

Although a number of dye sensitizers have been used in DSSCs, some of which yield higher conversion efficiencies then Ruthenium 505, this dye was chosen because of its stability, low cost and ease of availability. Furthermore, the data presented in this thesis was interpreted on a comparison basis, e.g. performance of low Au level to Au high level, rather than absolute conversion efficiencies, which did not warrant the use of a more expensive dye.

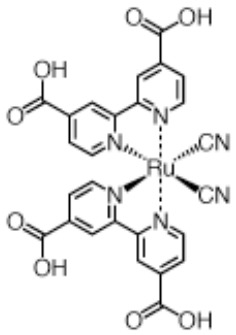

Figure 3-2 Chemical structure of Ruthenium 505

3.4 Characterization Techniques

3.4.1 Film Morphology

Since the films were deposited on isolated glass or quartz glass substrates, their morphology could be observed by Atomic Force Microscopy (AFM). Although the basic principle of AFM[6] is to use the height profile of the particles to obtain

morphology information (illustrated in Figure 3-3), film topography also reflects the distribution of particles and thus illustrated the influence of annealing on the smoothness of the films.

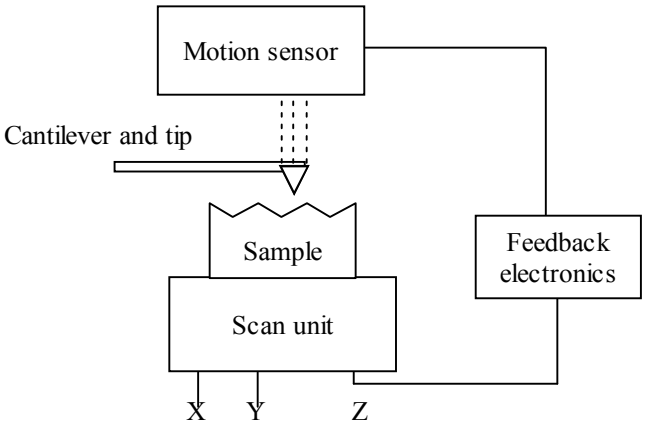

Figure 3-3 AFM working diagram. Adapted from reference [6].

One of the most important factors influencing the resolution that may be achieved with an AFM is the sharpness of the scanning tip. The best tips may have a radius of curvature of less than 5nm. For measuring particle size, the main influence of the tip size on the observed morphology is broadening. This arises when the radius of curvature of the tip is comparable with, or greater than, the size of the feature trying to be imaged. In this study, this problem did not exist, since the sizes of both the Au and TiO_2 particles used were larger than 5 nm; confirmed by TEM measurements. The particle size data obtained from the AFM images were also compared with measurement made by XRD and TEM analysis.

3.4.2 Crystallization Structure of films

X-ray Diffraction (XRD) [7]

In this study, the structure of the films and the average size of the Au nanoparticles were probed with a Brucker D8 advanced thin film XRD. Samples for this set of investigations were deposited on the quartz glass. The crystalline structures of composite films were determined by employing a collimated beam of X-rays from Cu Kα1 radiation with wavelength λ= 1.54056 Å to direct on a specimen such that it is diffracted by the crystalline phases in the specimen according to Bragg's law

$$n\lambda = 2d \sin\theta \qquad (3.1)$$

where n is the number of crystal plane, λ is the wavelength of X-ray radiation, *d* is the spacing between atomic planes and θ is the angle of incidence.

In order to get the crystal structure information from the films the diffractometer was operated with the in detector scan mode. The incoming X-ray irradiation was fixed at a glancing angle 1.5^{o}, and the detector scanned from $20\sim60^{o}$, using a step size of 0.02^{o} at 2 seconds per step. To get sufficient signal intensity the working voltage and current of the X-ray generator were set at 45 k eV and 40 mA respectively. The crystalline structure was identified by comparing the XRD diffraction pattern with standard PDF cards (Joint Committee on Powder Diffraction Standards; JCPDS).

XRD diffraction patterns not only provide information on the possible crystalline structure, but also on crystal size, by evaluating from the full width of half maximum (FWHM) of the diffraction peak and applying Scherrer's equation.[7] However, XRD still has a limitations as it only provides information on the average long-range order

of crystalline materials.

Transmission Electron Microscopy (TEM) [8]

TEM can offer two methods of specimen observation, diffraction mode and image mode. In diffraction mode, an electron diffraction pattern that originates from the sample area illuminated by the electron beam is obtained on the fluorescent screen. The diffraction pattern is equivalent to an X-ray diffraction pattern: a single crystal will produce a spot pattern on the screen, a polycrystal will produce a ring pattern (assuming the illuminated area includes a sufficient quantity of crystallites) and a glassy or amorphous material will produce a series of diffuse halos. The image mode produces an image of the illuminated sample area. The image can contain contrast brought about by several mechanisms: mass contrast, due to spatial separations between distinct atomic constituents; thickness contrast due to non-uniformity in sample thickness; diffraction contrast, which in the case of crystalline materials results from scattering of the incident electron wave by structural defects; and phase contrast.

TEM observations are carried out on an extra thin specimen (≤200 nm thick) that is bombarded with a highly-focused, mono-energetic beam of electrons in a high vacuum. The beam is of sufficient energy to propagate all the way through the specimen. A series of electromagnetic lenses then magnifies this transmitted electron beam. Diffracted electrons can be observed in the form of a diffraction pattern beneath the specimen. This information is used to determine the atomic structure of the material in the sample. Transmitted electrons form images from small regions of sample that contain contrast, due to several scattering mechanisms associated with interactions between electrons and the atomic constituents of the sample. Analysis of transmitted

electron images yields information about both atomic structure and defects present in the material. In comparison with XRD, TEM can directly supply both information on the crystalline structure and the image of the particles, such as the structure, shape and arrangement of the particles, as well as their relationship to each other on the atomic scale.

Regarding the requirement of an extra thin specimen for TEM observation, the sample preparation is very important. Generally, sample preparation for TEM is to alleviate sample thickness to 200 μm by sanding on the sandpaper, and then dimpling to 20 μm by dimple machine, finally ion milling to 20 nm by ion miller. In this study, two methods were used o obtain thin film samples, as illustrated in Figure 3-4. The first used to make longitudinal observations is to glue the film onto a copper grid, then to sand down the sample from the substrate side until 200 μm, followed by dimpling and ion milling(Figure 3-4 a). The second method used to make observations of cross sections involves gluing two films face to face, cutting to expose a cross section and gluing it to a copper grid. This is again followed by sanding, dimpling and ion milling (Figure 3-4 b).

In this study, the TEM observations were carried out on a JOEL-CX300 with an accelerating potential of 300 kV. Bright field images and selected-area electron diffraction patterns were taken to examine the crystal structure and identify the shape and size of the Au nanoparticles.

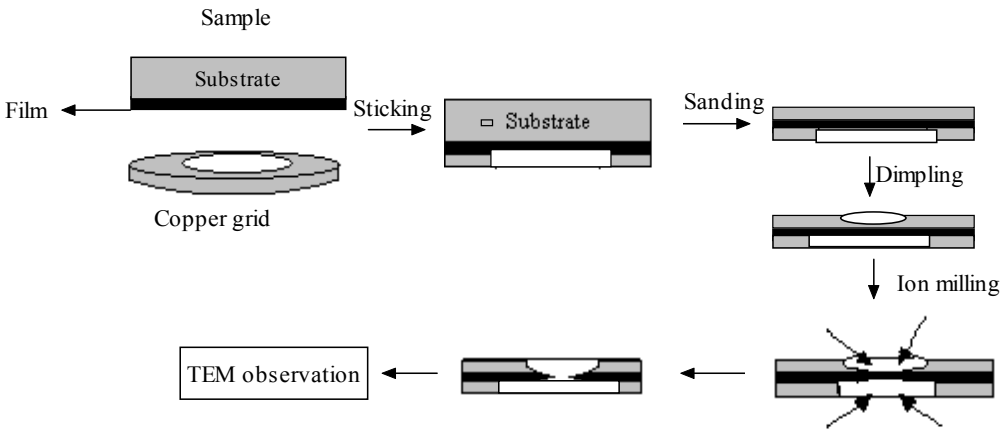

a) Sample preparation for observing longitudinal structure

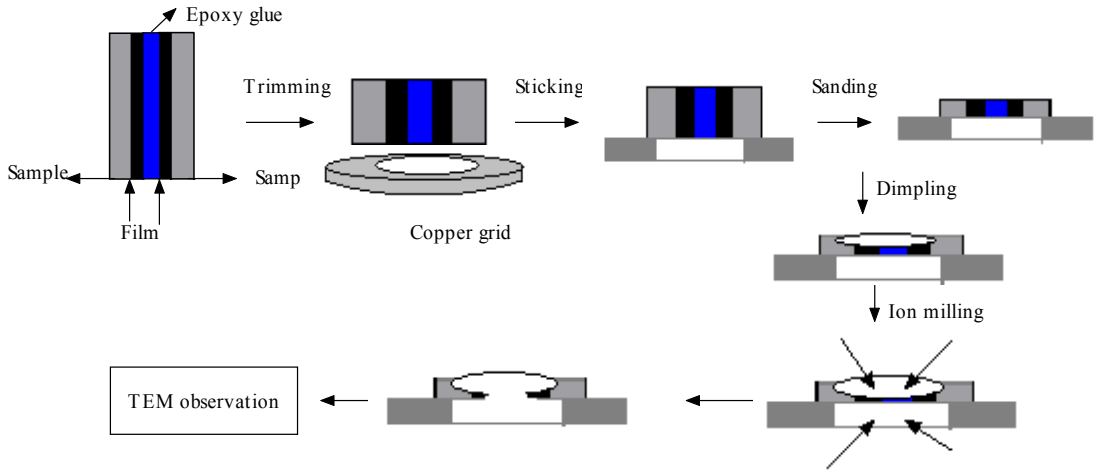

b) Sample preparation for cross-sectional structure

Figure 3-4 Sample preparation for TEM observation.

Raman Scattering [6]

Raman scattering was also employed to study the crystalline structure of the composite films. Compared with X-ray diffraction, Raman scattering acts as a local probe and is very sensitive to the crystallinity and microstructure of materials. The mechanism by which Raman scattering gets crystal structure information is by determining changes in photon energies after collisions between the incident photons and the material being investigated.

The collision between a photon of energy hv_0 and a molecule results in two different types of light scattering (Figure 3-5). The first, known as Rayleigh scattering, is an elastic collision between the incident photon and the molecule; since the photon neither loses nor gains energy (its energy remains equal to hv_0). For molecular systems, this is by far the strongest light scattering phenomenon. The second type of collision is Raman scattering. Raman scattering is an inelastic collision where the photon either gains energy from, or loses energy to, the molecule. The energy of the scattered light is $hv_{(0+1)}$ or $hv_{(0-1)}$. The energy gained or lost, hv_1 , corresponds to a vibrational energy transition within the molecule. Thus the energy of scattered light depends on the frequency of incident light, but the shift hv_1 from the Rayleigh scattering line is a constant corresponding to the vibrational energy. The Raman lines occurring at frequency $\nu_{(0-1)}$ are referred to as Stokes lines and the lines occurring at frequency $\nu_{(0+1)}$ are referred to as anti-Stokes lines. The Stokes lines are of higher intensity than the anti-Stokes lines due to the Boltzmann distribution, i.e, due to the higher population of molecules in the ground vibrational state (0) as compared to those in the excited state (1) at room temperature. Therefore, usually only the Stokes lines are utilized in the study of Raman scattering. Raman scattering within solids is an interaction between a photon (generally in the visible range) and the electronic cloud of the molecules or crystal. The difference in energy between the incoming and the outgoing photons corresponds to the energy of bond or lattice vibrations (phonons for a crystal) of the studied material.

Raman scattering obtains the conservations of energy and momentum, so because the momentum of the light is much smaller than those of the phonon, the vibrations observed by Raman spectroscopy are in the center of the Brillioum zone. Raman

scattering as a local probe is very sensitive to the crystallinity and microstructure of materials. Raman lines become weak and broad when the samples have local lattice imperfections[9].

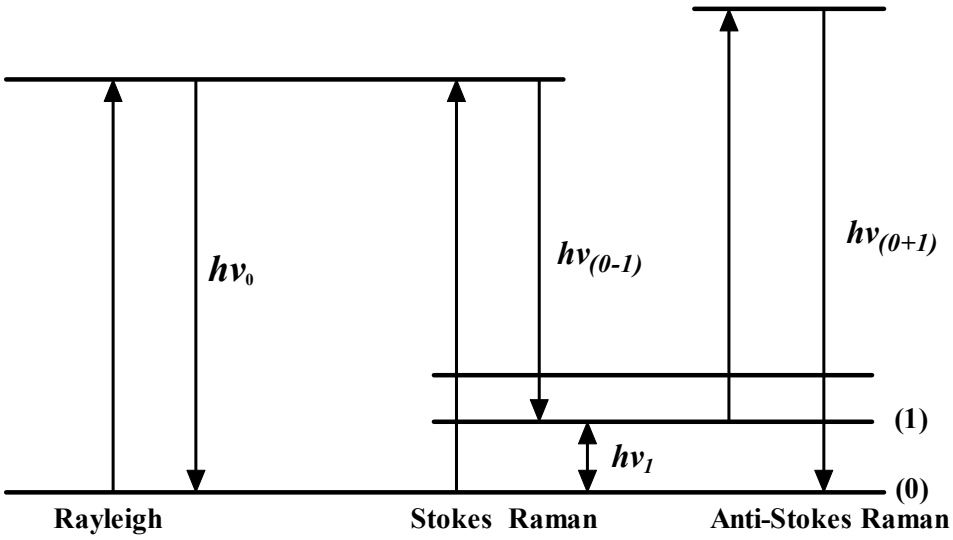

Figure 3-5 Energy level diagram for Raman scattering. monochromatic light of frequency ν_0 is scattered by the sample, either without losing energy (Rayleigh scattering) or inelasctically, in which a vibration is excited (Stokes band) or a vibrationally excited mode in the sample is de-excited (anti-Stokes band) adapted from reference [6].

In the present work the Raman scattering spectra were collected over the range 100 to 1000 cm^{-1} on a LabRam HR high resolution microRaman microscope (JOBIN YVON) equipped with a 40 mW Ar ion laser (green line at 514.53 nm) and the iris was set at 100 μm with 100% light pass.

3.4.3 Analysis of surface states

X-ray Photoelectron Spectroscopy and Ultraviolet Photoelectron Spectroscopy (XPS/UPS) [10]

Photoelectron spectroscopy (PES) is based on the photoelectric effect. Photons from a suitable source (an X-ray anode in the case of XPS, an ultraviolet lamp for UPS) impinge on the sample (Figure 3-6). Photoionization occurs according to

$$A + h\nu \rightarrow A^+ + e^- \qquad (3.2)$$

where the electron, e^-, is expelled from the sample with a certain amount of kinetic energy E_k. Depending on the energy of the incoming photon $h\nu$, emission of photoelectrons will take place from the valence band only (UPS) or from both valence and core levels (XPS). An electronic level of any atom present in the portion of sample probed by the technique will thus contribute to the flux of photoelectrons expelled, provided that the photoenergy, $h\nu$, is sufficient to eject the electron: (i) from the level considered and (ii) through the atom's outer electrons. The first condition gives rise to the basic equation of photoelectron spectroscopy (3.3)

$$E_k = h\nu - E_b \qquad (3.3)$$

where E_b is the binding energy of the electronic level considered. The second condition implies that any element, except hydrogen and helium (that do not have core levels), is detectable by means of its core levels (XPS) and that any valence band is visible both by XPS and UPS.

The valence state of the components and electronic state of the surface region of a sample can be studied by photoelectron spectroscopy which is based upon a single photon in/single electron out process.

In XPS, the photon is absorbed by an atom in a molecule or solid, leading to ionization and the emission of a core (inner shell) electron. By contrast, in UPS the photon interacts with the valence levels of the molecule or solid, leading to ionization by removal of one of these valence electrons. The kinetic energy distribution of the emitted photoelectrons (i.e. the number of emitted photoelectrons as a function of their kinetic energy) can be measured using any appropriate electron energy analyzer and a photoelectron spectrum can thus be recorded. To reach the required mean path for the

photoelectrons and to avoid surface-contamination (with adsorbed molecules like H_2O or O_2) UHV (Ultra-High-Vacuum) is needed for PES.

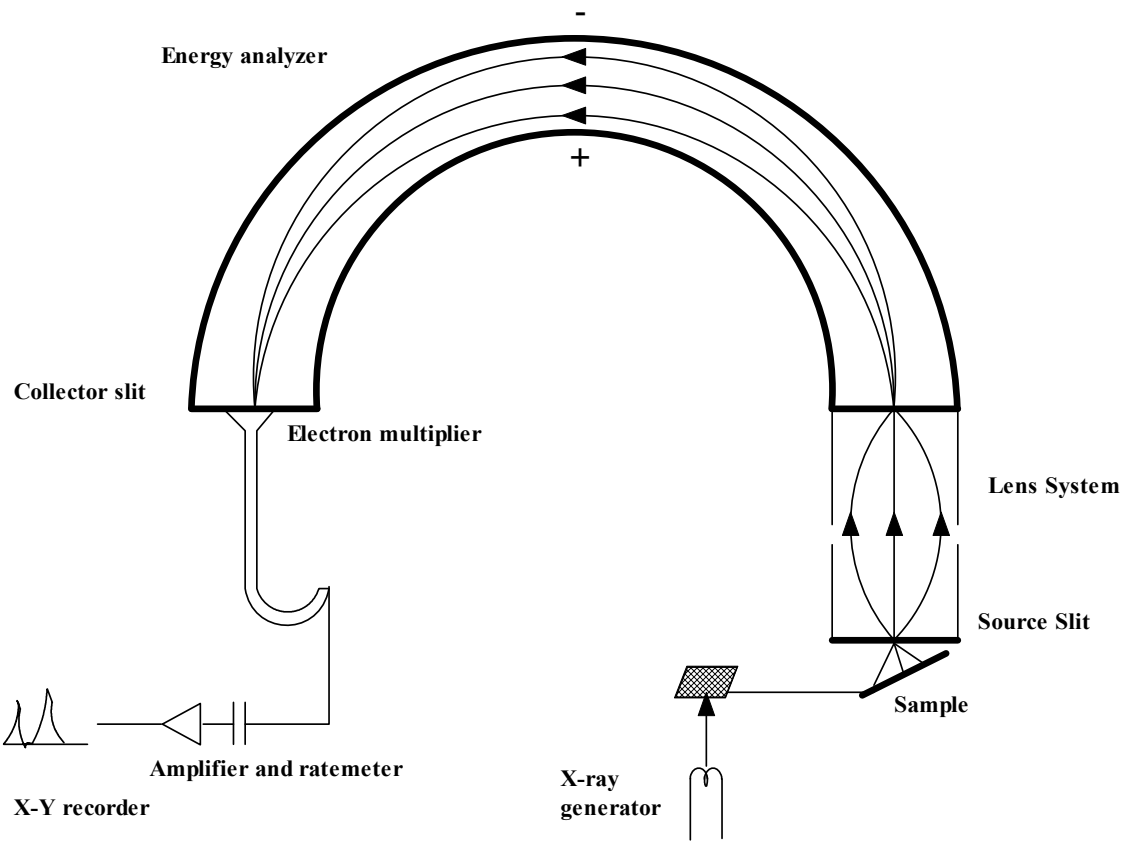

Figure 3- 6 Schematic representation of an X-ray spectrometer. Adapted from reference [9].

For the XPS measurements in the present work, the soft X-ray source used was Mg K radiation. The analysis was carried out by *XPS Speak Fit* software, FWHM (Full wave at half maximum) was fixed at 1; the percentage of Lorentzain-Gaussian peak was fixed as 80%.

In UPS measurements, the source of radiation was a He-discharge lamp emitting He I radiation of energy 21.2 eV. Analysis of the UPS spectra was preformed by reference to Figure 3-7. The electron affinity, E_A, was evaluated by the following procedure

throughout this study: the energy level of valance band maximum (VBM) E_{VBM}, was calculated by subtracting the excitation energy of He I (21.2eV) from the high-energy cutoff $E_{cutoff.}$ The energy amount by which the conduction band minimum (CBM) E_{CBM} is above the E_{VBM} yields the optical band gap of the material[11]. The low-energy cut-off in the spectrum corresponds to electrons leaving the surface with zero kinetic energy. The spectra were collected by the energy-dependent transmission of an electrostatic analyzer[12].

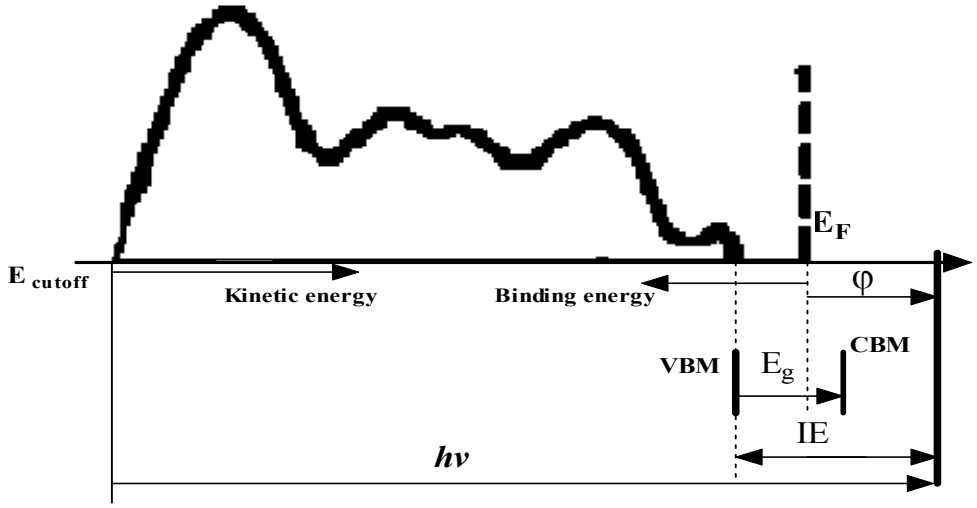

Figure 3-7 Schematic diagram for the identity spectra of UPS and identified the energy level. Adapted from reference [10]. (E_F: Fermi level, VBM: valence band maximum, E_g: band gap, CBM: conduction band minimum, IE: ionized energy, $E_{cut-off}$: high-energy cut off, φ: work function)

Photoluminescence [8]

In photoluminescence one measures physical and chemical properties of materials by using photons to induce excited electronic states in the materials system and analyzing the optical emission as these states relax (Figure 3-8). Typically, light is directed onto the sample for excitation and the emitted luminescence is collected by a lens and passed through an optical spectrometer onto a photodetector[8].

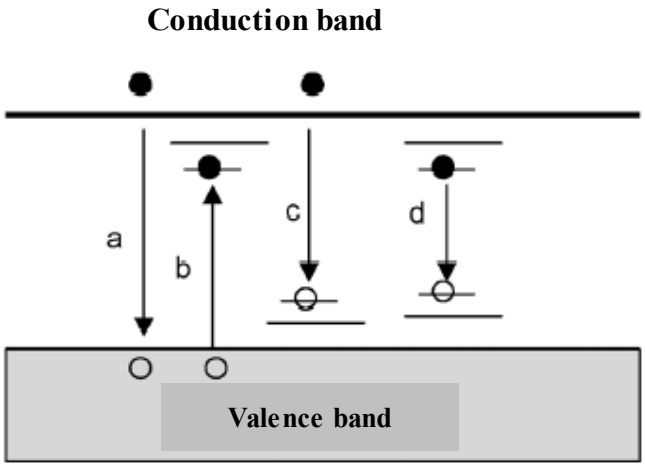

Figure 3- 8 Possible recombination processes leading to photoluminescence. a) electron hole pair recombination; b) inter-bandgap trapped electron recombine with hole; c) electron recombine with inter band gap hole; d) exciton recombination. Adapted from reference [8].

Photoluminescence (PL) spectroscopy is an extremely useful tool for obtaining information about the electronic, optic and photo-electric properties of materials, since it depends on electronic excitations and therefore is an important complement to spectroscopes that depends on lattice excitations (e.g. Raman). It has previously be postulated that the PL spectra of anatase TiO_2 can be attributed to three kinds of physical origins; self-trapped excitons, surface states and oxygen vacancies[13,14].

In this study, the PL spectra were obtained on a LabRam HR high resolution Raman microscope (JOBIN YVON) equipped with a 30 mW HeCd UV laser (325.09nm) over the ranges 330-649nm and 651~700nm; data cannot be collected at 650nm as this is 2x the wavelength of the excitation source. The iris was set at 500μm with 100% light pass.

3.4.4 Measurement of Optical Properties

Optical absorption spectroscopy is the most commonly applied technique for exploring

the quantum effects in semiconductor nanoparticles. Optical absorption follows the Beer-Lambert Law (Figure 3-9):[6,8]

$$I = I_0 \, Exp\,[-\alpha(\lambda)d] \qquad (3.4)$$

From UV/visible absorption spectra one can observe the development of discrete features and, if applicable, the enlargement of the energy gap in semiconductor quantum dots. In this work the optical absorption spectra were measured on a UV-vis spectrophotometer (UV1601, Shimadzu) over the range of 200 to 800 nm at room temperature. The spectral data were obtained with an accuracy of less than ±2 nm. Blank substrates were employed as references.

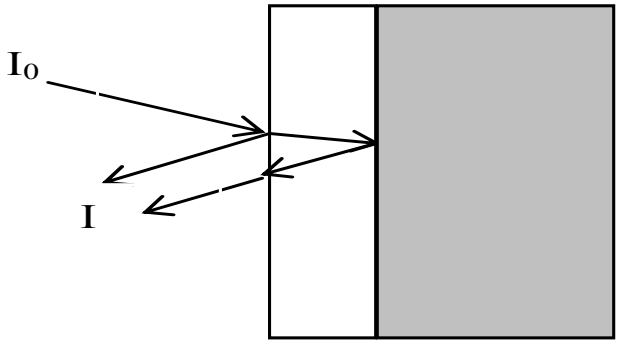

Figure 3-9 Schematic illustration of how back reflections can double the path length of thin films.

From an absorption spectrum the energy band gap of a semiconductor can be obtained, due to its band transition under irradiation. The band gap energy E_g of films was calculated by an established method, which assumes a transition from the valence band to the conduction band when incident photon with energy *hv* is absorbed. The variation of absorption coefficient, α, with photon energy is given by[24]:

$$\left(\alpha \cdot E_{photo}\right)^n = C \cdot \left(E_{photo} - E_g\right) \qquad (3.5)$$

$$\alpha = \left(A \cdot \ln 10\right) / d \qquad (3.6)$$

$$E_{photo} = h\nu = (1240/\lambda)\ eV \qquad (3.7)$$

where C is a constant, A is the measured absorbance d is the thickness of the films and n takes following values depending on the type of transition involved:

i) n = 1/2 → direct allowed transition;
ii) n = 3/2 → direct forbidden transition;
iii) n = 2 → indirect allowed transition;
iv) n = 1/3 → indirect forbidden transition.

TiO_2 is a direct band gap semiconductor, so according the equation 3.5 extrapolation of a plot of $(\alpha h\nu)^{1/2}$ *vs* E_{photo} to $(\alpha h\nu)^{1/2} = 0$ yield an absorption energy that corresponds to a band gap E_g. This is procedure is schematically in Figure 3-10 and is commonly referred to as a Tauc plot.

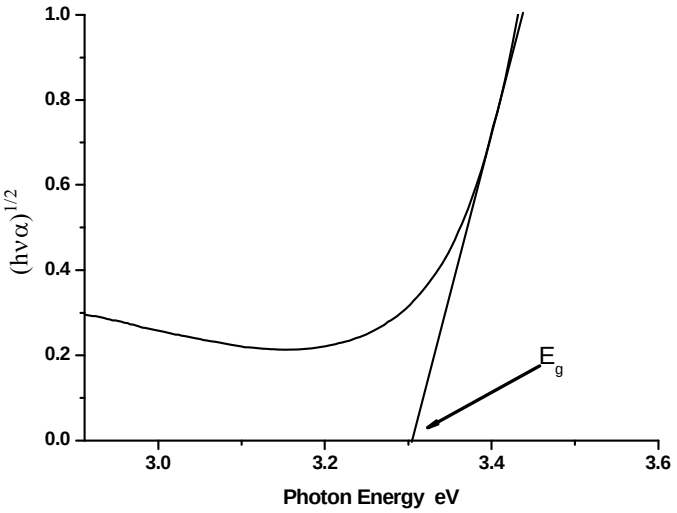

Figure 3-10 Schematic diagram of the method to determine the direct energy gaps of semiconductor films via UV-visible absorption spectroscopy.

3.5 Electrochemical Measurements

All the electrochemical experiments were carried out in a three compartment cell, as schematically shown in Figure 3-10. Except for the IMVS measurements (Section 3.5)

the electrolyte was 0.5 M Na_2SO_4 solution prepared in deionized water (18 M·ohm·cm). Samples were mounted on the copper wire via Ag epoxy resin as shown in Figure 3-11. The exposed parts of the connection and sample were masked by insulating epoxy resin. The electrochemical cell was designed with a quartz window to allow illumination with UV light. A platinum mesh acted as the counter electrode and Saturated Calomel Electrode (SCE) was used as the reference electrode. All potentials quoted in this thesis are versus SCE.

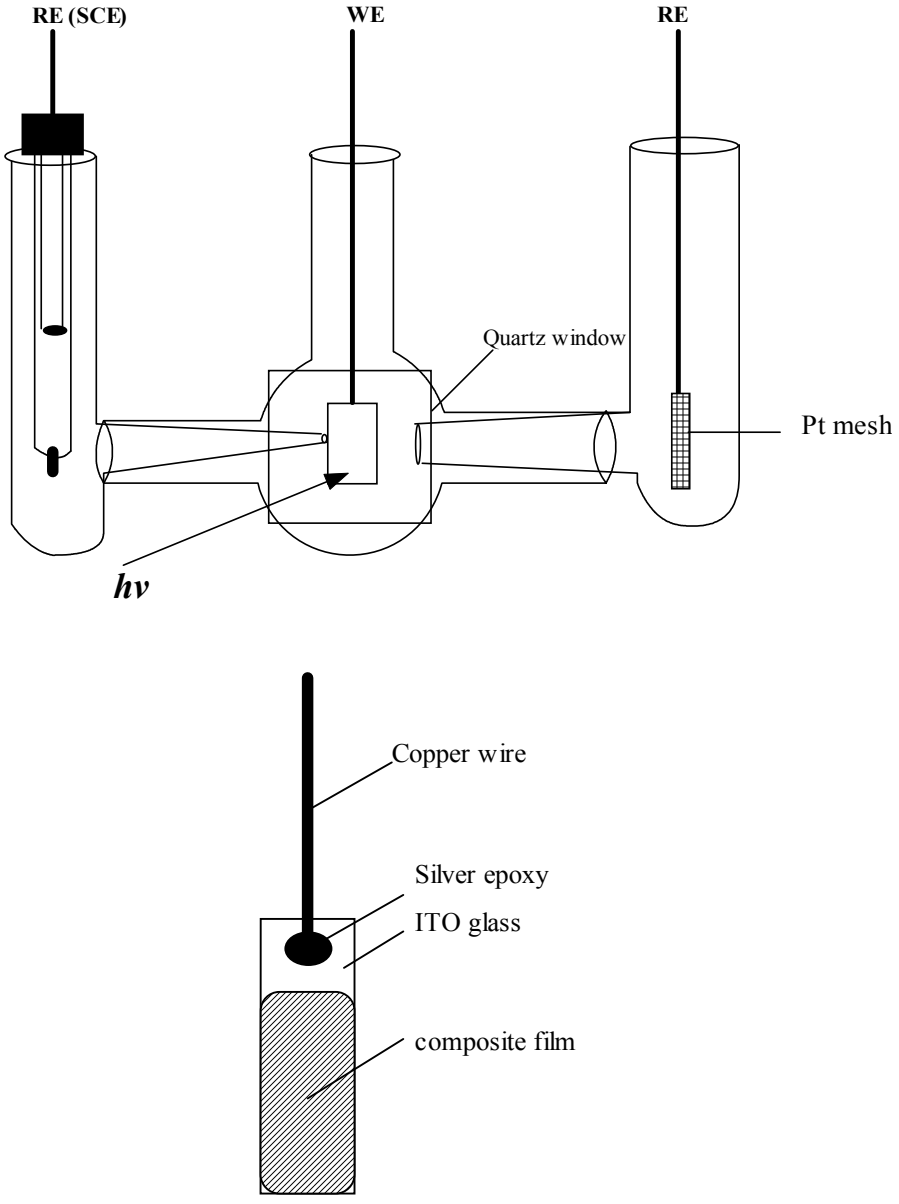

Figure 3-11 Schematic of the electrochemical/photoelectrochemical cell and working electrode design for the electrochemical experiments.

3.5.1 Cyclic Voltammetry (CV)

In cyclic voltammetry, a potential is ramped from an initial to a final value at a constant scan rate while the corresponding current is monitored. CV was carried out with the aid of an ACM field machine (ACM Instruments), this incorporates a potentiostat, waveform generator and frequency analyzer into a single instrument. The voltammograms were collected both in the dark and under illumination, over a scan range of -1000 mV to +1000 mV at a rate of 40 mV/min.

3.5.2 Electrochemical Impedance Spectroscopy (EIS)

The EIS technique involves applying small sinusoidal potential perturbations to an electrochemical system over a wide frequency range and measuring the magnitude and phase of the resulting current. Full details of the technique can be found in most electrochemistry text books[15]. In the present case the main aim of the EIS experiments was to obtain capacitive measurements from the composite films and thus investigate the influence of Au nanoparticles on the flat-band potential and donor densities within the TiO_2 particles and if possible draw conclusion about the presence and effects of any surface states.

For a passive system, i.e. one in which the presence of an oxide restricts electrochemical reactions to a very low rate the oxide/electrochemical interface can be approximated by the equivalent circuit shown in Figure 3-12 a), where R_{sol} is the uncompensated solution resistance and C_{ox} and R_{ox} are the space charge capacitance and leak resistance of the oxide. That is to say the charge transfer resistance, R_{ct}, and the double layer capacitance, C_{dl}, can be ignored. The relevant Nyquist plot (real against imaginary impedance) is schematically shown in Figure 3-12 b) and in this situation C_{ox} can be extracted from impedance data via the relationship:[15]

$$C_{OX} = \frac{Z''}{[(Z'')^2 + (Z'-R_{sol})^2]\omega} \qquad \ldots\ldots\ldots\ldots\ldots\ldots \qquad (3.8)$$

Here *Z''* and *Z'* are the imaginary part and the real part of the impedance respectively and ω is the angular frequency.

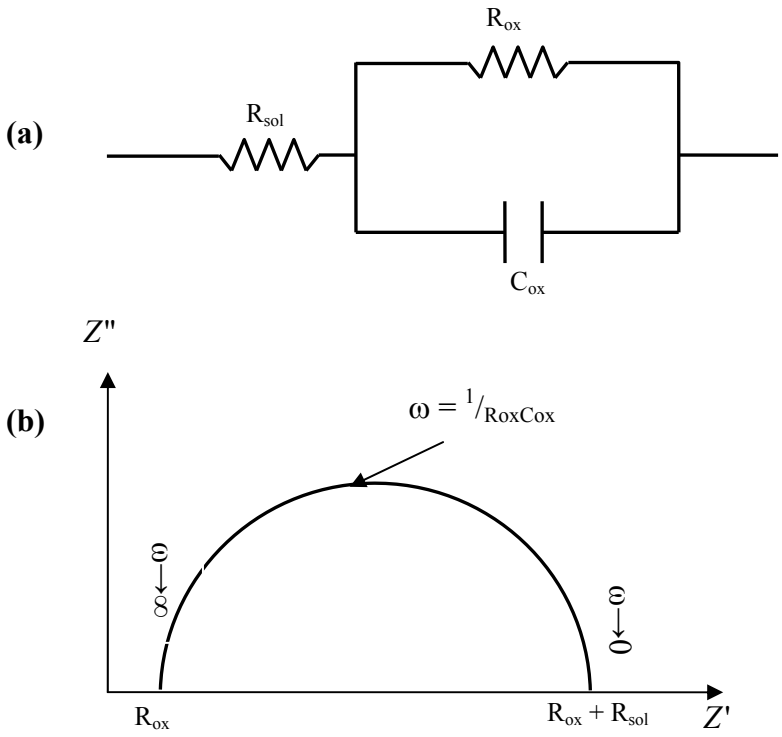

Figure 3-12 Representation of Electrochemistry Impedance Spectroscopy on the electrode a) the equivalent circuit for the electrochemical interface; b)The schematic Nyquist plot for the circuit shown in a). Adapted from reference [15].

The actual EIS experiments were carried out using the ACM field machine described in Section 3.3.1. Impedance measurements were then recorded from the composite films in 0.5M Na_2SO_4 at 100mV successive interval between 1000mV (SCE) and -1000mV (SCE) stepping in the negative direction. At each interval potential the sample was held 3 minutes prior to initiating the impedance measurement. The frequency range used was from 0.1 Hz to 10 kHz, unless otherwise stated and the signal was perturbed by RMS amplitude of ± 10mV.

The flat-band potentials and donor densities were determined via the potential dependence of the space charge capacitance, C_{sc}, given by the Mott-Shottky equation[16]:

$$\frac{1}{C_{SC}^{\ 2}} = \frac{2}{\varepsilon_S \varepsilon_0 e N_D A^2}(V - V_{fb}) \qquad (3.9)$$

where ε_s is the dielectric constant of the semiconductor , ε_0 is permittivity of free space, N_D denotes the donor density, A is the surface area of electrode, and V_{fb} is the flat band potential. V_{fb} and N_D can be obtained from a Mott-Schottky plot (Figure 3-14).

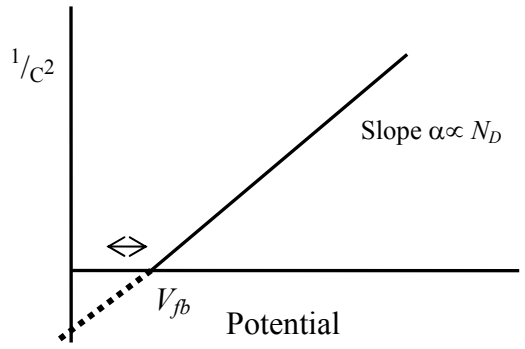

Figure 3-13 Representation of identifying the values on the Mott-Schottky plot. Adapted from reference [16]

3.6 Photoelectrochemical Experiments

Photocurrent measurements were performed by using a 300W xenon lamp and a monochromator. The photocurrents were generated by focusing the light with a fused silica lens thorough a quartz window of the electrochemical cell (Figure 3-11) onto the working electrode (composite films). The lock-in amplifier technique was used to separate the photocurrent from the passive current by chopping the light at a constant frequency of 29Hz. The photocurrent spectra were obtained by changing the wavelength in steps of 10nm. The instrumentation required for photocurrent experiments is schematically shown in Figure 3-14 and the electrolyte used was 0.5M Na_2SO_4 solution.

In order to enhance the accuracy, the photocurrent was corrected for the output of the lamp and the efficiency of the monochromator by using a calibrated photodiode (type S1227-1010BQ). Calibration was performed before and after every set of experiments. A calibration curve for the photodiode (photosensitivity) is shown in Figure 3-15. The photocurrent conversion efficiency ϕ_e can be calculated using; [17]

$$\phi_e = (photosensitivity) \times \left(\frac{h\nu}{\lambda} \right) \qquad \ldots\ldots \qquad (3.10)$$

Consequently the photocurrent conversion efficiency of the composite film, ϕ_F can be found from;

$$\phi_F = \frac{I_{P_F}}{I_{P_{PD}}} \times \phi_e \qquad \ldots\ldots\ldots\ldots\ldots\ldots\ldots\ldots\ldots\ldots\ldots\ldots\ldots\ldots (3.11)$$

where I_{P_F} and $I_{P_{PD}}$ are photocurrents observed from the oxide and the photodiode respectively.

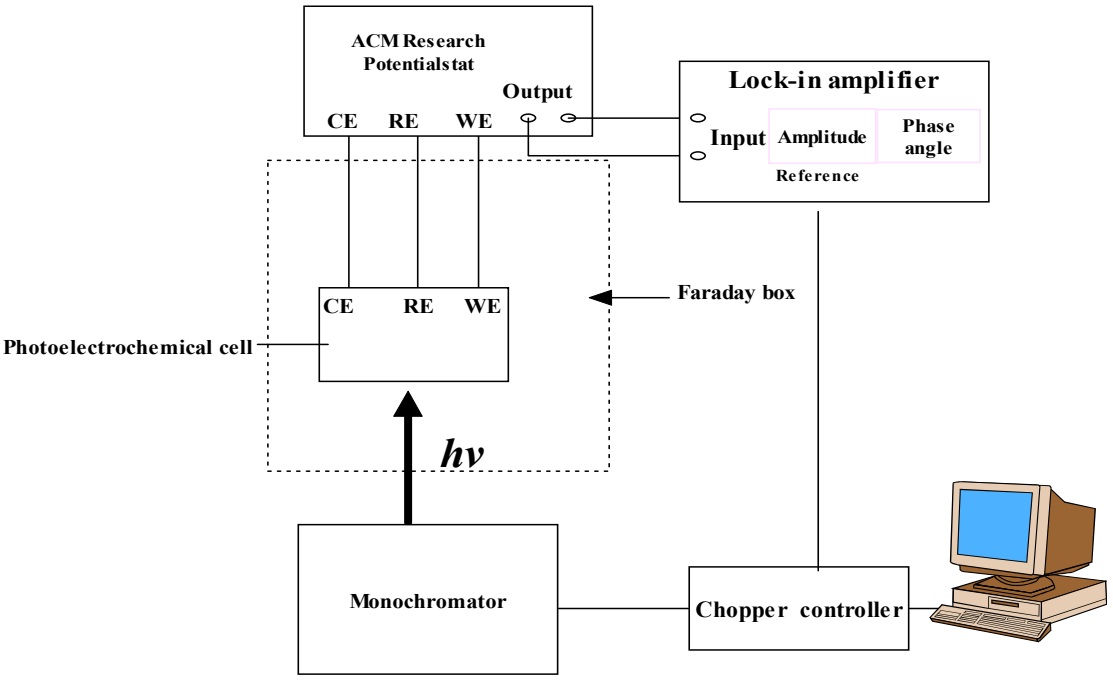

Figure 3-14 Schematic diagram of the experimental arrangement for photocurrent measurements.

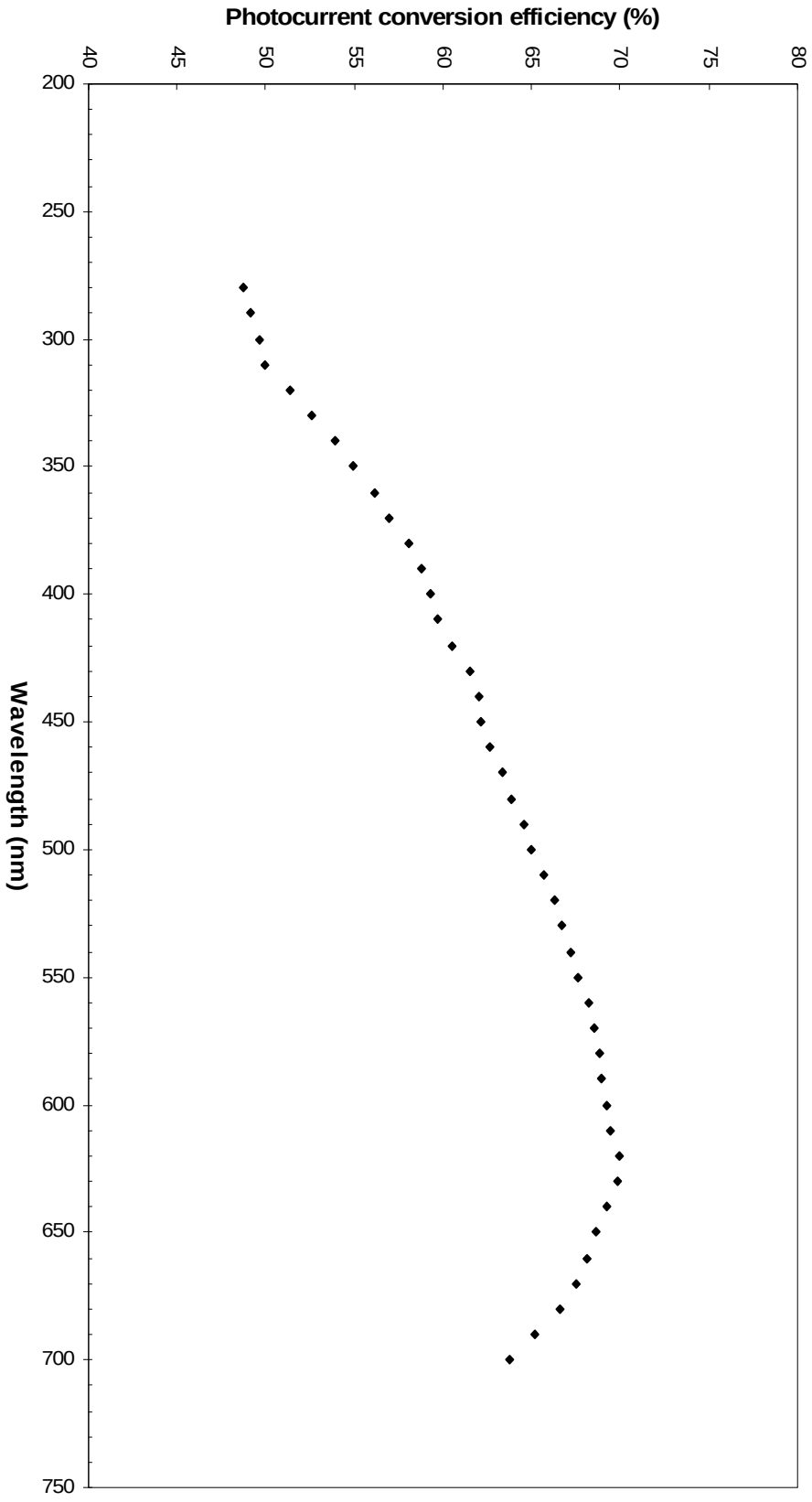

Figure 3-15 Photocurrent conversion efficiency of the photodiode.

3.7 Intensity Modulated Photovoltage Spectroscopy (IMVS)

The aim of IMVS is to examine the effect of surface modification of dye-covered TiO_2 electrodes on the conduction-band edge potential and recombination kinetics. IMVS measures the modulation of the photovoltage in response to modulation of the incident light intensity; a small sinusoidal perturbation of the light intensity superimposed on a larger steady background level (Figure 3-16). The illumination intensity is thus time dependent[18]:

$$I(t) = I_0(1 + \delta e^{i\omega t}) \qquad (3.12)$$

where $\omega = 2\pi f$ is the angular modulation frequency and δ is much less than unity. Measurement of the phase and magnitude of the photovoltage under open-circuit conditions, relative to the ac component of the illumination, gives information about charge transfer kinetics and transport.

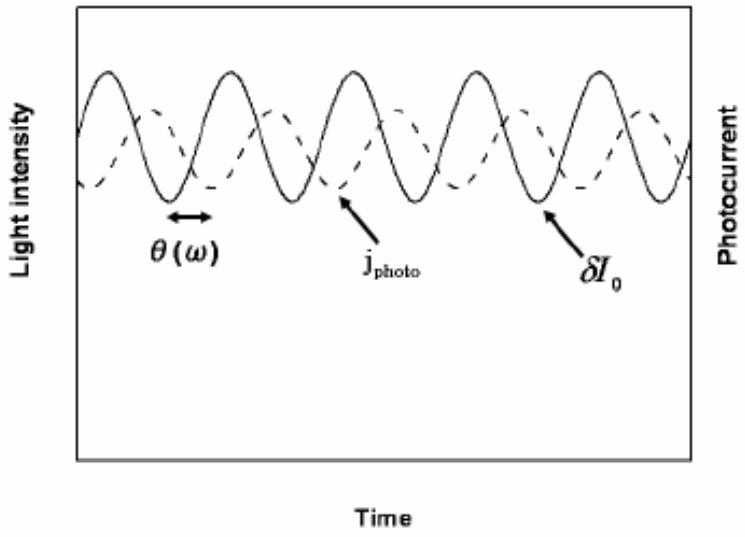

Figure 3-16 Simple diagram illustrating the IMVS experiment. Modulation of light intensity induces a phase shifted modulation in the photocurrent. Where δI_0 is the modulated light intensity, j_{photo} is the corresponding photocurrent and θ(ω) is phase shift. Adapted from reference[18].

The theory behind IMVS has previously been described in the works of Peter and

Schlichthorl *et al.*[18, 21 23], so the following only outlines the main points. Optical excitation of the sensitizing dye molecules leads to an electron injection current density (J_{inj}) into the conduction band of the semiconductor. This process is known to be very fast, occurring in the femtosecond-to-picosecond domain[19,20]. At open-circuit, all of the electrons injected into the conduction band must eventually undergo reaction at the semiconductor/solution interface. Figure 3-17 illustrates the possible reaction pathways, with corresponding rate constants, which may occur at the surface of an illuminated TiO_2 electrode in contact with a redox electrolyte, namely: charge trapping by a surface state (k_1), detrapping from a surface state (k_2) and recombination via the conduction band (k_3) or surface state (k_4). If it is assumed that recombination is irreversible, then at open-circuit and constant light intensity (i.e. steady state conditions) the recombination current density equals J_{inj}.

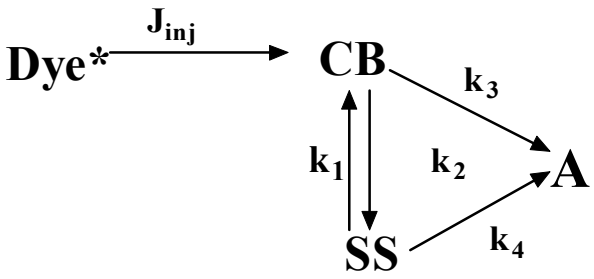

Figure 3-17 Schemes for electron transfer kinetics. J_{inj} is the electron injection current from excited dye molecules into the TiO_2 conduction band, $k_1$and k_2 are the respective rate constants for electron capture by surface state and the thermal emission of electrons back into the conduction band, whilst k_3 and k_4 are the respective rate constants for back electron transfer from the conduction band and surface states to an electron acceptor at the nanocrystalline semiconductor/redox electrolyte interface. Adapted from reference [23].

Electron diffusion to the substrate contact gives rise to a time delay between electron injection and collection. This delay manifests as a phase lag in the photocurrent response to intensity modulated light. Accordingly the diffusion length is given by Eq. 3.13[21, 22]

$$L_n = (D_n \tau_n)^{1/2} \qquad (3.13)$$

where the diffusion coefficient D_n and electron lifetime τ_n are the major parameters to influence charge diffusion. In an IMVS experiment, the technique used for the work presented in this thesis, the intensity dependence of the electron lifetime comes from the influence of surface states on the rate of interfacial electron transfer to the electrolyte. The electron life time is then related to the frequency at which the imaginary component of the photoresponse is maximized, f_{max}, , via equation 3.16[23]:

$$\tau_n = \frac{1}{2\pi f_{\max}} \qquad (3.14)$$

In practice, plotting the real and imaginary components of the photovoltage response against one another yielding a semicircle, the top of which occurs at f_{max}.

A schematic diagram of the apparatus used to conduct the IMVS experiments is illustrated in Figure 3-18. The light source used was a UV light excitation diode (LED), because its intensity could easily be modulated and focused on an electrode's surface, at a wavelength of 380 nm, i.e. of higher energy (3.26 eV) than the band gap of the TiO_2 films. The intensity LED was modulated by about ±0.5% by imposing a small a.c voltage (20mV) on top of a constant d.c voltage (4V), and the photocurrent signal was detected via a preamplifier and fed into a frequency response analysis (Solartron 1250). The electrolyte used was I^-/I^{3-} in acetonitrile, with an Ag wire acting as a pseudo reference electrode and Pt flag counter electrode. The electrochemical cell, shown in Figure 3-19 was sealed with epoxy resin and the measurements were preformed inside a Faraday box to reduced electromagnetic noise disturbance.

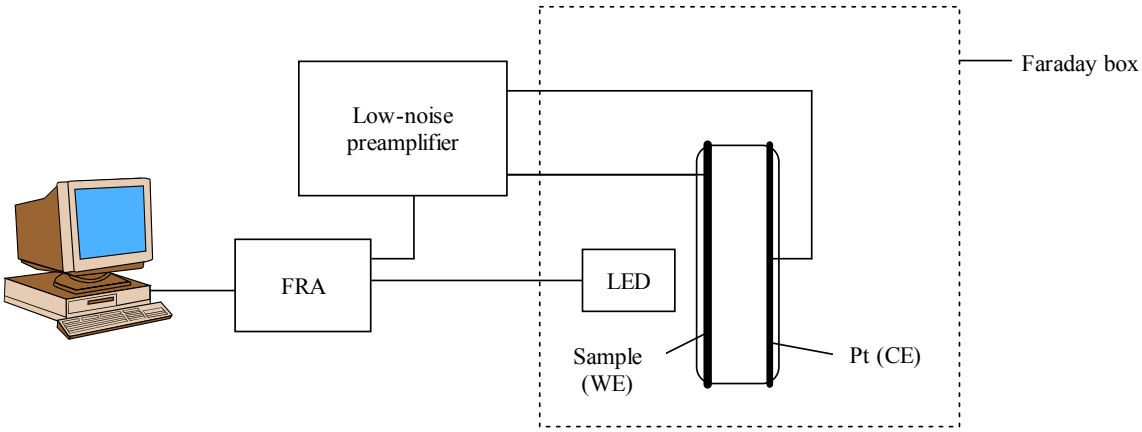

Figure 3-18 Schematic diagram of setup for Intensity Modulated Photovoltage Spectroscopy experiments.

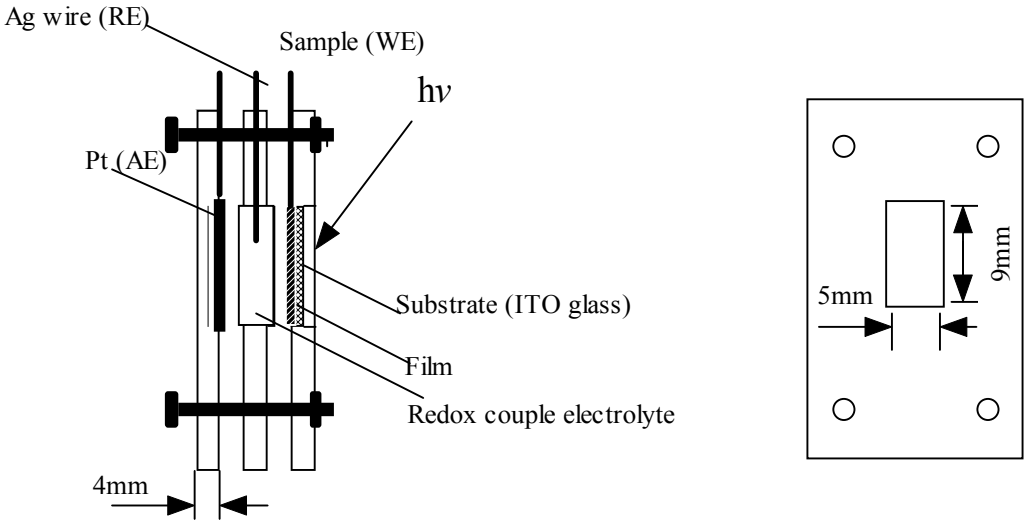

Figure 3-19 Schematic diagrams of the electrochemical cell used in the IMVS experiments.

Reference

(1) O'Regan, B.; Grätzel, M. *Nature* **1991**, *353*, 737-740.

(2) Johnson, B. F.; Davis, F. D. *Comprehensive Inorganic Chemistry*; Pergamon: New York, **1973**.

(3) John D. W.; A., N.; Sommerdijk, J. M. *Sol-Gel Materials Chemistry and Applications*; Gordon and Breach Science Publishers: Netherlands, **2001**.

(4) Takahashi, M.; Tsukigi, K.; Uchino, T.; Yoko, T. *Thin Solid Films* **2001**, *388*, 231-236.

(5) Kalyanasundaram, K.; Grätzel, M. *Coord. Chem. Rev.* **1998**, *177*, 347-414.

(6) Grim, P. C. M.; Hadziionannou, G. In *Characterization of composite materials*; Ishida, H., Ed.; Manning Publitions Co.: Boston, **1994**.

(7) Cullity, B. D. *Elements of X-Ray Diffraction*; Third edition ed.; Prentice-Hall International: London , **2001**.

(8) Brundle, C. R.; Evans, Charles A.; Wilson, S. *Encyclopedia of materials characterization*; Manning Publications Co.: Greenwich, **1992**.

(9) Zhang, W. F.; He, Y. L.; Zhang, M. S.; Yin, Z.; Chen, Q. *J. Phys. D: Appl. Phys.* **2000**, *33*, 912-916.

(10) Defosse, C. *Characterization of heterogeneous catalysts*; Delannay, F., Ed.; Marcel Dekker, Inc: New York, **1984**.

(11) Yamaguchi, H.; Yamada, T.; Kudo, M.; Takakuwa, Y.; Okano, K. *Appl. Phys. Lett.* **2006**, *88*, 202101-3.

(12) Brause, M.; Skordas, S.; Kempter, V. *Surf. Sci.* **2000**, *445*, 224-234.

(13) Zhu, Y.; Ding, C.; Ma, G.; Du, Z. *J. Solid State Chem.* **1998**, *139*, 124-127.

(14) Zhang, W. F.; Zhang, M. S.; Yin, Z.; Chen, Q. *Appl. Phys. B: Lasers Opt.* **2000**, *70*, 261-265.

(15) Southampton Electrochemistry Group *Instrumental Methods in Electrochemistry*; Ellis Horwood Limited: Chichester, England, **1985**.

(16) Gomes, W. P.; Cardon, F. *Surf. Sci.* **1982**, *12*, 155-215.

(17) Blackwood, D. J. *Ph. D Dissertation*, University of Southampton, **1986**.

(18) Peter, L. M.; Wijayantha, K. G. U. *Electrochem. Commun.* **1999**, *1*, 576-580.

(19) Tachibana, Y.; Moser, J. E.; Grätzel, M.; Klug, D. R.; Durrant, J. R. *J. Phys. Chem.* **1996**, *100*, 20056-20062.

(20) Asbury, J. B.; Ellingson, R. J.; Ghosh, H. N.; Ferrere, S.; Nozik, A. J.; Lian, T. *J. Phys. Chem. B* **1999**, *103*, 3110-3119.

(21) Peter, L. M. *Chem. Rev.* **1990**, *90*, 753-769.

(22) Dloczik, L.; Ileperuma, O.; Lauermann, I.; Peter, L. M.; Ponomarev, E. A.; Redmond, G.; Shaw, N. J.; Uhlendorf, I. *J. Phys. Chem. B* **1997**, *101*, 10281-10289.

(23) Schlichthorl, G.; Huang, S. Y.; Sprague, J.; Frank, A. J. *J. Phys. Chem. B* **1997**, *101*, 8141-8155.

(24) Tauc, R. G.; Vancu, A. *Phys. Stat. Sol.* **1966**, 15, 627-637.

Chapter 4 Characterization of Au/TiO_2 composite films

Characterizations of Au/TiO_2 composite films were carried out on the films which were prepared by sol-gel method and deposited on the fused quartz glasses, and followed by the different temperature (200^{o}C, 500^{o}C and 800^{o}C) heat-treatment. For comparing the difference between TiO_2 and Au/TiO_2 composite films, the Au composite films were synthesized in different Au concentration. In order to investigate the influence of Au particles on the properties of TiO_2 film, the comparison between TiO_2 film and Au/TiO_2 composite films with different Au concentration (1%, 5%, 10%, 25% and 50%) on the morphology observation, crystal structure, optical properties and photoelectric properties were explored.

4.1 Components of Composite film

As described in Chapter 3, the composite films were prepared by mixing different Au concentrations with the Ti containing precursor at the designed Au:Ti molar ratio. After spin-coating and sintering at high temperature, the actual Au:Ti ratios in the composite films were determined by EDX (Energy Dispersive X-Ray) attached to an SEM. The results are illustrated in Table 4-1. It can be seen that the measured Au levels were lower than the designed levels. The reason may be because of the deposition method, spin-coating, which may lead to a loss of the heavy Au particles due to the higher centrifugal force acting upon them compared to the lighter TiO_2.

Table 4-1 Chemical composition of the composites as determined by EDX.

Designed Au atomic percentage for composite film	Actual Au concentration in composite film at%
1%Au/TiO_2	0.88
5%Au/TiO_2	2.4
10% Au/TiO_2	5.4
25% Au/TiO_2	24.8
50% Au/TiO_2	33.2

4.2 Crystallization of Au particles in the composite films

During the composite film deposition procedure, it was found that the color of composite films changed as it was heated on the hot-plate at 200^{o}C, the extent of which depended on the Au concentration. The initial color of all the films was yellow, whereas after hotplate heating films with the lowest Au concentration turned yellow, whilst blue and then purple were observed as the level of Au in the films increased. That is the higher the Au concentration, the darker the color of the heat-treated composite film. The XRD data, obtained by glancing scan in low degree, showed that the Au particles were already crystallized at the end of the 200^{o}C hotplate heating (as shown in Figure 4-1a)), i.e. even before the 500^{o}C sintering step. In the synthesis processes, the composite films were subjected to the evaporation of solvent on the 200^{o}C hotplate. In most sol-gel processing routes, Au nanoparticles are usually formed by the reduction of Au complex molecules (in the present case $HAuCl_4 . xH_2O$). According to Johnson *et al.*[1] the sequence of $HAuCl_4$ thermal decomposition in films is:

$$HAuCl_4 \cdot xH_2O \xrightarrow{100^{o}C} AuCl_3 \xrightarrow{160^{o}C} AuCl \xrightarrow{200^{o}C} Au \qquad (4.1)$$

Thus Au ions are already reduced to metallic gold at 200^{o}C and Au particles form afterwards. During the 200^{o}C hotplate heating, as the solvent evaporated the confinement on the Au particles from the matrix was relaxed allowing them to grow, and thus the particle size changed with Au concentration. This indicates that Au

particle crystallization is related to an electrostatic interaction between the gold species and the embedding matrix. After 500°C sintering, the XRD patterns of Au particles became sharper and evidence for TiO_2 crystals appeared (Figure 4-1 b)). From the XRD patterns in Figure 4.1, it can be seen that the TiO_2 was not crystallized until after the 500°C sintering stage.

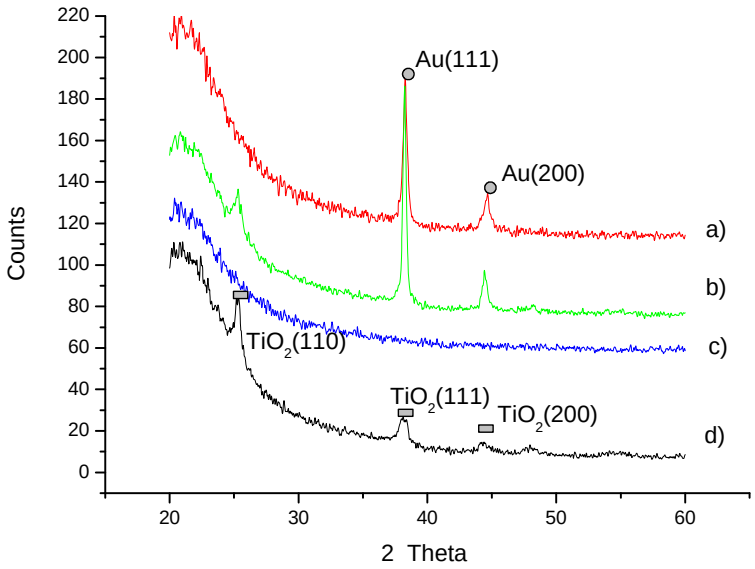

Figure4- 1 XRD spectra of 50%Au composite film and pure TiO_2 film at different stages of sample preparation, a) as deposited composite film, b) Au composite film after 500°C sintering, c) TiO_2 film as deposited, d) TiO_2 film after 500°C sintering.

The procedures involved in a typical sol-gel process of metal alkoxide are schematically described in Figure 4-2[2]. In this case, the metal (M) has a coordination number of four and is surrounded by four alkoxy (OR) ligands. The first chemical reaction is hydrolysis, which is promoted by introducing water to the sol. For thin film preparations, sols are usually only partially hydrolyzed in order to allow them to be applied onto a substrate by spinning. Condensation reactions begin as soon as the hydroxy groups are generated, occurring between either an alkoxy and a hydroxy group or two hydroxy groups with the dominant route depending on the degree of prior hydrolysis. Hydrolysis and condensation reactions continue concurrently in the

sol and eventually lead to the formation of a rigid network. At this point, the backbone of the oxide has been formed via metal-oxygen-metal bonds. However, the material is amorphous and still contains trapped water and alcohol, which has to be removed by drying at 200°C. After drying, the gel is still amorphous (Figure 4-2 c) and crystals of TiO_2 only formed during subsequent 500°C heat-treatment (Figure 4-2 d).

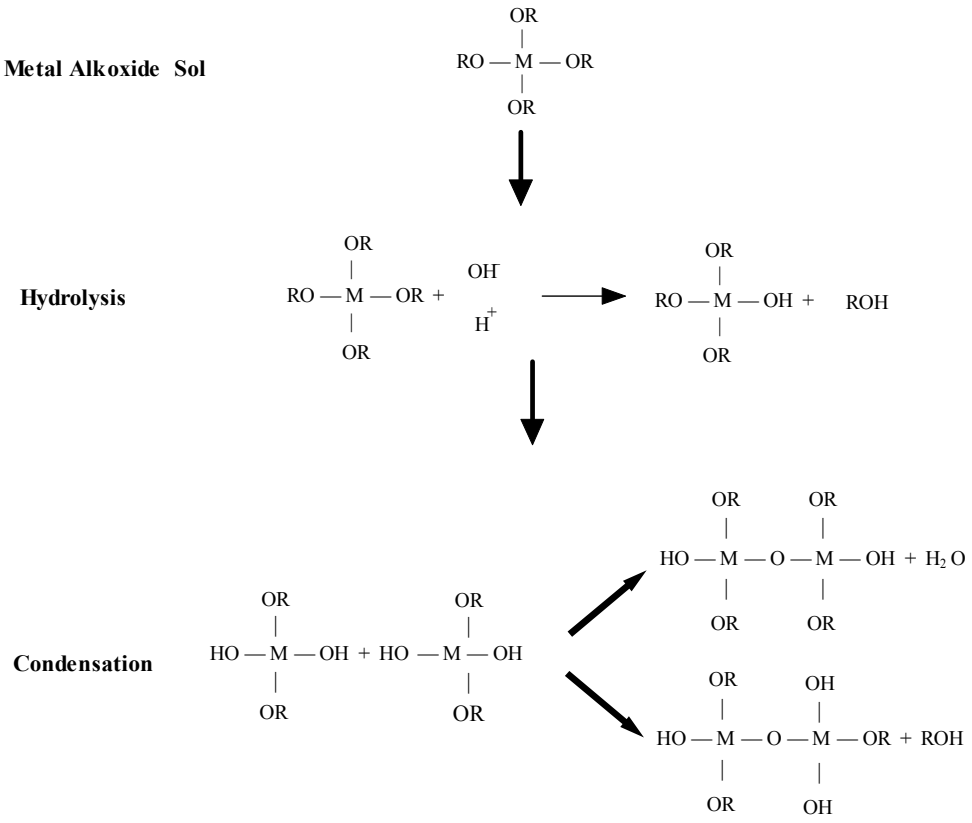

Figure4-2 Schematic representation of the chemical reaction in a sol-gel process. (Adapted from reference [2])

4.3 Morphology of composite films

The morphology of the composite films was described by AFM, as illustrated in Figure 4-3. By comparing the morphology between as-deposited composite films and those sintered at 800°C, it was found that at all Au levels the roughness decreased upon sintering. However, as the Au concentration increased the morphology of composite films was observed to become coarser. Also as the Au concentration was increased "hills" emerged out of the surface of the sintered composite films.

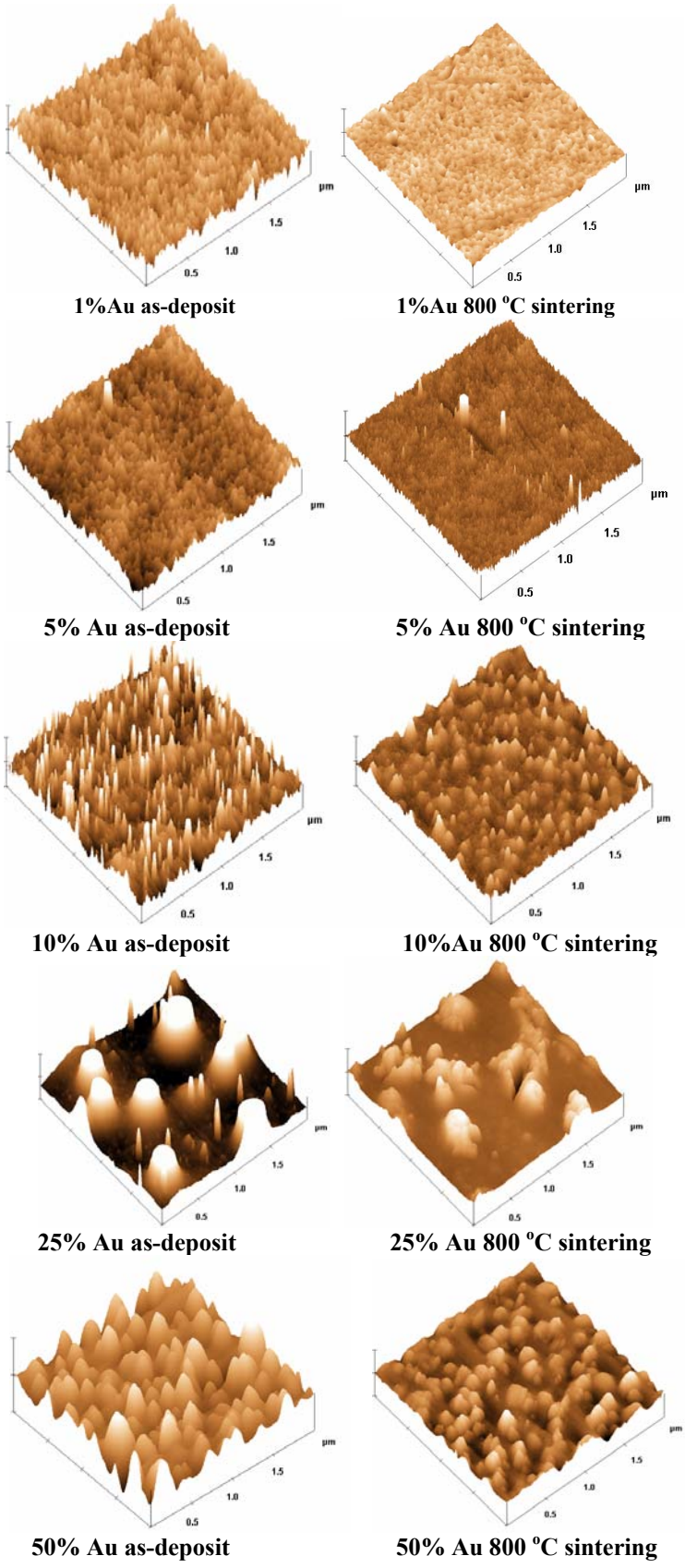

Figure4-3 AFM morphology of Au/TiO_2 composite films as deposited and after sintering at 800°C.

From the crystal identification results of the XRD low angle glancing scan, it is known that the crystal structure of Au particles had already formed in the as-deposited states, so the hills could be formed by distortion of crystallized Au particles. It was noticed that the morphology of 1% Au composite film was different from other composite films, with there being no hills protruding out of its surface, such that it presented morphology similar to that of a pure TiO_2 film. The morphology difference between low and high Au concentration composite films arises from the sol-gel processes. During synthesis Au acid was added into the gel of TiO_2, thus the acidity increased as the quantity of Au increased, which could have interrupted the condensation process. Although it is hard to identify TiO_2 particles from Au particles from AFM pictures, when these are combined with the XRD and TEM data one can make an educated assignment.

Since AFM only can reflect the height difference of the composite surface, TEM observation is still needed to obtain information about exact shape of the Au and TiO_2 particles. Figure 4-4 shows that the Au nanoparticles are embedded in the TiO_2 films, but their size and shape vary with concentration. It appears that the Au particles are crystallized independently. In the 1%Au/TiO_2 composite film, most of the Au particles were located at intergranular positions and their shapes were irregular. With increasing Au concentration, the shape of the Au particles became more regular and their size increased due to aggregation. For example, in the 5% Au/TiO_2 film the Au particles appeared spherical whilst in the 50% Au/TiO_2 film the Au particles change into polygons, i.e. these were faceted. Figure 4-4 shows that except for some abnormally large particle sizes in the 25% Au/TiO_2 composite film, the particle distribution and particle size are uniform in each of the different composite films. It was also observed

that in 25% Au/TiO_2, a number of small Au particles remained along with the more than 100nm particle size ones formed by aggregation. These big particles will cause scattering of any irradiation light, and thus influence light absorption. This TEM information will be helpful to the explanation of the optical properties of Au composite films.

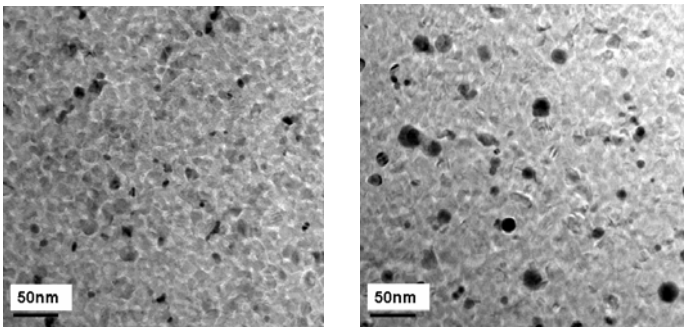

1% Au/TiO_2 **5%Au/TiO_2**

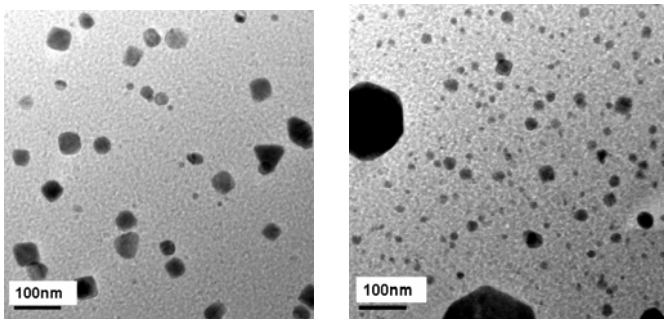

10% Au/TiO_2 **25%Au/TiO_2**

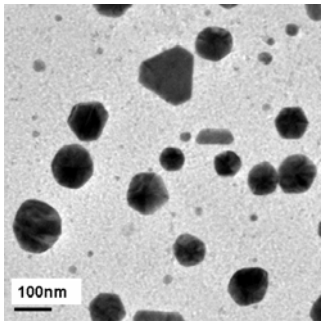

50% Au/TiO_2

Figure4-4 TEM images of sintered Au/TiO_2 composite films at different Au concentrations. Note that the scale is larger at the three highest Au levels.

As yet it is unclear why the 25%Au loading had larger particles than the 50%Au one, possibly it is related to the nucleation and growth of the particles. For example, it may

be that up to a loading of 25%Au nucleation is rate determining, this would lead to a small number of large particles, but if at very high Au levels may be growth dominates over nucleation there would be a large number of smaller particles.

4.4 Effect of heat-treatment on the crystallization of composite films

The extent of crystallization is an important parameter for a semiconductor, because it is relative to the electrical and the optical properties of materials. In addition, different techniques were used in this study. Although XRD is the most common method to identify crystal structures, it only gives information about the long-range average crystallinity. Therefore, in this study, Raman and TEM diffraction techniques were also used to study the localized crystal structure. By comparing the structure information obtained from the different techniques, a detail account of how the different concentrations of Au particles influence the TiO_2 films crystal structure was obtained.

4.4.1 XRD results of composite films

As-deposit

Figure 4-5 shows the X-ray diffraction (XRD) patterns for the as-deposit Au/TiO_2 films at Au concentration of 1%, 5%, 10%, 25%, 50% (at%), which were pre-treated by spin coating on a hotplate at 200^{o}C for 10 minutes (sample color changed from light yellow to dark purple due to the different Au oxidation states) then dried in a 80^{o}C oven for 30 minutes. There is no any peak could be discerned in the XRD for 1% Au. For the 5%, 10%, 25% and 50% compositions, peaks could be identified as belonging to (111) and (200) of a face-centered cubic gold phase, however, no peaks of the TiO_2 matrix were found. This indicates that the gold was reduced from Au^{3+} to Au^{0} and crystallization started even at the 200^{o}C deposition temperature, possibly due

to the chemical stability of gold and the high mobility of Au atoms[4]. With increasing Au concentration the intensity of the XRD peaks was enhanced, indicating high crystallization of the Au particles in high Au concentration composite films.

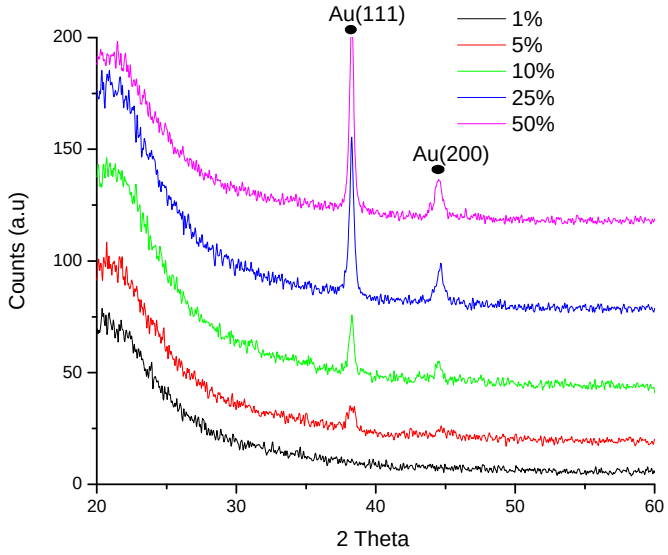

Figure4-5 XRD patterns of Au/TiO_2 composite films as-deposit.

After 500 °C sintering

The XRD patterns of Au/TiO_2 films after 500 °C sintering are shown in Figure 4-6. It is evident that now both Au and TiO_2 were crystallized in the composite films. Identification of the XRD pattern showed that the structure of TiO_2 phase was anatase, which agrees with that reported previously[3] . However, the intensity of the TiO_2 peaks decreased with increasing Au concentration, suggesting lower crystallinity. In Figure 4-6 it can also be seen that with Au concentrations above 10% the intensity of the gold peaks were stronger than those of the TiO_2 in composite films, despite the dominant ratio of Ti atoms over Au atoms in the films. This difference is attributed to the nucleation of the crystallization of Au particles during the 200°C pre-treatment, such that in the 500°C sintering stage the behavior of Au nanoparticle was mainly agglomeration. This may suppress the fluctuation of the surface free energy around the

Au particles and thus delay the later crystallization of the TiO_2 particles. Therefore, compared with the crystallization of Au particle, the crystallization of TiO_2 was weak. From these XRD patterns it can be ascertained that the phases of Au and TiO_2 were not mixed together, even though they were deposited from the same precursor. This may be due to the difference in their nucleation temperatures.

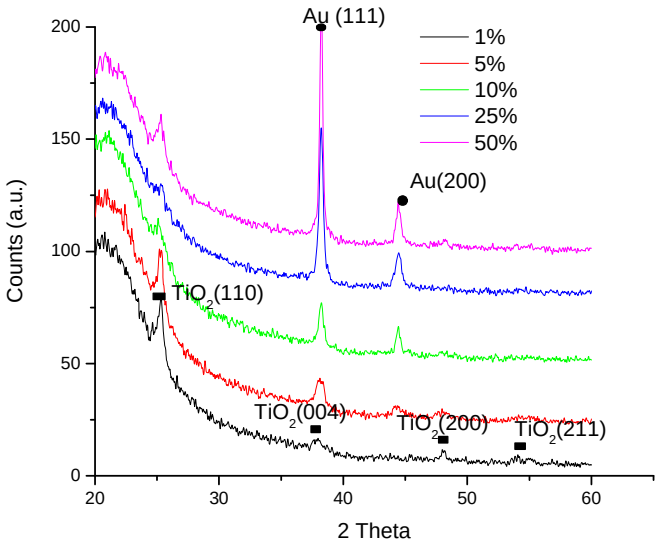

Figure4-6 XRD patterns of Au/TiO_2 composite films after 500 °C sintering.

After 800 °C sintering

Figure 4-7 illustrates the XRD patterns of Au/TiO_2 composite films after 800°C sintering. The XRD patterns of Au and TiO_2 were the same as those after 500°C sintering (Figure 4-5). This is different from previous work in which the TiO_2 particle after 800°C sintering presented the rutile structure[4]. This could be due to the fact that in the present work hydrolysis of the dilute TiO_2 precursor solution was suppressed by working in a dry glove box. The formation of the rutile phase has been shown to depend on the degree of condensation in the gel structure[5,6].

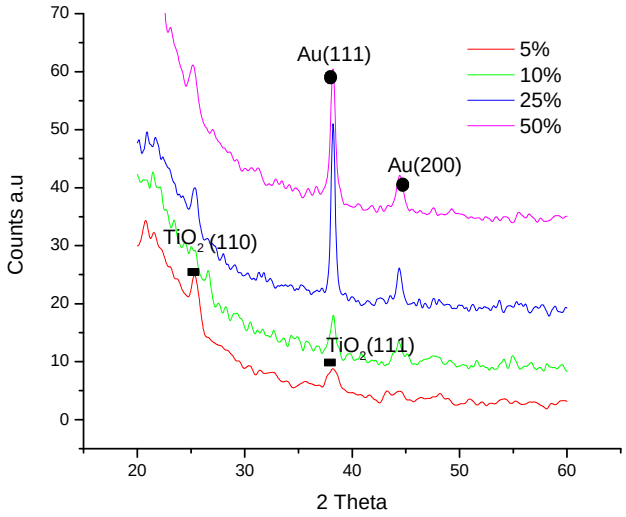

Figure4-7 XRD patterns of Au/TiO_2 composite films after 800°C sintering.

From the XRD patterns, it can be seen that the Au crystal structure of composite film became dominate as the Au concentration increased. This could be due to the signal collection method, i.e. glancing scan mode which supplies crystal information from the near surface. For investigating the crystal structure of composite films, XRD also has another limitation in that it only gives average information from the composite film. Therefore, to investigate any differences of crystallization in the TiO_2 matrix, TEM diffraction patterns were obtained from selected areas. It was observed that the TiO_2 diffraction pattern changed from a dot-ring to a smooth-ring which indicates that the TiO_2 crystallinity became weak with increasing Au concentration (Figure 4-8). It should be pointed out that in these diffraction patterns information about the crystallization of the Au particles is obscure. This could be due to the fact that the diffraction was carried out on selected areas that were dominated by TiO_2 particles, the primary focus of this part of the investigation. Furthermore, on one hand to obtain a diffraction pattern the sample thickness has to be thin enough to let electron beam go through, thus the larger Au particles >100 nm in diameter would not be contribute to

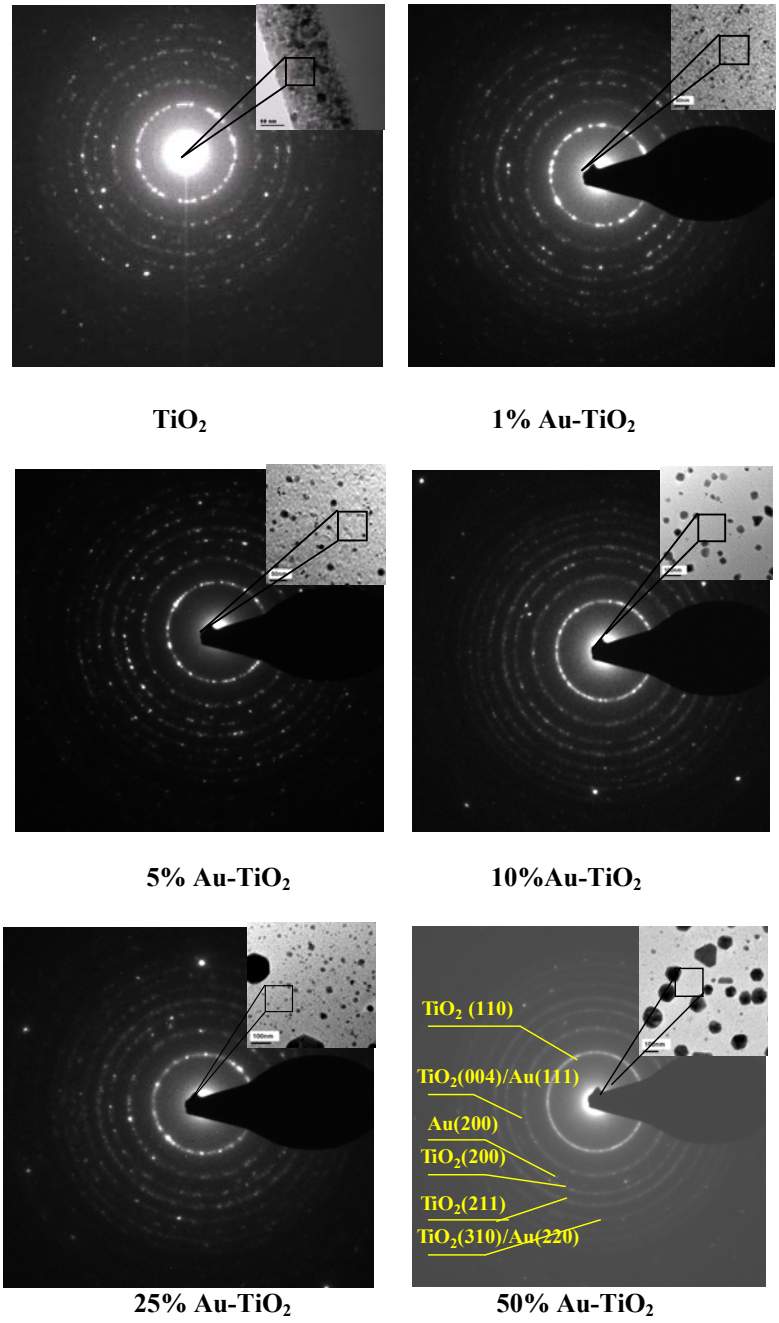

TiO_2 1% Au-TiO_2

5% Au-TiO_2 10%Au-TiO_2

25% Au-TiO_2 50% Au-TiO_2

Figure4-8 TEM diffraction pattern of Au/TiO_2 composite films. With increasing Au concentration, the dot-ring became blurred. This indicates that the crystallization composite film was incomplete.

the diffraction pattern, eliminating many of the particles in the 25% and 50% Au films. On the other hand, particles that are too small (< 50 nm in diameter) and present only at low levels will also only contribute weakly to the diffraction pattern. From the morphology of the Au particles seen in the TEM images the Au particles in 1% and

5% composite films are likely too small and/or too few in number to be revealed in the selected area diffraction patterns. As a result bright diffraction dots from Au particles can only be seen in the higher Au percentage composite films, where a large number of small Au particles existed.

The diffraction rings in the 50% composite films are identified in Figure 4.8. These rings from the center outwards belong to anatase TiO_2 (110) (004) (200) (211) (assigned by referring to PDF card 21-1272) and Au (111) (200) (220) (assigned referring to PDF card 04-0784) respectively. The TiO_2 (004) and Au (111) rings overlap, as was also seen in the XRD spectra. The identified Au diffraction rings were confirmed by checking against the equation:

$$(\frac{r_n}{r_1})^2 = \frac{M_n}{M_1} \quad (4.2)$$

r_n: radius of the rings in diffraction pattern

M_n: Miller index in the crystalline $M = h^2 + k^2 + l^2$

4.4.2 Micro-phase identification of composite films by Raman spectroscopy

Although XRD reveals the long-range order of materials and gives average structural information within several unit cells, it has limitations when used for the investigation of nanocrystallization. An alternative method to explore crystallization is microRaman scattering. Raman scattering as a local probe is very sensitive to the crystalline and microstructures of materials; Raman lines become weak and broad when the samples have local lattice imperfections[7]. Moreover, due to the Au particle dispersed on the surface of composite film, Raman scattering is enhanced, i.e. Surface Enhanced Raman scattering (SERS)[8]. Although the reason that Au particles can enhance Raman

scattering without any traces is not well understood, the study of Raman scattering on different Au concentration samples should give information about the Au influence on the atomic vibrations under excitation.

Raman spectra of composite films after different temperature treatments

Figure 4-9 illustrates the Raman spectra of composite films after 500°C sintering for 30mins. There are four bands in all the spectra which are typical of anatase TiO_2, which has a D_{4h} symmetry point group so the bands have previously been assigned to the Raman-active vibration modes E_g(144cm^{-1}), A_{1g}(395cm^{-1}), B_{1g}(514cm^{-1}) and either B_{2g} or an overtone E_g(639cm^{-1}) respectively; previously reported locations are given in brackets [9] . The lowest-frequency E_g mode is known to be closely related to the grain size of the TiO_2 nanocrystals[7], its occurrence of lower E_g 151 cm^{-1} mode as a strong band indicates that the TiO_2 nanocrystal possess a certain degree of long-range order in the anatase phase, whereas the weak broader peaks in the high-frequency region indicate a lack of long-range order.

After 800 °C sintering of the composite films the Raman spectra were as shown in Figure 4-10. It can be seen that the peaks are now stronger, and it indicates that intensity of lower E_g mode is related to the degree of crystallization of the films. The E_g mode blue-shifted with increasing Au content but not as dramatically as under 500°C sintering and, except for the 1% load, this peak appeared at higher wavenumbers than its the 500°C sintered counterpart.

Figure 4-11 shows that with increasing Au concentration the strongest mode, lower E_g, associated with grain size, blue-shifted to higher frequencies. This blue-shift, along

with peak broadening, indicates that the particle size of the TiO_2 is getting smaller. It was noticed that this shift was dramatic for small gold additions (e.g. 1% and 5% shifts ~5cm^{-1}) but less conspicuous at high levels (e.g. 25% and 50% shifts <2cm^{-1}). The E_g mode also appeared to gain strength and become broader as the Au concentration increase up to 25%. However, a further addition of Au to 50% caused a large decrease in the Raman intensity observed. The intensity of the other peaks followed that of the lower E_g mode, but these were all too broad and weak to abstract any meaningful peak shift information. Broad, weak peaks in the high-frequency E_g mode are indicative of some local lattice imperfections in these composite films, perhaps due to the unsaturated bonds at the surface.

Overall the broadening and blue-shifting of the Raman peaks indicate that the TiO_2 particle size decreases with increasing Au concentration, which is consistent with the results obtained by XRD and TEM. Also, in all three techniques, anatase was the only TiO_2 phase, other than amorphous, revealed in these composite films even after 800^oC. In this measurement, Au particles only played a role in the enhancement of Raman scattering of TiO_2. This indicates that the Au was not mixed with TiO_2 in the lattice structures; i.e. no peaks that could be assigned to vibrations involving Au atoms were observed. Therefore one possible reason for the apparent TiO_2 particle size shrinkage effects may be that the Au particles induced more defects into the lattice. To test this hypothesis, measurements on the surface state of the composite films and TiO_2 were carried out by XPS, UPS and photoluminescence spectroscopy and the results of these investigations are presented in section 4.7.

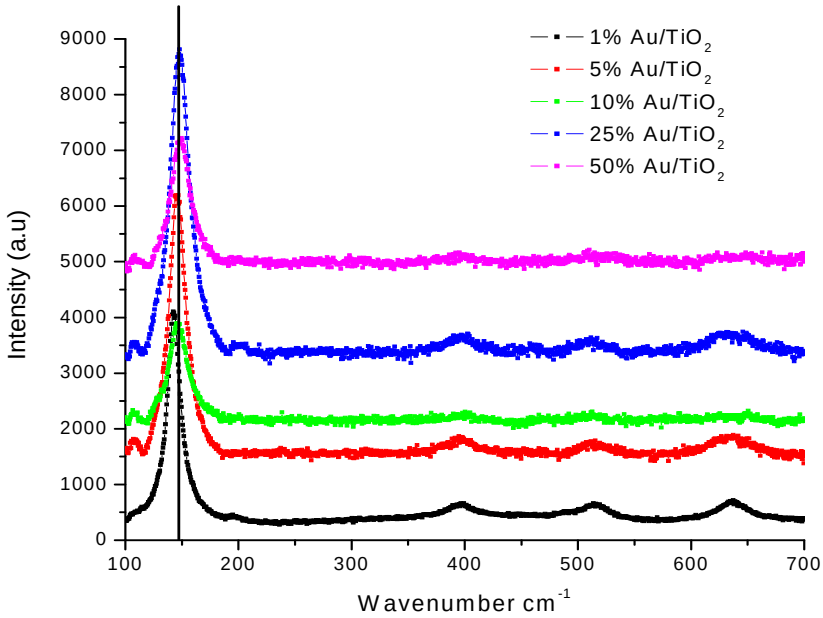

Figure4- 9 Raman scattering spectra of Au/TiO_2 films after 500°C sintering for 30 mins. Ar -ion laser 514nm at 30mW. Peaks shift with increasing Au concentration.

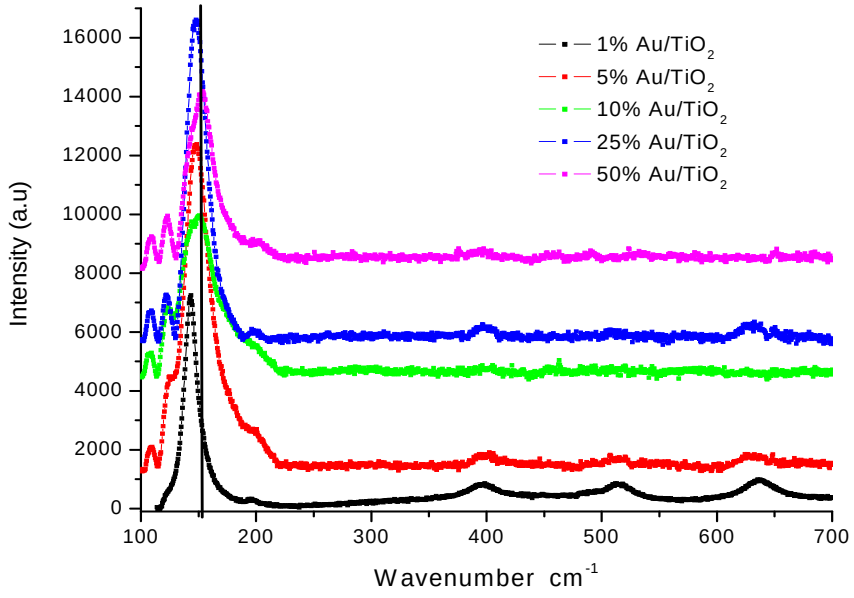

Figure4-10 Raman scattering spectra of Au/TiO_2 films after 800°C sintering for 30 mins. Ar-ion laser 514nm at 30 mW. Peaks shift with increasing Au concentration.

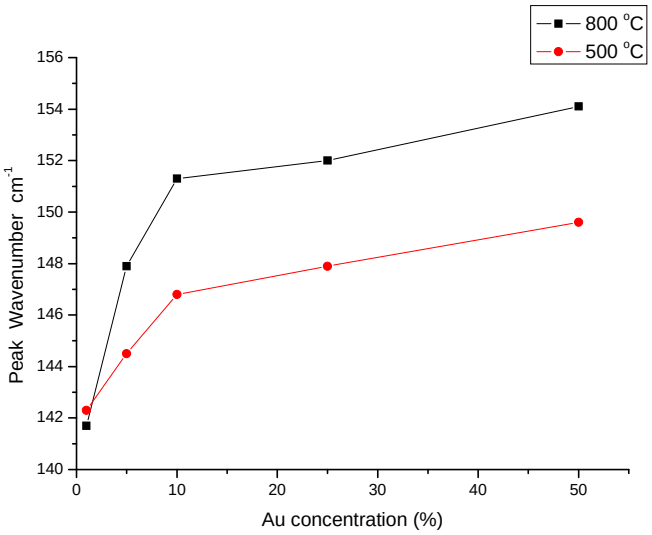

Figure4-11 Shift in peak position of the lower E_g Raman band with Au concentration for composite films after 500 °C and 800 °C sintering for 30mins.

4.5 Au and TiO_2 particle sizes change in composite films

Particle size is an important parameter in the optical absorption properties (e.g. SPR) of Au composite films. From the TEM plain view pictures in Figure 4-4, Au particle size changed from about 10nm in a 1% Au/TiO_2 composite film to 180nm in a 25%Au/TiO_2 composite film. Figure 4-12 show the Au particle sizes and TiO_2 particle size in the various films，in which TiO_2 particles were obtained from XRD and Au from TEM images. The particle size of TiO_2 crystallites were evaluated from XRD via the Debye-Scherrer's equation[10]:

$$L = \frac{k \cdot \lambda}{B_r \cdot \cos\theta} \qquad (4.3)$$

Here B_r is the instrumentally subtracted diffraction peak breadth, i.e. the broadening caused by the instrument is subtracted from the full width of half maximum (FWHM) of the recorded peaks; λ is the wavelength of the X-ray radiation used, 1.54056 Å; θ is the Bragg angle of the diffraction line; L is the average crystallite size measured in a direction perpendicular to the surface of the specimen; k is a constant taken as 0.9 [10]in

this study. It is evident that the changes in the sizes of the two types of particle are inversely related, i.e. when one increases the other decreases, plus the changes in the Au particles are much more dramatic than those of the TiO_2 particles. It is hard to have a clear explanation for why the 25% loading had larger particles (although fewer of them) than the 50% loading; this observation was repeatable and always occurred. However, it is possibly related to the nucleation and growth of the particles. For example, it may be that up to a loading of 25% nucleation is rate determining, this would lead to a small number of large particles, but if at very high Au levels may be growth dominates over nucleation there would be a large number of smaller particles.

Table 4.2 shows a comparison of the data obtained from TEM and XRD. In the XRD patterns, the strongest Au peak overlapped with a strong TiO_2 peak, so Scherrer's equation could not be used to evaluate Au particle sizes accurately. However, comparing the results of XRD and TEM for TiO_2 displayed in Table 4.2 reveals good agreement between the two techniques, thus the easier to obtain XRD data was used for analysis of the sintered films.

Table 4-2 Comparison of the TiO_2 particle sizes in the composite films determined by XRD and TEM.

Composite films	1%Au	5% Au	10% Au	25% Au	50%Au
Particle size from TEM images (nm)	14.4±4.1	14.1±3.2	10.6±4.0	9.5±1.5	14.5±3.6
Particle size calculated from XRD diffraction pattern (nm)	17.1	17.1	12.1	9.5	12.8

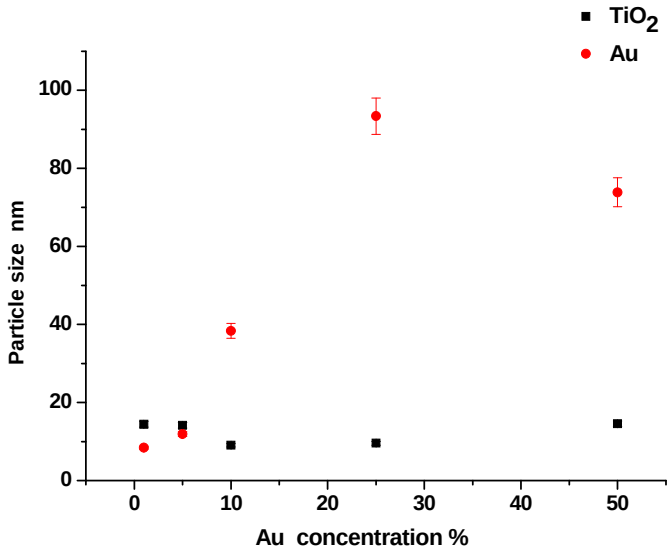

Figure4-12 Comparison of average Au nanoparticle size from TEM with TiO_2 particle size after 800 °C sintering.

Figure 4-13 shows the average TiO_2 particle size changes in different composite films after sintering at 500°C and 800°C, as determined from XRD peak broadening based on equation 4.3. It was found that at 800°C, the TiO_2 particle size decreased with the increase of Au particle size. This could be but then remained fairly constant over the range 5% to 25%, however, at the highest level of 50% the TiO_2 particle size increased again close to that seen in the pure TiO_2. The results after 800°C sintering were somewhat similar, except that the TiO_2 particle size continuously decreased from 5% to 25% Au levels and the TiO_2 particle size in 50% specimen was close to that in the 10% one.

This particle size difference in the composite film could influence the band structure and even the electron transport properties. For example, quantum confinement effects can increase the band gap of a small nanocrystalline semiconductor, whilst increasing a Au particle's size will make its properties closer to that of bulk gold.

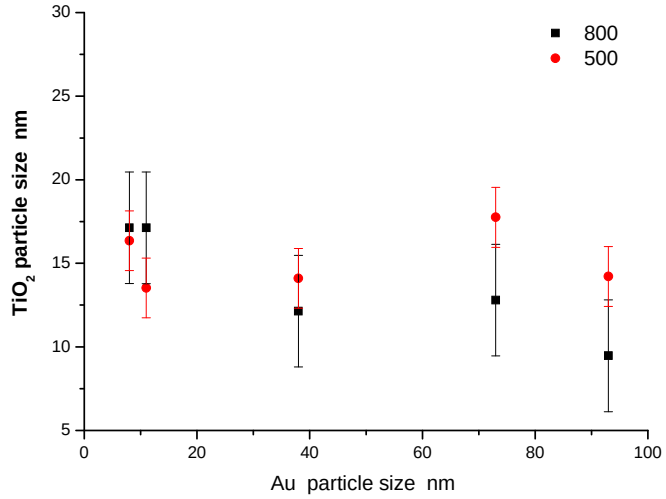

Figure4-13 Average particle size of TiO_2 in composite films after 500°C and 800°C sintering calculated from XRD by Scherrer's equation.

4.6 Optical absorption properties of Au/TiO_2 composite films

The visible absorption spectra for the as-deposit Au/TiO_2 composite films are shown in Figure 4-14, in which there are three noteworthy features, namely the change in the SPR peak wavelength position, its intensity and its width. It is evident from Figure 4-14 that the composite film with only 1% Au did not exhibit any surface plasmon resonance (SPR) peak. This may be due to the fact that Au concentration was too low for SPR to take place, or at least its intensity is too weak to be detected. However, at Au concentrations of 5% and above the SPR peak was clearly evident, showing a marked red-shift as the Au concentration increased. The surface plasmon resonance frequencies of nanometer-size noble metal particles dispersed in a dielectric medium are given by the Mie-Drude equation [11]

$$\varpi_p = \left(\frac{4\pi n q^2}{m^* \varepsilon_0} \right)^{1/2} \bullet \left(2\varepsilon_{matrix} + 1 + \chi_{\text{int}erband} \right)^{-1/2} \qquad (4.4)$$

where, n is the surface electron density, q is the charge constant, m* is the effective mass of an electron in the noble metal, ε_0 is the permittivity of free space, ε_{matrix} is the

dielectric constant of the matrix and $\chi_{\text{int}erband}$ is the dielectric susceptibility due to inter-band transition. As a particle's size increases the ratio of surface atoms to bulk atoms decreases leading to a reduction in the surface electron density, thus Equation 4.2 predicts a decrease in the SPR frequency, i.e. a red-shift. Therefore the observed red-shift in the SPR peak wavelength with increasing Au content corresponds to increases in the Au particle size, which is consistent with the earlier TEM observation (Section 4.3). In addition, it has been also reported that the dielectric constant of Au has a dependence on particle size[11]. Hövel *et al.* [12]and Chen *et al.*[13] reported that interfacial chemical interaction and charge transfer between the noble metal particles and the matrix may influence the free electron density and consequently change the SPR frequency.

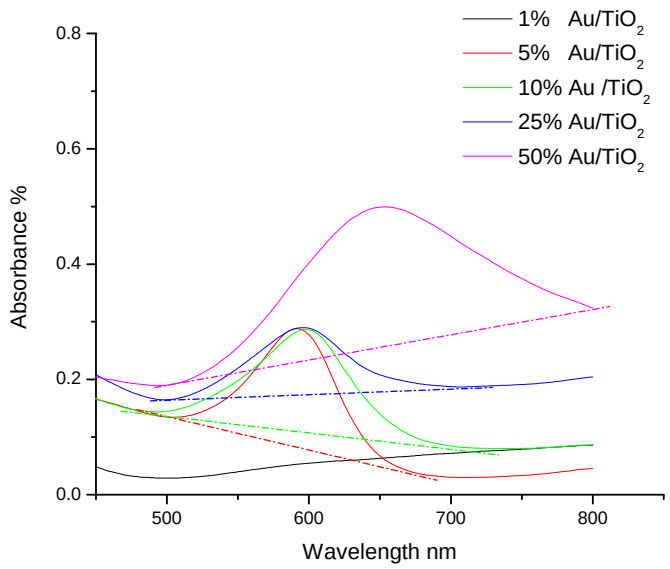

Figure4-14 Optical absorption spectra of as-deposit Au/TiO_2 composite films measured by UV-visible spectroscopy.

From Figure 4-14 it appears that the SPR signal's intensity, width and red-shifting are all related to the Au concentration, i.e. the results from this present study indicate that the width of the peaks are proportional to the total volume of individual Au particles.

As shown in Figure 4-4, increasing Au concentration levels led to gold dominated surfaces and wider particle size distributions. As a result, the collective effect of the resonance from these Au particles with different particle sizes forms a broad and intense SPR peak. Also, as the volume of Au particles on the surface increases so does the summation of the SPR activity, as well as the observed intensity. In contrast, relatively little aggregation occurs in composite films with low Au concentrations so these have a narrower distribution of Au particle sizes and thus show a sharper SPR peak. Finally, because the low Au concentration composite films have lower volumes of Au particles the intensity of the SPR signal is lower.

The SPR spectra of composite films after sintering at 500^{o}C and 800^{o}C are illustrated in Figure 4-15 and Figure 4-16 respectively. The tendency of the shift of SPR peak wavelength with Au concentration is similar to that of the as-deposited films shown in Figure 4-17 and discussed above. However, as shown in Figure 4-17 all the SPR peaks of the sintered films are red-shifted relative to those of the as-deposit films, with the shift being larger after sinter at 800^{o}C than at 500^{o}C. To illustrate this clearly, a series of UV spectra of Au/TiO_2 composite films before and after sintering are shown in Figure 4-17. This red-shift on sintering is consistent with the observed increase in Au particle size reported in Section 4.3.

Sintering the composite films caused crystallization of the TiO_2 matirx from amorphous to anatase; as confirmed by the XRD and Raman spectra presented in Section 4.3 and 4.4. This crystallization will have caused the dielectric constant of matrix to increase[14], which according to Equation 4.4 will red-shift the SPR peak

wavelength. Hence the red-shift between the as-deposited and sintered samples results from a combination of increased Au particle size and crystallization of the TiO_2 matrix. It is also evident from Figure 4-14, 4-15, and 4-16 that the SPR intensity in the sintered films was stronger than that in their as-deposit counterparts. The confinement of Au particles by the matrix does not change, i.e. ε_{matrix} in equation 4.4 remains constant, so in this case the SPR intensity can be mainly attributed to the Au particle size. However, in this present study, after sintering, the TiO_2 matrix underwent a phase transition, from amorphous to anatase, on heating and thus the Au particles became confined in a denser phase, which increased the interaction between the Au particles and the matrix.

However, the behavior of the 25% Au composite film did not follow the trend expected from the other compositions, it is having a smaller SPR peak than expected. This may be due to the few large very Au particles in the 25% composite film (even larger than see in the 50% film Section 4.3) that could scatter the light and thus decrease the observed SPR intensity. Furhtermore, in addition to the few very large particles (>100nm; that may be too large to give SPR) the 25% composite films still contains many small Au particles that were of a similar size as those in the 5% composite films. This explains why the SPR peak wavelength is in a similar position to the 5% Au composite films, i.e. SPR position is still a function of the effective Au particle size.

TEM also revealed that with high Au concentrations the distance between Au particles was less than that in dilute composite films, thus any interface effects between Au particles cannot be ignored in this study. Furthermore, the TEM diffraction pattern

showed that the extent of TiO_2 crystallization decreased at higher Au levels (Figure 4-12). These results indicate that the SPR performance of the Au/TiO_2 composites does not only depend on the Au particle sizes, as described in Mie's theory, but is also related to the interface effects between both Au-Au particles and Au-TiO_2 particles. This is consistent with Ung *et al*'s[15] effective medium theory (MG theory), which is an extension of Mie's theory.

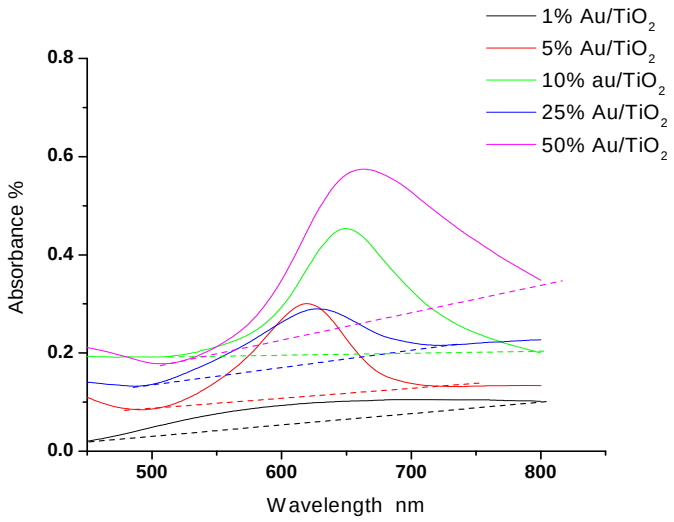

Figure4-15 UV-visible spectra of Au/TiO_2 composite films deposited on quartz glasses taken 500 ^oC sintering for 30mins.

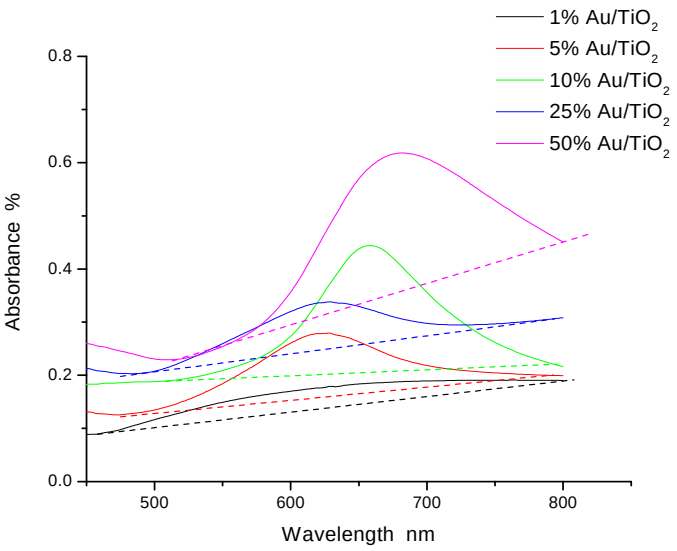

Figure4-16 UV-visible spectra of Au/TiO_2 composite films deposited on quartz glasses taken 800 ^oC sintering for 30 mins.

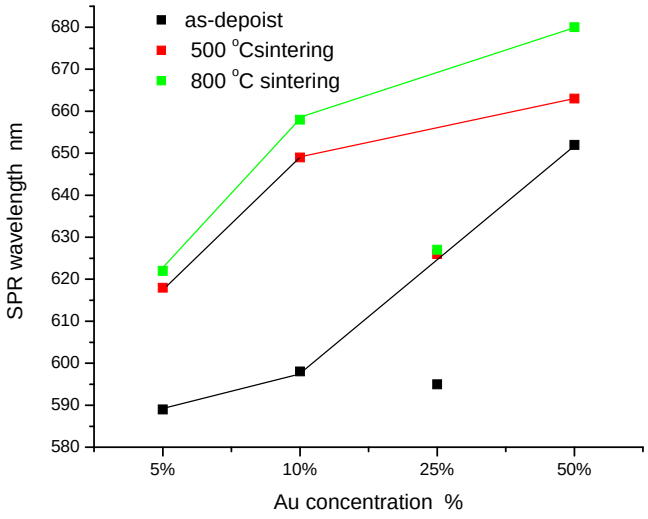

Figure4-17 Wavelength change of Au/TiO_2 composite films after different heat treatments.

4.7 Band gap of composite films

The magnitude of the band gaps of the TiO_2 in the composite films formed at different sintering temperatures were measured by the method introduced in Chapter 3, Section 3.5 and illustrated in Figure 4-18 line A. For pure TiO_2 films (i.e. no gold), it shows that the band gap was decrease with increasing sintering temperature, since the crystal structure of TiO_2 is changed with the sintering temperature, i.e as-deposited TiO_2 is amorphous, forms anatase structure after 500°C sintering and forms rutile after 800°C sintering[4]. These structures are different from each other in terms of density and atomic arrangement. Among these three films, rutile has the most compact density and the smallest interstitial distance of atoms. The crystallization of the TiO_2 influences the electron distribution and thus its band gap structure, e.g. rutile has a band gap of 3.05 eV whereas the less dense anatase has a wide band gap of 3.2 eV.

Similarly, for the Au containing composite films, the band gap of films shows a red-shift with decreasing Au concentration, as shown in Figure 4-18 line B. However, a

comparison of lines A and B in Figure 4-18 shows at all gold levels the band gap is closer in value to that of the amorphous pure TiO_2 than either of the two crystalline forms. This is consistent with the insertion of Au particles decreasing the crystallization of TiO_2, as discussed in Section 4.4. Although the particle size of TiO_2 also decreased on increasing the Au concentration, the large magnitude of the effective mass of an electron in TiO_2 means it is unlikely that a quantum size effect will induce a significant change in its band gap[16]. Therefore, in this study, the influence of Au particle on the band gap is believed to be mainly due to its influence on the TiO_2's crystallization.

Moreover, in TiO_2, both the valence band (VB) and conduction band (CB) contain contributions from the O 2p and Ti 3d orbitals, indicating hybridization between these states, which also means that transitions across the band gap will involve both O 2p and Ti 3d states. The electronic and optical properties of TiO_2 may be altered considerably by doping and/or defect structures. The dopant may either be inserted substitutionally or interstitially, whilst defects may be created by the removal of atoms from the lattice. In TiO_2 the defects could be oxygen vacancies or Ti cation interstitials. It was reported by von Oertzen *et al.*[17], that oxygen vacancies influence the energy gap, but Ti interstitials do not. The bottom of the CB, mainly from the Ti 3d orbital, is populated increasingly with increasing vacancy concentration. The occupation of the bottom of the CB by electrons would lead to a significant reduction in the photon energy required for electron excitation and hence associated photocatalytic reactions. Early experiments by Cronemeyer demonstrated that the reduction of rutile by heating removes oxygen atoms from the crystal structure, resulting in a blue color[18].

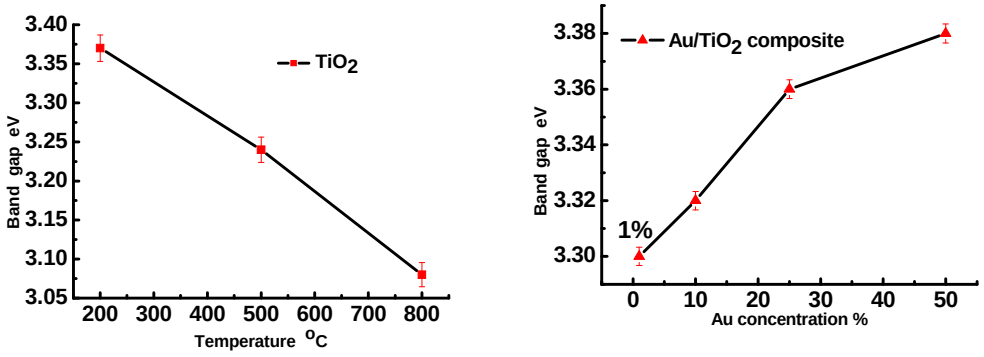

Figure4-18 Band gaps of pure TiO_2 film after different crystallization treatments (left) and composite films with different Au concentrations after 500 °C sintering (right).

4.8 Surface states of Au/TiO_2 composite films

To further analyze the electronic surface states of composite films, X-ray Photoelectron Spectroscopy (XPS), Ultra-violet Photoelectron Spectroscopy (UPS) and photoluminescence (PL) measurements were performed.

4.8.1 Influence of Au particles on the XPS spectra

Figure 4-19 illustrates the XPS profile, along with a fitting simulation (using software *XPSPEAK Version 4.0*), of Au $4f_{7/2}$ in a 50% composite films sintered at 500 °C. The binding energy peak displays the typical XPS profile of Au^0 ($4f_{7/2}$=84.0eV with Δ=3.67eV)[19] and the simulation graph confirms a single chemical state of Au^0. This indicates that the Au precursor was completely reduced and that the Au particles did not undergo oxidation during sintering. Figure 4-20 shows Ti binding energy profiles, with simulations, of composite films with different Au concentrations. The typical binding energy of Ti in TiO_2 is 458.8 eV (2p3/2=458.8eV, $\Delta = 5.54$eV)[19]. It can been seen that the Ti binding energy for the TiO_2 sample without Au coincides with the reference and shows a single chemical state Ti^{4+}. However, with increasing Au

concentration, the XPS peak shifts to lower binding energies and splits into two chemical states (Ti^{4+} and Ti^{3+}). The introduction of the Ti^{3+} chemical state could be due to surface strain and lattice distortion induced by the incorporation of the Au particles into the matrix. Here, surface strain is more likely than lattice distortion as the Au was not incorporated into the lattice. The reason for binding energy shift is that the electrons with Ti^{4+} feel a higher attractive force from the nucleus than the electrons in the Ti^{3+} [20]. As studied by Wang and Hwang, Au tends to attach to TiO_2 particles by binding with O vacancy sights, cause a reconstruction in the arrangement of surface atoms in the TiO_2 leading to a change in surface chemistry [21]. If surface O atoms are removed from the lattice, the two electrons previously associated with the anion have to be retained in the lattice in order to preserve electric neutrality. There is some debate as to whether these electrons are associated with a vacancy site to form Vo^{2+} donor sites, or whether two adjoining Ti^{4+} atoms are transformed into two Ti^{3+} sites[22]. In this present study, the situation is more reasonable if explained by the latter.

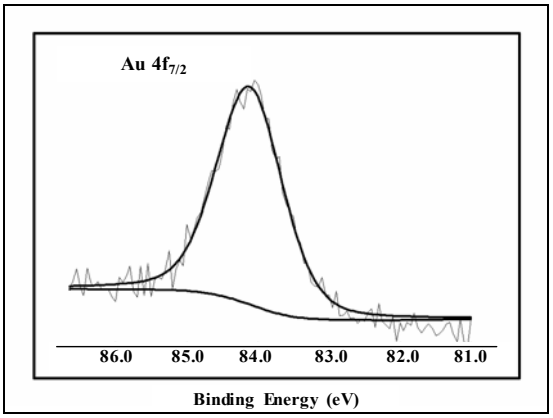

Figure4-19 XPS profile of Au $4f_{7/2}$ of 50% Au/TiO_2 composite film.

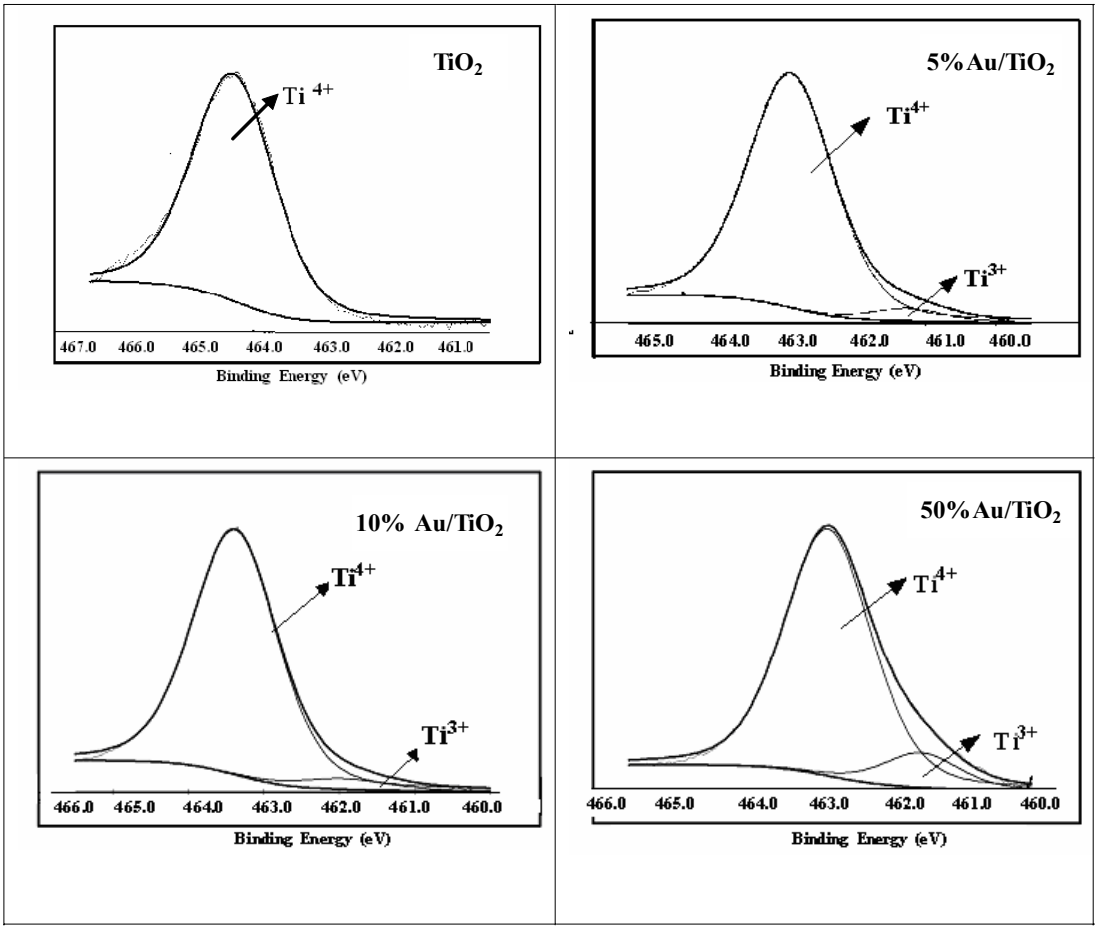

Figure4-20 XPS spectra with simulation of TiO_2 film and Au composite films after 500 ^oC sintering.

4.8.2 Influence of Au particles on the UPS spectra

Figure 4-21 illustrates the UPS spectra of composite films sintered at 500 ^oC which reveals the density of states of the valence band. The spectra were analyzed as shown in Chapter 3 Section 3.4.3. The secondary electron cut-off point corresponds to loss of electrons, which had just enough kinetic energy to overcome the work-function of the substrate. The cut-off in spectra was employed to derive values of the ionization energy (Φ) of the composite films by subtracting off the width of spectrum from the energy of the incoming UV photon (21.2eV). For the pure TiO_2 specimen Φ=3.2eV is found, whereas for the 5%Au/TiO_2 and 50%Au/TiO_2 composites values of Φ were 4.2eV and 4.7eV respectively. As shown in Figure 4-21, the cutoff is shifted to low

binding energy with Au concentration increasing. This indicates that work function of composite film is increased with Au concentration increasing. This result is similar as the case of Pt/TiO_2, in which the work function increase was contributed to the trapping of the accompanying electrons to the Pt clusters[23].

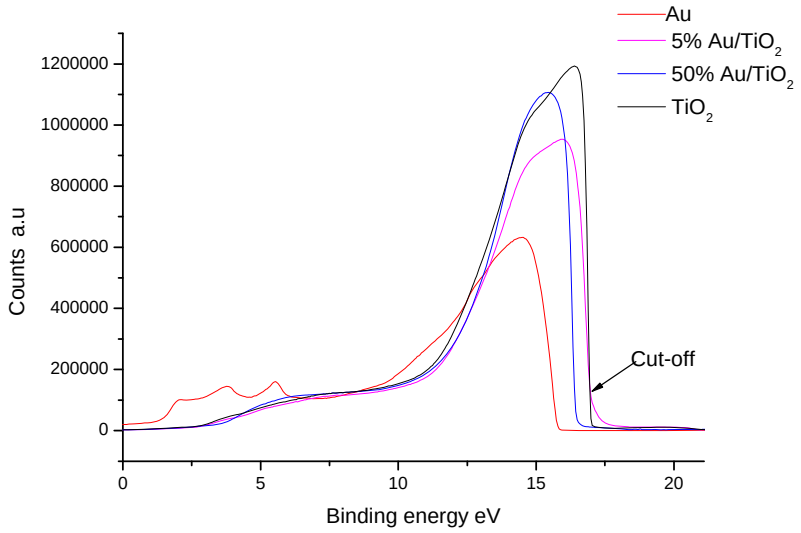

Figure4-21 UPS spectra of Au/TiO_2 composite films

4.8.3 Influence of Au particle on the Photoluminescence spectra

No luminescence appears in conventional bulk TiO_2, but nanostructured TiO_2 presents luminescence phenomena. This is due to the fact that a large number of interfaces, with more random atomic arrangements, lead the translation periods in these regions to be substantially broadened. This mean new luminescence bands caused by some electronic transitions, which are forbidden in conventional materials, can be observed for nanostructured TiO_2 [24]. Also, the surface states responsible for the visible emission are likely to be formed by surface unsaturated atoms on the TiO_2 nanocrystallites, related to Ti^{4+}, $Ti^{3+}$and Ti^{2+} [25]. Figure 4-22 presents the recorded photoluminescence (PL) spectra. It can be seen that there are three main peaks in these spectra: Peak A

370~450nm; Peak B 450~550nm; and Peak C 550~650nm. Zhang *et al.*[24], reported that Peaks A and B are due to Ti^{3+} and Ti^{4+} respectively. Peak C in the 550~650nm range is due to surface plasmon resonance from the gold particles; excited by the 514nm Ar-ion laser used to collect the Raman spectra spectral band of Au that is its resonance[26].

The 1% Au sample showed strong PL for both peak A and peak B, however, the addition of higher levels of Au led to a dramatic decrease in PL intensity. The effective quenching of the nanocrystalline TiO_2 photoluminescence by the Au can be attributed to the two following pathways[27]. Firstly, the electron is trapped by the oxygen vacancy, while the hole is trapped by the doped Au particle. Secondly, the excited electron can transfer from the valance band to the new levels that exist above the conduction band introduced by doped Au particles, which can also decrease the photoluminescence. Nevertheless, Figure 4-22 does suggest that for Au levels above 10% Peak A recovers to some extent, whilst Peak B continues to be quenched. This could be interpreted as a transformation of some of the Ti^{4+} and Ti^{3+}, which would be in good agreement with XPS data presented above.

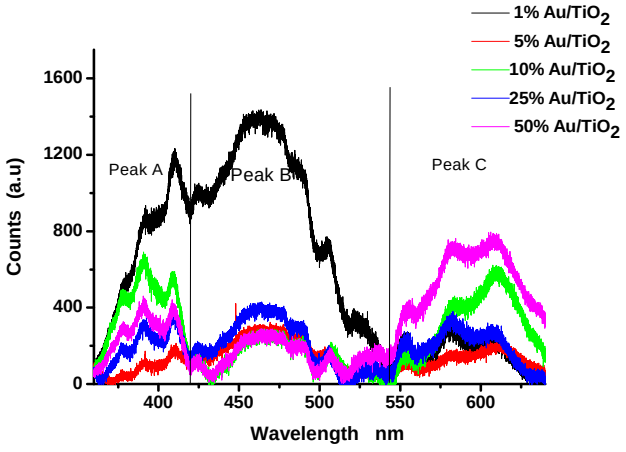

Figure4-22 Photoluminescence of Au/TiO_2 films under UV radiation (325.15nm).

4.9 Summary

In this chapter, the influence of adding Au particles to TiO_2 films prepared by sol-gel method was investigated. TEM and XRD data revealed that generally the Au particle size increased as its concentration. The exception to this was the 25%Au level, which had few Au particles that were even larger than in the 50%Au composites. As yet it is unclear why the 25%Au loading had larger particles than the 50%Au films, possibly it is related to the nucleation and growth of the particles. For example, it may be that up to a loading of 25% nucleation is rate determining, this would lead to a small number of large particles, but if at very high Au levels may be growth dominates over nucleation there would be a large number of smaller particles.

The crystallization of TiO_2 matrix was found to decrease as the size of the Au particles increased, with the least crystallization with 25%Au, i.e. the composition that contained the largest Au particles, rather than at 50%, i.e. the highest Au loading. This suggests that the distortion from a small number of large Au particle size out weighs the distortion from a larger number of smaller particles. Optical absorption measurements revealed that the TiO_2's band gap increased as crystallinity decreased due to the presence of large Au particles.

With respect to the SPR emitted by the Au particles, it was found that its intensity was not only a function of the Au particle size, but also their concentration and the crystallinity of the TiO_2 matrix. The SPR peak wavelength was observed to red shift as the average Au particles size increased. Again the SPR from the 25% Au loading requires a further explanation, as although it had the largest Au particles its SPR peak wavelength did not red-shift as much as anticipated; in fact it was close to that of the

5% Au specimen. However, TEM images revealed that as well as the few very large particles the 25%Au composite also contained many much smaller ones, which were of a similar size to those observed at 5%Au loadings. It is thus postulated that it is these smaller Au particles that dominate the SPR signal, in deed it is possible that the larger (>100nm) ones are too large to produce the SPR effect, i.e. they may take on the properties of bulk gold. Furthermore, the weak intensity of 25%Au SPR may be because the large Au particles cause scattering of the emitted light.

The nature of surface states present in a TiO_2 film were also investigated, as these are important to both dye attachment and electron transport. It has been shown that the addition of Au particles introduced additional surface states into the TiO_2 films. From the result of the XPS and photoluminescence investigations it was postulated that the Au particles caused some of the Ti^{4+} surface states to split into a mixture of Ti^{4+} and Ti^{3+} states. A possible explanation for the extra Ti^{3+} states could be that the Au particles prefer attach to the oxygen vacancies of the TiO_2 and in doing so create the Ti^{3+} state. Because Ti^{4+} acts as in the TiO_2's conduction band it is possible that the Au induced Ti^{3+} states effect the valence band in the semiconductor and thereby influence the efficiency of metal ligand charge transfer reactions.

The conclusion for this chapter could be:

Au particle size was increased with the Au concentration due to the aggregation. The addition of Au particles in the TiO_2 film would induce the surface plasmon resonance （SPR） in the visible region. This SPR intensity was relative to the Au particle size and Au particle concentration, but the SPR peak position was only dependent on the Au particle size. The addition of Au particles also influences the properties of TiO_2.

film. TiO_2 particle size change was relative to Au concentration. The smaller Au particle size gave more confinement on the TiO_2 particle growth, and hence made the crystallization of TiO_2 film decrease. With the increase of Au concentration in the composite film, the surface state of TiO_2 film was changed from Ti^{4+} into Ti^{3+} and Ti^{2+}.

Reference

(1) Johnson, B. F.; Davis, F. D. *Comprehensive Inorganic Chemistry*; Pergamon: New York, **1973**.

(2) John D. W.; A., N.; Sommerdijk, J. M. *Sol-Gel Materials Chemistry and Applications*; Gordon and Breach Science Publishers: Netherlands, **2001**.

(3) Zhao, G.; Kozuka, H.; Yoko, T. *Sol. Energy Mater. Sol. Cells* **1997**, *46*, 219-231.

(4) Kalyanasundaram, K.; Grätzel, M. *Coord. Chem. Rev.* **1998**, *177*, 347-414.

(5) Bersani, D.; Antonioli, G.; Lottici, P. P.; Lopez, T. *J. Non-Cryst. Solids* **1998**, *232-234*, 175-181.

(6) Bersani, D.; Capelleti, R.; Lottici, P. P.; Gnappi, G.; Montenero, A. *Mater. Sci. Forum* **1997**, 87, *239-241*.

(7) Zhang, W. F.; He, Y. L.; Zhang, M. S.; Yin, Z.; Chen, Q. *J. Phys. D: Appl. Phys*. **2000**, *33*, 912-916.

(8) Fleischmann, M.; Tian, Z. Q.; Li, L. J. *J. Electroana. Chem.,* **1987**, *217*, 397-410.

(9) Nyquist, R. A. *The Handbook of Infrared and Raman Spectra of inorganic Compounds and Organic Salts*; Acadmic Press: San Diego, **1997**.

(10) Cullity, B. D. *Elements of X-Ray Diffraction*; Third edition ed.; Prentice-Hall International: London , **2001**.

(11) Kreibig, U.; Vollmer, M. *Optical Properties of Metal Clusters*; Springer: Berlin, Germany, **1995**.

(12) Hövel, H.; Fritz, S.; Hilger, A.; Kreibig, U.; Vollmer, M. *Phys. Rev. B* **1993,** 4*8,* 18178 LP-18188.

(13) Chen, W.; Cai, W.; Wang, G.; Zhang, L. *Appl. Surf. Sci.* **2001,** *174,* 51-54.

(14) Xu, X. H.; Wang, M.; Hou, Y.; Zhao, S. R.; Wang, H.; Wang, D.; Shang, S. X. *Cryst. Res. Technol.* **2002,** 3*7,* 431-439.

(15) Ung, T.; Liz-Marzan, L. M.; Mulvaney, P. *J. Phys. Chem. B* **2001,** *105,* 3441-3452.

(16) Memming, R. *Semiconductor Electrochemistry;* WILEY-VCH: Weinheim, **2001**.

(17) von Oertzen, G. U.; Gerson, A. R. *J. Phys. Chem. Solids* **2007,** *68,* 324-330.

(18) Cronemeyer, D. C. *Phys. Rev.* **1959,** *113,* 1222 LP - 1226.

(19) Moulder, J. F.; Stickle, W. F.; Sobol, P. E.; Bomben, K. D. *Handbook of X-ray Photoelectron Spectroscopy;* Perkin-Elmer Corporation: Eden Prairie, **1992**.

(20) Niemantsverdriet, J. W. *Spectroscopy in Catalysis;* Wiley-VCH Verlag GmbH: Weinheim, **2000**.

(21) Wang, Y.; Hwang, G. S. S*urf. Sci.* **2003,** 5*42,* 72-80.

(22) Grant, F. A. *Rev. Mod. Phys.* **1959,** 3*1,* 646- 674.

(23) Hiehata, K.; Sasahara, A.; Onishi, H. *Nanotechnology* **2007,** *18,* 084007.

(24) Zhang, L. D.; Mo, C. M. *Nanostructured Materials Proceedings of the Second International Conference on Nanostructured Materials* **1995,** 6*,* 831-834.

(25) Zhang, W. F.; Zhang, M. S.; Yin, Z.; Chen, Q. *Appl. Phys. B: Lasers Opt.* **2000,** *70,* 261-265.

(26) Liao, H. B.; Wen, W. J.; Wong, G. K. L. *J. Opt. Soc. Am. B* **2006,** 2*3,* 2518-2521.

(27) Cong, Y.; Zhang, J.; Chen, F.; Anpo, M. *J. Phys. Chem. C* **2007,** *111,* 6976-6982.

Chapter 5 Effect of Au nanoparticles on photon-electron conversion

In this chapter the influence of Au nanoparticles on the photon-electron conversion was investigated by measuring the electrochemical behavior and photocurrent characteristics of composite films, both in the absence and presence of a dye sensitizer. The experiments were capable of revealing the influence of Au nanoparticles on electron-hole separation and recombination processes as well as on the surface states of the composite films, which can indirectly influence the photon-electron conversion. The experiments were carried out on the composite films directly deposited on the ITO conductive glasses. Unfortunately, the Au nanoparticles were found not to be as beneficial as anticipated, therefore a modification was made to the composites to try to improve photon-electron conversion. This was the introduction of an extra TiO_2 blocking layer between the composite layer and the back contact electrode. These modified structures are denoted as Au/TiO_2-TiO_2 composite films. The influence of the blocking layer on the Au/TiO_2 composite film is reported towards the end of this chapter.

5.1 Influence of Au particle on the open-circuit potential of TiO_2 films

Figure 5-1 illustrates the relationship of Au particle size with the open circuit potential of the composite films in 0.5M Na_2SO_4 in the dark current and under 340nm light irradiation. It can be seen that at small Au particles distributed in the composite films adopted more negative open-circuit potentials than a pure TiO_2 film, but with big Au particle the films took up more positive potentials. Under 340nm illumination the open-circuit potentials of all the films showed negative shifts, consistent with a n-type

semiconductor in which Fermi level will move to negative direction under irradiation. Furthermore, Figure 5-1 also shows that the magnitude of the photovoltage ($|V_{oc,dark}|$-$|V_{oc,light}|$) generally increased with Au particle size; the exception being the 25% Au composite with largest Au particle size (around 90nm) that showed the smallest photovoltage.

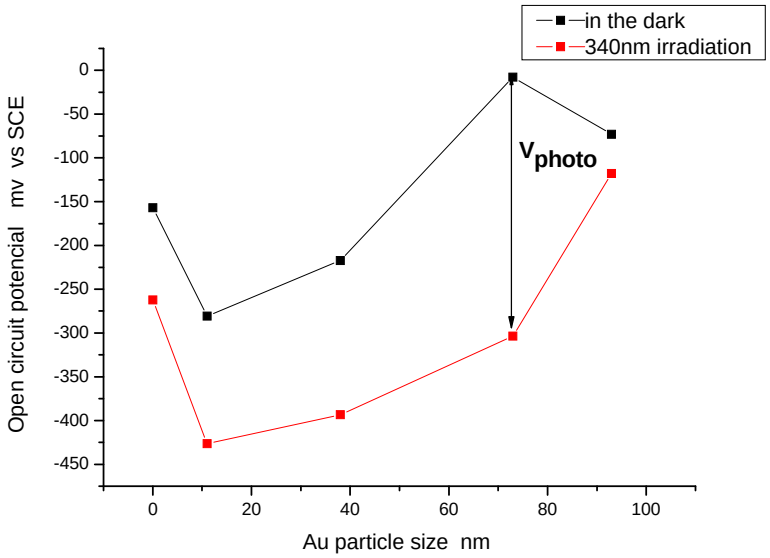

Figure 5-1 Open-circuit potential s displayed by Au/TiO_2 composite films in 0.5 M Na_2SO_4 as a function of Au particle size in the dark and under 340 nm irradiation. The difference between light and dark conditions yields the photovoltage.

Table 5-1 Photovoltage of composite films

Au concentration of composite films (%)	TiO_2	1%Au/TiO_2	5%Au/TiO_2	25%Au/TiO_2	50%Au/TiO_2
Photovoltage of composite films without dye-sensitization (mV)	105	145	176	44	295

The magnitude of the photovoltage represents the energy difference between the Fermi-level of the TiO_2 film and SCE （Saturated Calomel Electrode） reference electrode in the electrolyte under irradiation, thus the larger phototovoltages with Au additions suggest more negative Fermi-levels in the composite films. This is consistent

with the results obtained by Kamat *et al*.[1], whose previous studies showed that noble metal or metal ion doped semiconductor nanocomposites exhibit negative shifts in their Fermi levels compared to the pure semiconductor. By shifting the Fermi level closer to the conduction band, semiconductor-metal composites facilitate charge rectification and improve the photocatalytic efficiency. In the present study, it was found that low levels of Au caused a negative shift in the Fermi-level. This could be the result of a higher degree of electrons accumulating at the composite/electrolyte interface with Au particles causing the composite system be more reductive than the pure TiO_2 system.

Returning to the positive shift in the open-circuit potential caused by the larger Au particles relative to pure a TiO_2 film, especially for 70nm size and 90nm size of Au partilces. A positive shift in the open-circuit potential should mean increased band bending, which gives a greater potential for photovoltage (although not seen for the 90nm Au composite) and this is beneficial to solar cells. For 70nm Au composite film, the good conductivity of the Au dominates, forming a Schottky barrier at the TiO_2 surface, which increases band bending of space charge layer and thus shift open-circuit potential positively allowing the large photovoltage. The lack of a large photovoltage in the 90nm Au composite can be explained by reference to its TEM cross-section image of 90nm Au composite film in Figure 5-2. This appears to show that the large Au particles dispersed in the film are connected to each other forming a net with the back contact electrode. In metal electrodes, electron transfer occurs mainly around the Fermi level and is independent of illumination[2]. So the continuous Au network could mean that the observed small photovoltage is controlled by the ITO glass back contact rather than the TiO_2 in the composite.

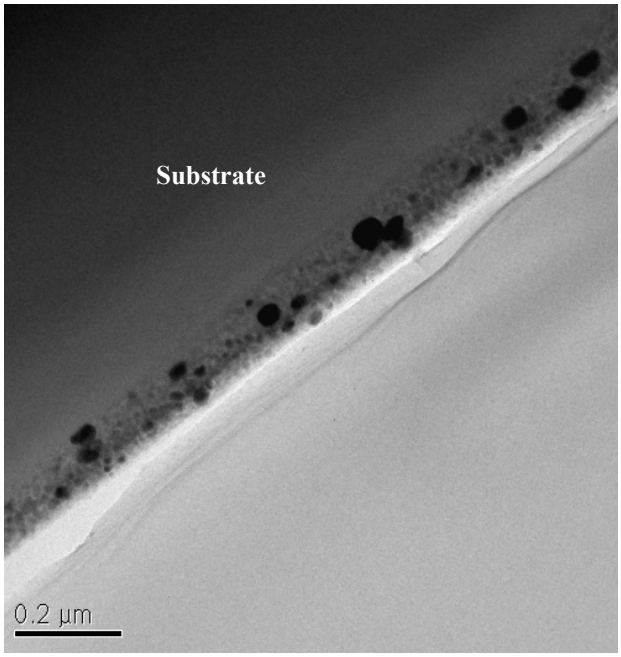

Figure 5-2 TEM cross section view of 25% Au/TiO_2 composite film with average 90nm Au particle size.

5.2 Influence of Au particle on the polarization behavior of TiO_2 films

Figure 5-3 shows cyclic voltammograms for Au/TiO_2 composite films in 0.5M Na_2SO_4 in (a) the dark and (b) under illumination at 340nm. It can be seen that in the dark all the samples showed the typical rectifying behavior of an n-type semiconductor. However, the result of adding Au particles was not that which might be expected, the addition of 1% gave rise to an anodic wave at about 0.0V vs. SCE, but further additions of Au caused the magnitude of this feature to decrease significantly as well as its onset to shift to more positive potentials. A possible explanation for this anodic wave is that is the oxidation of the Au nanoparticles to AuO. Although this would not be expected at such low potentials with bulk gold, surface energy size effects may allow the early oxidation of nanopartilces. Such an explanation is consistent with the decrease in magnitude and positive shift of the oxidation wave with increasing Au content and thus larger particle size (See Chapter 4, Section 4.5). Under 340nm

irradiation, the addition of the Au particles significantly reduced the magnitude of the photocurrent obtained, as compared with the pure TiO_2 film.

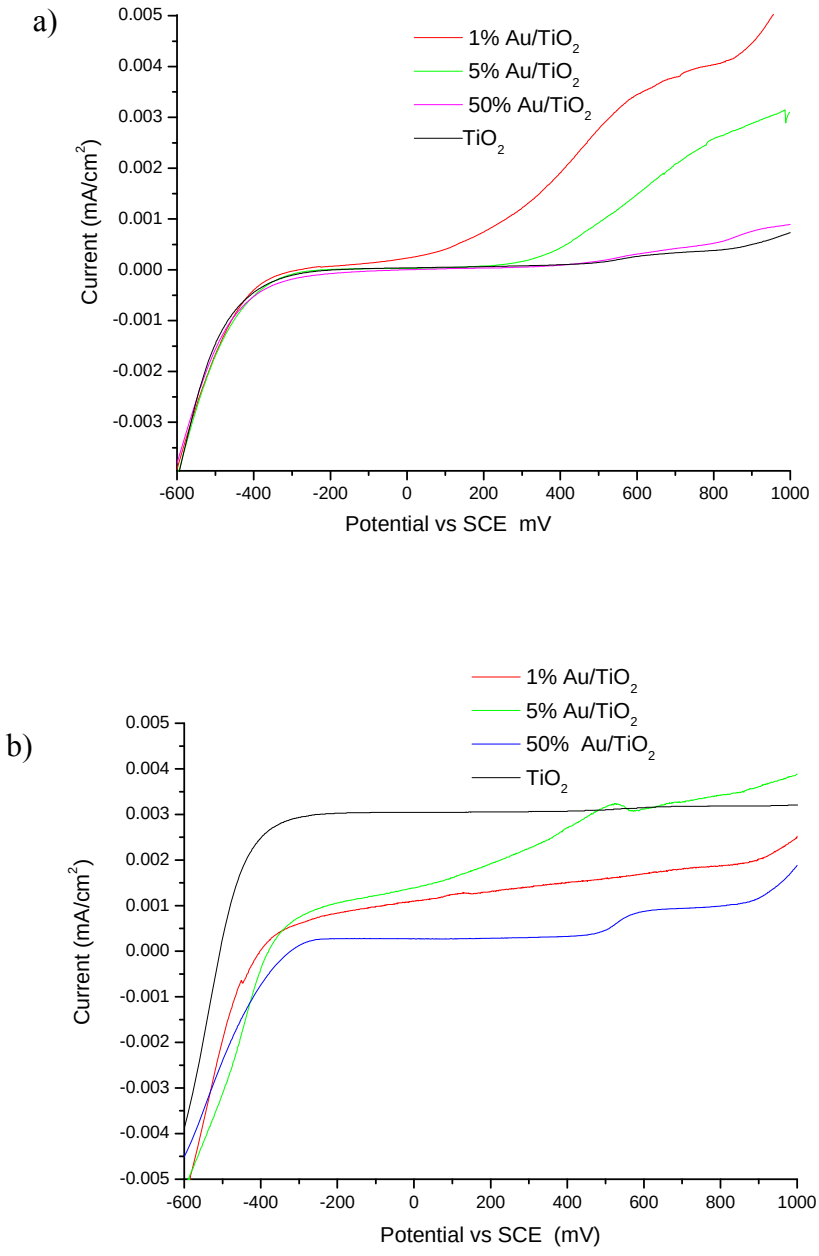

Figure 5-3 I-V curves for Au/TiO_2 composite films in 0.5M Na_2SO_4 a) in the dark and b) under 340 nm irradiation.

5.3 Influence of Au particles on the impedance measurement of TiO_2 films

The expected equivalent circuit for the compact composite films is illustrated in Figure 5-4 where R_{sol} is the solution resistance, R_{ox} is the leakage resistance of the composite

film, R_{ct} is the charge transfer resistance which is inversely proportional to the reaction rate, C_{ox} the capacitance of the composite and C_{dl} is the double layer capacitance. The introduction of the conductive Au particles into the film should reduce the magnitude of R_{ox} but increase that of C_{ox} (large Au/TiO_2 interface area can potentially store additional charge), both of which lead to a decrease in the impedance of the composite. Therefore at high Au levels the EIS response should be dominated by R_{ct} and C_{dl}, whilst at lower Au concentration R_{ox} and C_{ox} will contribute more strongly and perhaps even dominate. Each of the two parallel RC networks in the circuit will have their own time constants ($\propto {}^{1}/_{RC}$), if these are significantly different one could see two semicircles in a Nyquist plot (Z_{real} vs $-Z_{imaginary}$)

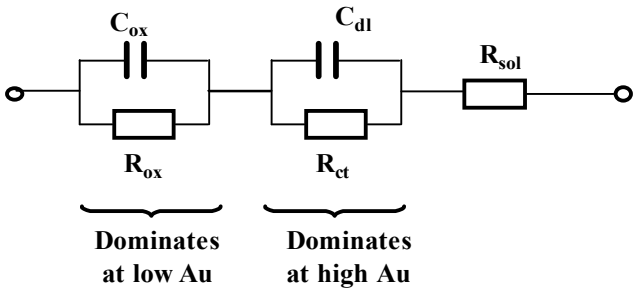

Figure 5-4 Illustration of equivalent circuit of reaction at the composite/electrolyte interface. R_{sol} is the solution resistance, R_{ox} is the leakage resistance of the composite, R_{ct} is the charge transfer resistance, C_{ox} the capacitance of the composite and C_{dl} is the capacitance of double layer.

Figure 5-5 illustrates Nyquist diagrams of Au composite films over the frequency range 0.1Hz to 10 kHz in 0.5M Na_2SO_4 solution; see Chapter 3 Section 3.5 for the experimental arrangement. The Nyquist plots on the present compact electrodes consist of a single semicircle, in contrast to the double semicircles reported in previous works on porous TiO_2 films[3,4]. The single semicircle implies either one of the two parallel RC networks dominates over the whole investigated frequency, or the two times constants are sufficiently close so that the two semicircles cannot be resolved and merge together. Evidence for the latter explanation comes from the observation

that the single semicircles are slightly flattened (their height is less than half their extrapolated diameter) indicating that these could be two merged semicircles.

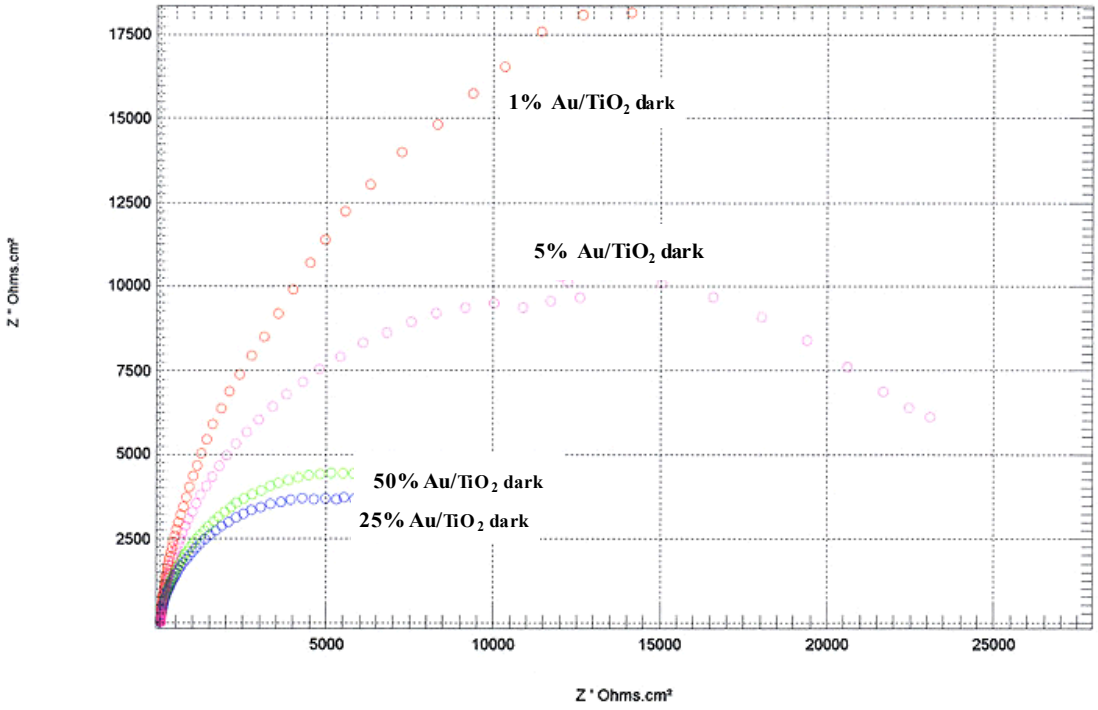

Figure 5-5 Nyquist plots of Au composite films in 0.5M Na_2SO_4 measured under dark condition.

As it was not possible to resolve the Nyquist plot, it was decided to define a total polarization resistance, R_p, ($R_p = R_{ct} + R_{ox}$) which could be obtained from the extrapolated diameters of the semicircles, and a total interface capacity C, ($1/C \approx 1/C_{ox} + 1/C_{dl}$) which could be obtained from the apex of the semicircles (the angular frequency of which is equal to $^1/_{RC}$); in practice a software package was used to simulate the Nyquist plots and extract R_p and C values. The polarization resistance is a measure of the conductivity of the composite films, whilst the interface capacity is proportional to the how fast the charges move away the interface. Figure 5-6 shows the dependence of R_p on the Au level in the composite films and it can be seen that R_p falls by up to an order of magnitude as the first 5% Au is added, but further additions have less effect. Furthermore, it was found that if the EIS experiments were repeated

whilst the composites were illuminated with UV light the R_p values decreased, consistent with the photogeneration of carriers that should reduce R_{ox}. However, the R_p of composite films with high Au level were less sensitive to the light, reflecting the increased metallic character of Au particles; i.e. R_p is becoming dominated by R_{ct}. From the polarization resistance spectra, it indicates the higher the polarization resistance more current required to move the potential, so that the more photons are required to shift the V_{oc}.

Figure 5-7 shows how the interface capacitance depends on Au concentration whilst illuminated by 340nm irradiation. At low Au levels C_{ox} dominates, which mainly consists of the space charge capacitance[2], the magnitude of which depends on the electrode's potential. However, with increasing Au concentrations, the composite surface becomes dominated by the metallic Au particles and the interface capacitance reflects the Helmholtz double layer, which is unlikely to vary significantly with film composition and is almost independent of variations in the electrode's potential.

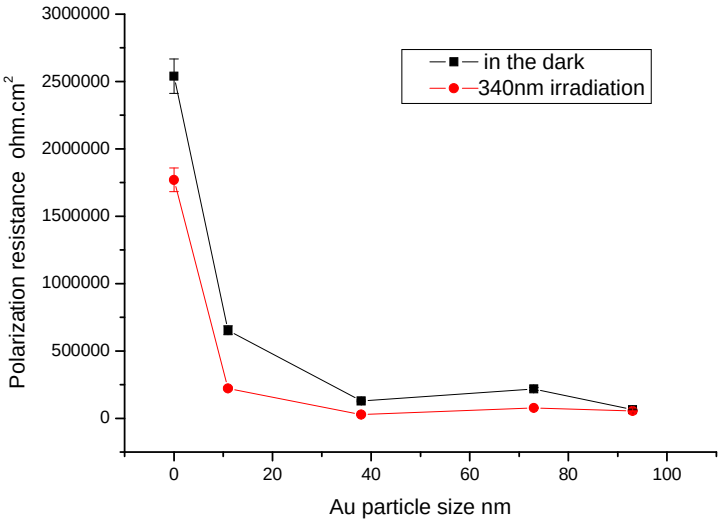

Figure 5-6 Influence of Au particle size on the polarization resistance in the dark and under 340 nm irradiation.

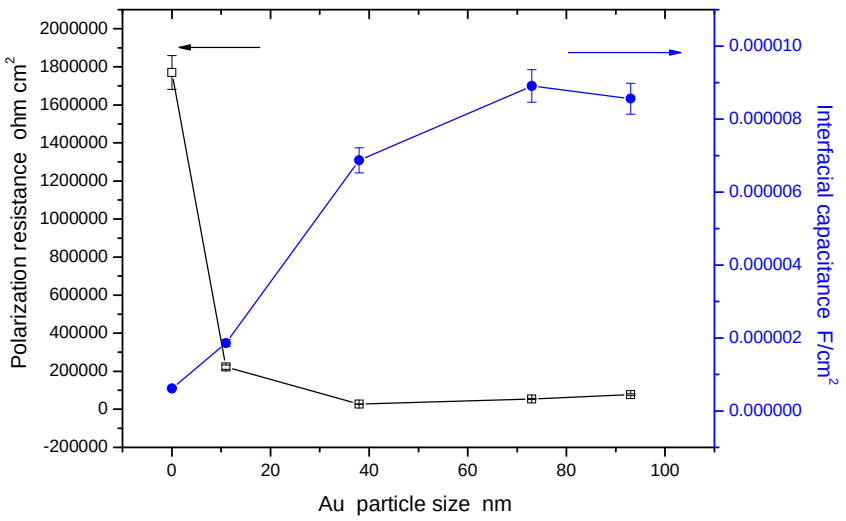

Figure 5- 7 Influence of Au particle size on the polarization resistance and interfacial capacitance under 340 nm light irradiation.

5.4 Influence Au particle on the flat-band and carrier density

The electrochemical behavior of a semiconductor is mainly determined by its flat-band potential V_{fb}, the band gap and charge carrier density N (N_D or N_A). Hence, a detailed knowledge of these parameters is indispensable for an understanding of a material's electrochemical behavior.

The flat-band potential V_{fb} can be determined according to Equations (5.1, 5.2) by extrapolation:

$$\frac{1}{C_{SC}{}^2} = \frac{2}{\varepsilon_S \varepsilon_0 e N_D S^2}(V_B - V_i) \qquad (5.1)$$

Where V_B is the electrode potential and the intersection potential V_i is refer to V_{fb} by;

$$V_i = V_{fb} + \frac{kT}{e} \qquad \cdots\cdots\cdots\cdots\cdots\cdots \qquad (5.2)$$

Where k is the Boltzmann constant, T is the temperature, and e is the elementary charge. Determination of the V_{fb} according to Equation (5.1, 5.2) is correct when the

space charge layer capacitance is small compared with Helmholtz layer capacitance such that the potential drop caused by the applied potential falls entirely across the space charge region within the semiconductor. Figure 5-8 shows Mott-Schottky plots for the Au/TiO_2 composite films collected at a frequency of 10Hz. It can be seen that there appears to be two linear regions with different slopes, however, the intercept on the potential axis of the lower region appears is independent of the Au concentration at -500mV and this is believed to represent the flat-band potential of the TiO_2 portion of the composite. The positive slopes of the Mott-Schottky plots are consistent with an n-type semiconductor, which is as expected for TiO_2.

Returning to the appearance of two linear regions in the Mott-Schottky plots, the slope indicates the donor/acceptor density in the space charge region near the surface and deviations from a single linear slope are known to result from a number of different phenomena, for example inhomogeneous doping (e.g. a deep donor level) or surface reactions[2]. Table 5.2 shows the donor densities extracted from both the upper (N_D2) and lower regions (N_D1) and these are displayed graphically as a function of Au concentration in Figure 5-9; the dielectric constant of anatase, 55[5,6], was used in the calculations. It can be seen that except for the Au highest loading (50%，average particle size 70nm) the N_D1 values are almost independent of Au level at about 2 x10^{18} cm^{-3}, which is around an order of magnitude above that normally reported for pure TiO_2 crystalline films (typical 2 to 5 x$10^{17}cm^{-3}$)[5-7]. The N_D1 value of the 50% composite was more than two orders of magnitude lower, perhaps an indication that the majority of the composite now took on metallic behavior. The N_D2 values were smaller than the N_D1 values, suggesting that any deep level must be an acceptor, and were more in keeping with the donor densities expected for pure TiO_2. Once again the

50% Au specimen behaved differently, having a larger N_D2 than N_D1. The transition between region 1 and region 2 is close to where the smaller Au particles were postulated to oxidize in Section 5.1.1. It has been reported that small (<5nm) Au particles are good hole consumers[8,9], so in an n-type semiconductor their presence could result in a higher donor density than pure TiO_2, which is consistent with the observed N_D1 values; consumption of holes releases electrons. However, if the small Au particles are oxidized they would release the holes lowering the donor density, effectively acting as an acceptor level; again this is consistent with the N_D2 values being close to reported values for pure TiO_2. Although this is a possible explanation for the behavior of the low Au composites, it does not explain the change in donor concentration for the 25% Au specimen where the gold particles were larger than 100nm in diameter, unless there were also a number of smaller, undetected, Au particles in this sample (Chapter 4 Section 4.3).

For the 50% Au composite, region 2 is not only different from the other composites in terms of its higher N_D2 than N_D1, but also if it is extrapolated to the potential axis it would intercept at a much more negative potential. A possible explanation for this is that the high metallic character of the 50% film could mean that in this case region 2 occurs when the space charge extends completely across the composite so that the ITO back contact is probed.

Table 5-2 Donor carrier density ND in different Au composite films obtained from Mott-Schottky equation.

Au concentration of composite films (%)	1%	5%	25%	50%
Lower Donor density N_D1 (cm^{-3})	2.7×10^{18}	1.8×10^{18}	2.2×10^{18}	7.9×10^{16}
Upper Donor density N_D2 (cm^{-3})	5.5×10^{17}	1.4×10^{18}	5.5×10^{16}	1.3×10^{16}

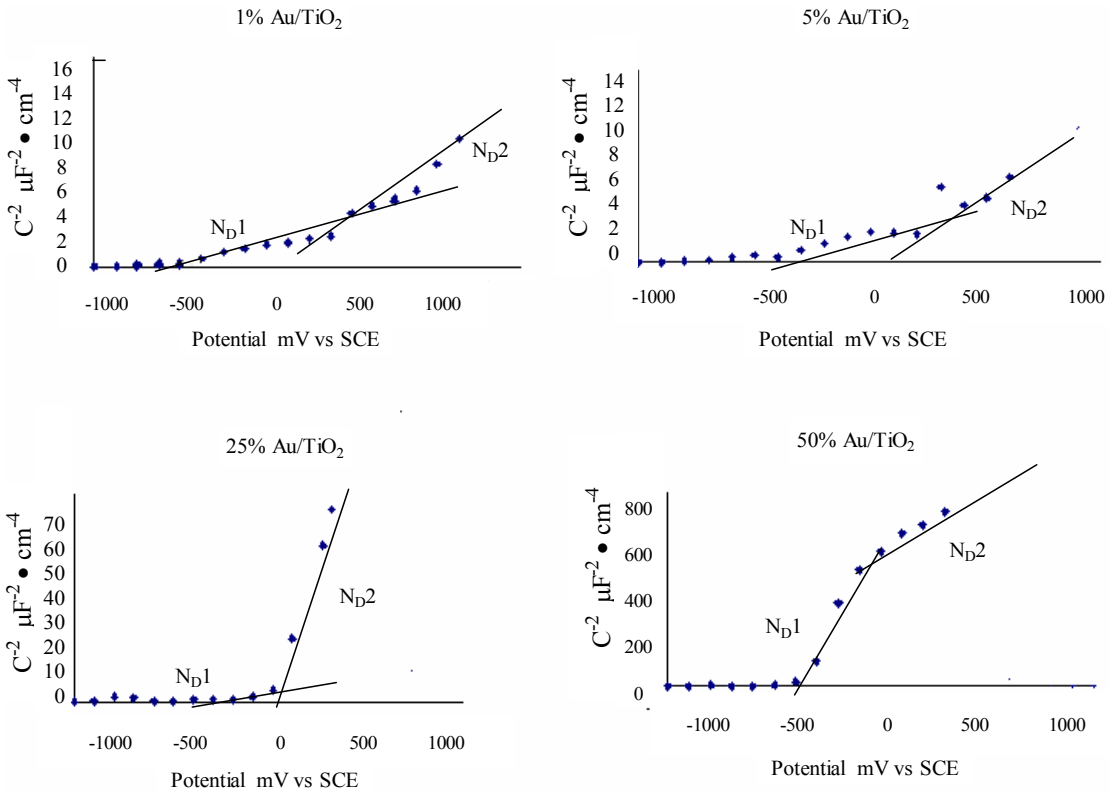

Figure 5-8 Mott-Schottky plots of the space charge capacity vs. electrode potential for Au/TiO_2 composite films in the dark.

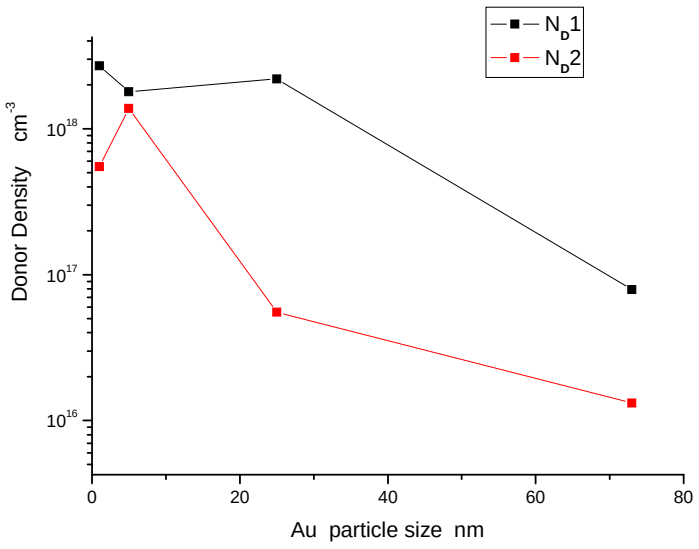

Figure 5-9 Relation of charge carrier density N_D to the Au particle size obtained from the Mott-Schottky equation. Charge carrier density of TiO_2 was according to the reference [5-7].

5.5 Influence of Au particles on the electron lifetime

Electron diffusion to the substrate contact gives rise to a time delay between electron injection and collection. This delay manifests as a phase lag in the photocurrent response to intensity modulated light. Accordingly the diffusion length is given by Eq. 5.3:

$$L_n=(D_n\tau_n)^{1/2} \qquad (5.3)$$

Where the diffusion coefficient D_n and electron lifetime τ_n are the major parameters to influence charge diffusion. Most previous work investigated the IMPS performance of DSSC, which provides information about the electron diffusion coefficient. Less work has focused on IMVS, the response of which is related to the electron lifetime under open-circuit conditions[10,11]. The intensity dependence of the electron lifetime comes from the influence of surface states on the rate of interfacial electron transfer to the electrolyte. As reported by Peter *et al.*[11]and Schlichthorl l *et al.*[12], the electron lifetime decreases as the light intensity increases, i.e. the back reaction of electrons with the electrolyte becomes faster. IMVS plots are always presented as dimensionless "complex gain" of the photoelectrode. So far, two types of IMVS spectra have been reported: Peter *et al.*[11] obtained spectra in the fourth quadrant, whilst Schlichthorl *et al.*[12] obtained spectra in the second quadrant.

In this study, IMVS spectra collected from the Au/TiO_2 composite films in 0.5M LiI/0.05M I_2 in acetonitrile using a UV LED (380nm) as the modulation source and shown in Figure 5-10, were in the second quadrant and thus similar to the results obtained by Schlichthorl *et al.*[12]. The IMVS semicircles in Figure 5-10 shrink with increasing Au concentration; a similar phenomenon was reported by Schlichthorl *et al.,* when investigating different chemical treatments to shift the energy of the conduction

band edge, who explained their results in terms of a decrease in the number of surface states. Thus it is proposed that the Au nanoparticles could reduce the number of surface states, such as oxygen vacancies. As stated in Chapter 3, Section 3.5, the electron life time, $\tau_{n,}$ is related to the frequency at which the imaginary component is maximized, f_{max}, i.e. the frequency at the top of the IMVS semicircle, via equation 5.4:

$$\tau_n = \frac{1}{2\pi f_{\max}} \qquad (5.4)$$

Figure 5-11 shows that τ_n initially increased with increasing Au concentration up to a maximum of 1%, however, at higher Au levels τ_n started to decrease. In the case of n-type semiconductor electrodes under depletion conditions the energy bands are bent up so that the hole moves toward the surface. Therefore when an n-type electrode is in contact with a media without any hole acceptors, so that the holes cannot be transferred across the interface, these must accumulate at the surface where they could trap photogenerated electrons[2]. Small Au particles are good hole consumers for the surrounding TiO_2 particles, due to their high surface area to bulk ratio, so their presence can increase the measured electron lifetime. However, at higher concentrations the larger Au particles produced tended to dominate the electrode/electrolyte interface resulting in metallic behavior and reduced electron lifetimes. The τ_n observations are consistent with the report by Valden *et al.* that Au particles below ~3.5nm manifest a marked increase in the reaction rate per surface site but large Au particles have no significant effect [9].

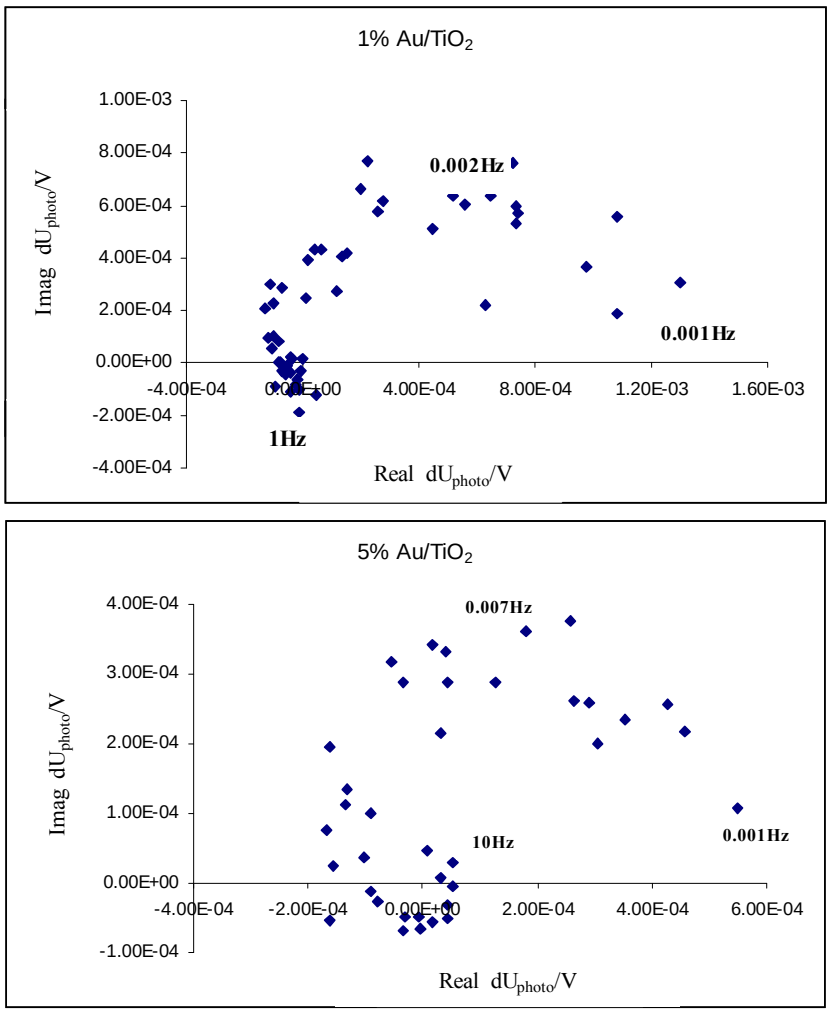

Figure 5-10 IMVS spectra of different Au concentration composite films in 0.5 M LiI/0.05M I_2 in acetonitrile under irradiation by a modulated LED (λ=380nm).

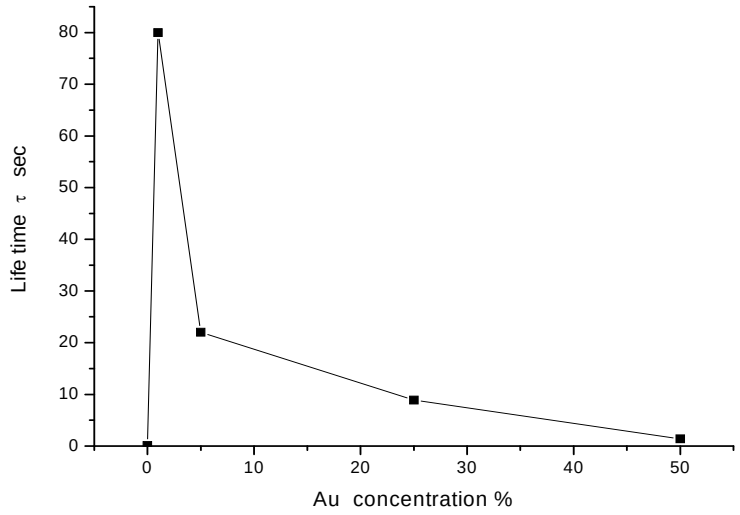

Figure 5-11 Electron lifetime obtained from the IMVS spectra.

Table 5-3 Electron lifetime of Au composite films obtained from IMVS.

Au composite films (%)	TiO_2	1%Au/TiO_2	5%Au/TiO_2	25%Au/TiO_2	50%Au/TiO_2
Electron lifetime (s)	0.09	80	22	8.9	1.3

5.6 Influence of Au nanoparticles on photocurrent of TiO_2 films

Photocurrent spectra of dye-sensitized TiO_2 and Au/TiO_2 composite films are illustrated in Figure 5-12 a). There are three parts to be noticed: a) in the UV region, the photocurrent intensity decreases with increasing Au concentration; b) the adsorption band edge red-shifts for 1%Au, but the blue-shifts with higher Au loadings (Figure 5-12b)); c) weak photocurrent was seen in the visible region (Expanded view Figure 5-12c)).

With regards to the damping of TiO_2 photocurrent in UV region by adding Au particles, Zhao *et al.*[13] have suggested that the Au particles form Schottky barriers with the TiO_2 particles, lowering the electron transport rate and thus causing the photocurrent to decrease. However, these authors ignored the influence of Au particle size and location on the photocurrent. In the current study, Au particles of different sizes were implanted in the TiO_2 films. It was found that larger particles had a stronger effect than small ones. The influence of Au particle on surface optical absorption (i.e. in the space charge layer) could be more than just decreasing electron transport in the TiO_2 film. From the UV-visible absorption spectra shown in Figure 5-13, it appears as if the SPR peak of the Au particles and the UV absorption peak of TiO_2 seems to be inversely related, i.e. the intensity of SPR increased with Au concentration, but the intensity of UV absorption peak of TiO_2 decreased. However, the two processes take place at different parts of the spectrum, so there is no conflict on energy distribution

between UV absorption and SPR absorption. Nevertheless, the decrease of UV absorption could be due to the fact that UV light was reflected or scattered, before it reached the TiO_2 particles. It was also noticed that compared to the UV-visible absorption spectra, SPR absorption by the Au particles was not obvious in the photocurrent spectra. The reasons could be that either the photocurrent caused by SPR of Au particles was too weak to be visible or the energy absorbed by the SPR process cannot lead to excite electrons being injected into the conduction band of TiO_2.

The shifts in the onset of photocurrent edge in the UV region could be due to reduction in the crystallinity of the TiO_2 matrix on the addition of Au particles, which in tern left to an increase in the semiconductors band gap. It has already be shown that the introduction of Au particles decreases the crystallinity of the TiO_2 (Chapter 4, section 4.3) and Figure 5-14 shows that sintering, i.e. improved crystallization, causes a red-shift of absorption edge in pure TiO_2 films. This argument is in contrast to that put forward by Zhao *et al*'s[13] in which the damping of the photocurrent in UV region was proposed to be due to Schottky barriers between the Au and TiO_2 particles. Since photocurrent depends on optical absorption and then electron transport, it is postulated the photocurrent in the present work was damped in the primary optical absorption step.

With respect to the small photocurrent in the visible region, it was found that a 1% Au/TiO_2 film exhibited higher photocurrent than other composites. This enhancement could attribute to the small Au particle size in the 1% acting as a photocatalyst to improve the efficiency of dye-sensitization. As shown in Figure 5-15, the tail of the optical absorption spectra of the dye ($RuL_2(CN)_2$; L = 2,2'-bipyridyl-4,4'-dicarboxylic

acid) overlaps with the SPR of the Au particles. However, on further increasing the Au concentration, the photocurrent reduced, with a 50%Au/TiO_2 film, yielding less visible photocurrent than the plain TiO_2 film. This decrease could be due to the high Au concentrations resulting in large Au particles. This high loading of Au particles in the TiO_2 film could change the film from semiconductor domination to metal domination, thus lowering the effective photon-electron conversion area. This is consistent with impedance results the R_p reduced with increasing Au levels.

a)

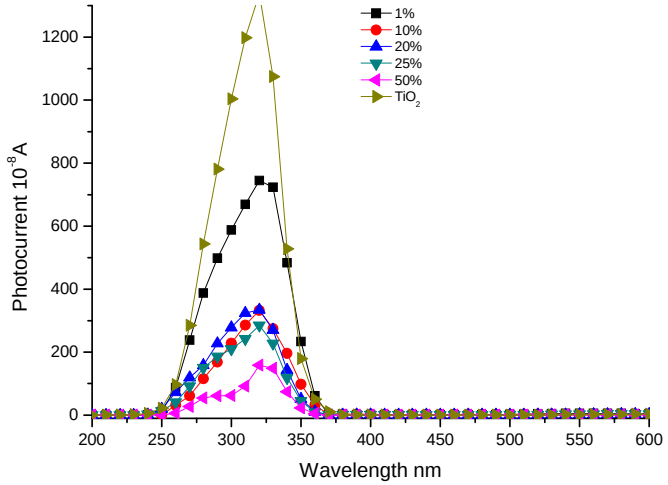

b)

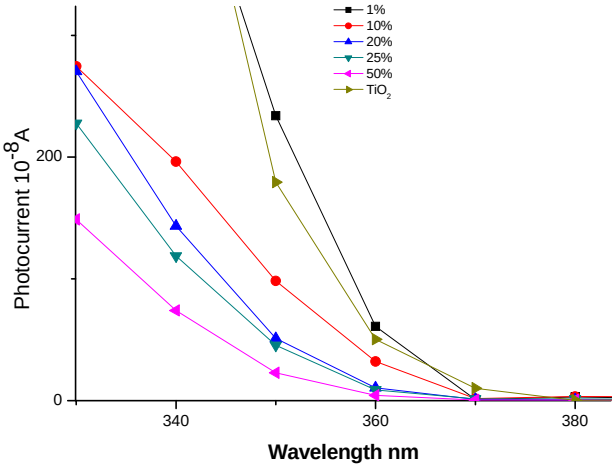

c)

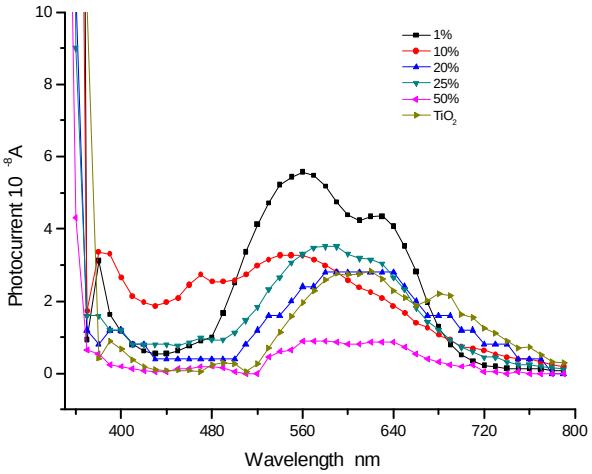

Figure 5-12 Photocurrent of Au/TiO_2 composite films with different Au concentration synthesized on ITO glass. a) photocurrent in UV region, b) photocurrent edge in UV region, c) photocurrent in visible region.

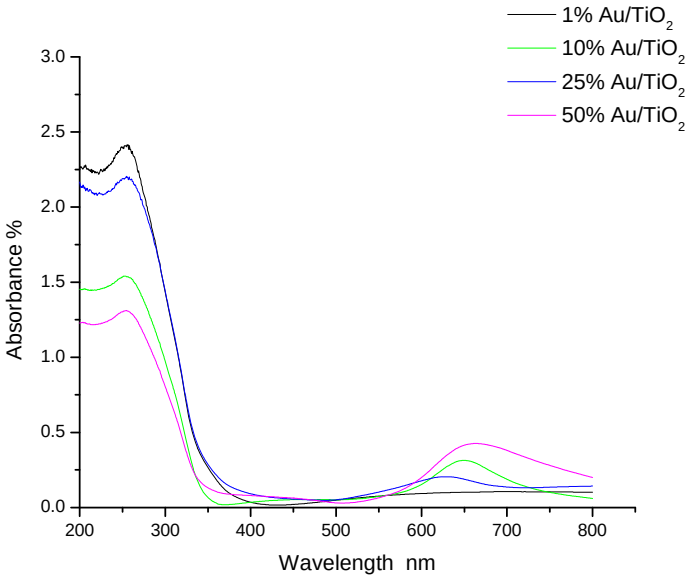

Figure 5-13 UV-visible absorption spectra of Au/TiO_2 composite films with different Au concentrations..

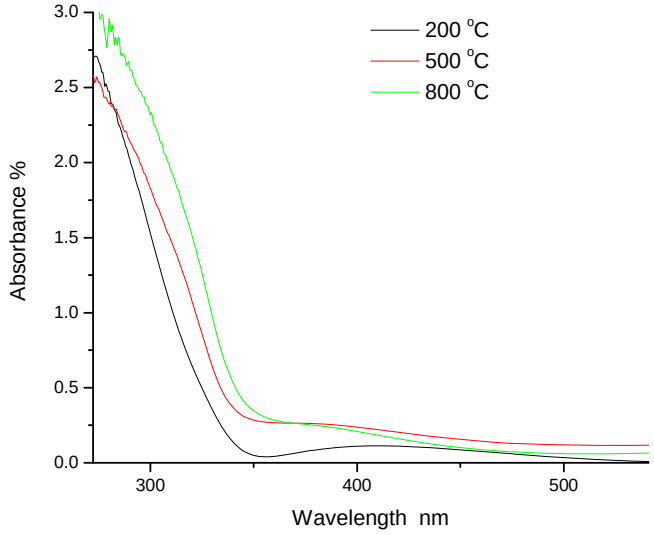

Figure 5-14 Illustration of the UV absorption band edge movement of a pure TiO_2 film caused by sintering at different temperature.

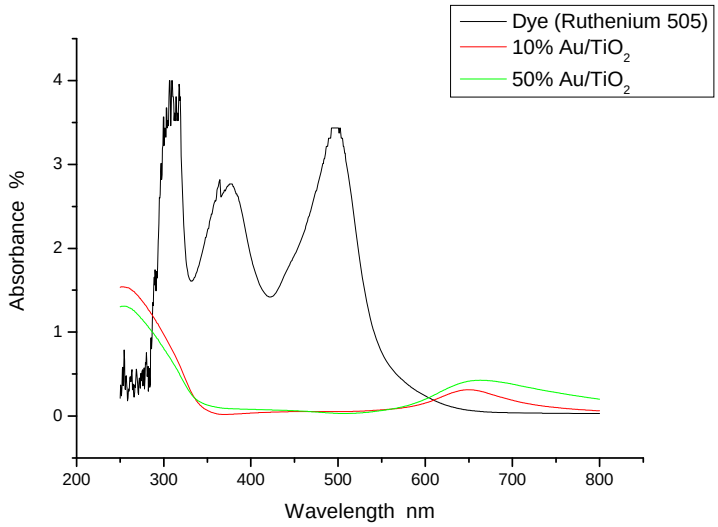

Figure 5-15 UV-visible absorption spectra of the dye ($RuL_2(CN)_2$; L = 2,2'-bipyridyl-4,4'-dicarboxylic acid) and the SPR peak of Au/TiO_2 composite films

5.7 Modification of electrode structure

From the influence of Au particles at different concentration on the surface characteristics and photoelectrochemistry of TiO_2 films, it was concluded that Au composite films were not as beneficial for solar cell applications as anticipated. One

reason could be that the surface states of TiO_2 film were changed by the introduction of Au particles. Surface states are known to play a vital role in the electron diffusion [14], the main mechanism by which the charge is transported from the TiO_2/electrolyte interface to the back contact electrode. Therefore, in order to gain an improvement a modification on the electrode structure was carried out to reduce the dark current back reaction (Figure 5-16).

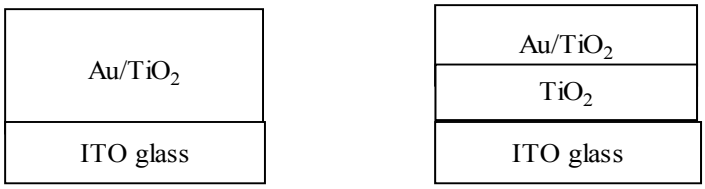

a) before modification (two identical layers) **b) after modification**

Figure 5-16 Comparison of electrode structures between Au/TiO_2 composite film and Au/TiO_2-TiO_2 composite films.

In the modified structure, a TiO_2 under layer was deposited and heat-treated at 500^oC for 30mins, prior to depositing the Au/TiO_2 composite film. This type of lower TiO_2 layer was reported by Hart *et al.* to act as a blocking layer to reduce the dark current formed between the back contact electrode and the electrolyte[15]. Both the original and modified composite films had approximately the same overall thicknesses. The results illustrated in following sections are based on this modified electrode structure.

The morphology of the modified electrode as revealed by AFM is illustrated in Figure 5-17. The Au particles are presented similar as those in the unmodified electrodes (Figure 4-3), but the Au particles covers a higher fraction of the surface area in modified electrodes.

5.7.1 Optical absorption of Au/TiO_2-TiO_2 composite films

The difference between Au/TiO_2 and Au/TiO_2-TiO_2 composite films in the UV-visible

spectra is the extra peak at 400nm, i.e. between the SPR and the TiO_2 absorption peaks (Figure 5-18). One explanation for this peak is that it might not be absorption but reflection at the Au/TiO_2 composite/TiO_2 film interface[16], this still reduces the amount of light reaching the detector so the spectrometer would record it as absorption.

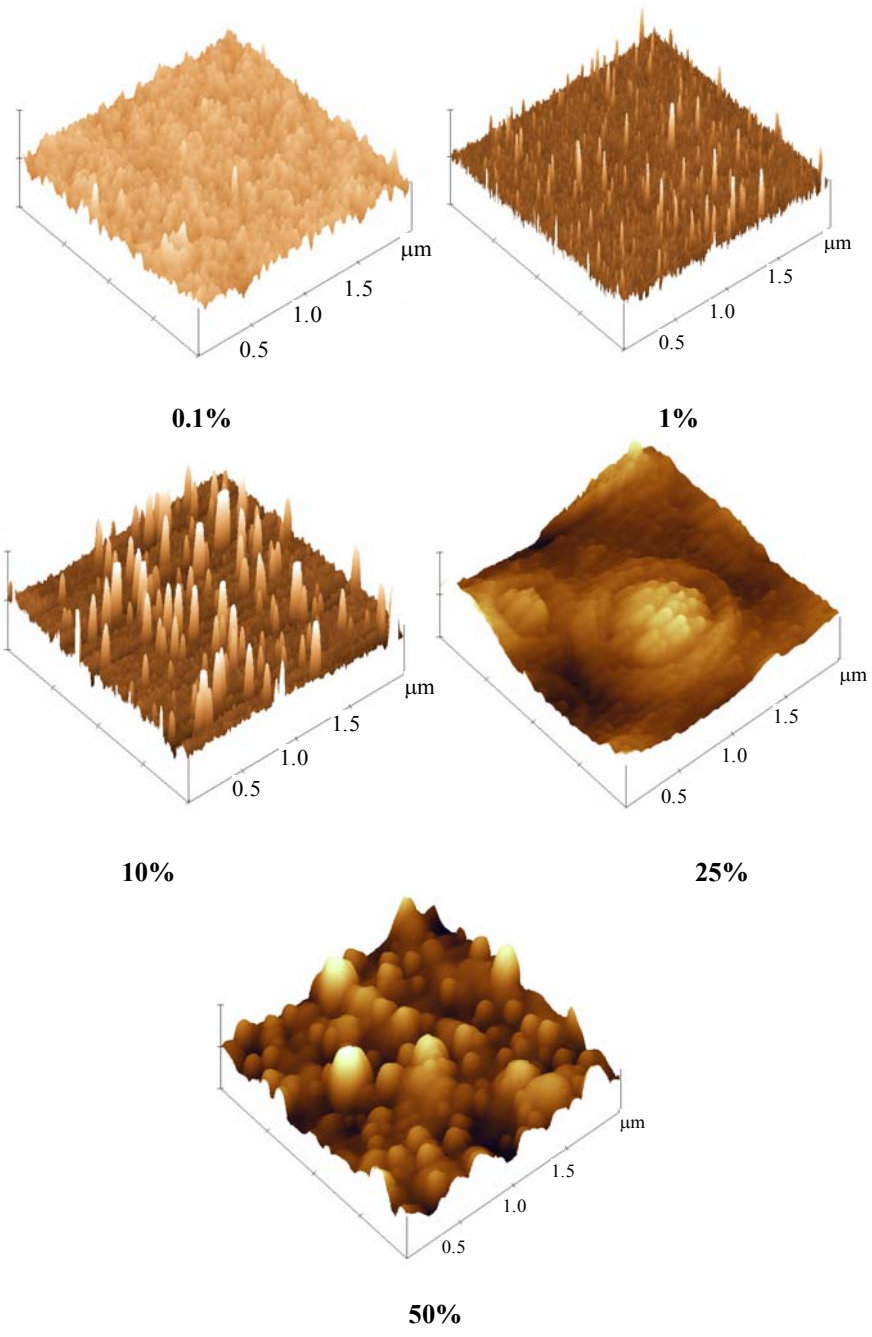

Figure 5-17 Morphology of different Au/TiO_2-TiO_2 composite films after 500 ^oC sintering.

The UV-visible spectra in Figure 5-18 were used to construct of Tauc plots (Chapter 3, Section 3.4.4) enabling the band gaps of the modified films to be obtained. Figure 5-19 shows that the band gap of the modified films was generally lower than that of the standard films. This was especially true at the 50% Au level, where the modified composite had a band gap of 3.2eV, close to that expected for anatase. The presence of anatase was confirmed by the microRaman spectra shown in Section 5.7.5. However, it is not certain rather this anatase is in the blocking layer or the top Au/TiO_2 layer.

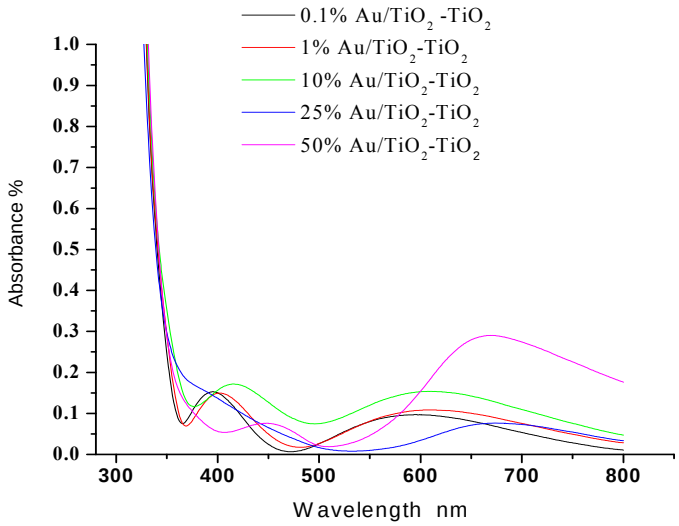

Figure 5-18 UV-visible spectra of Au/TiO_2-TiO_2 composite films with different Au concentration.

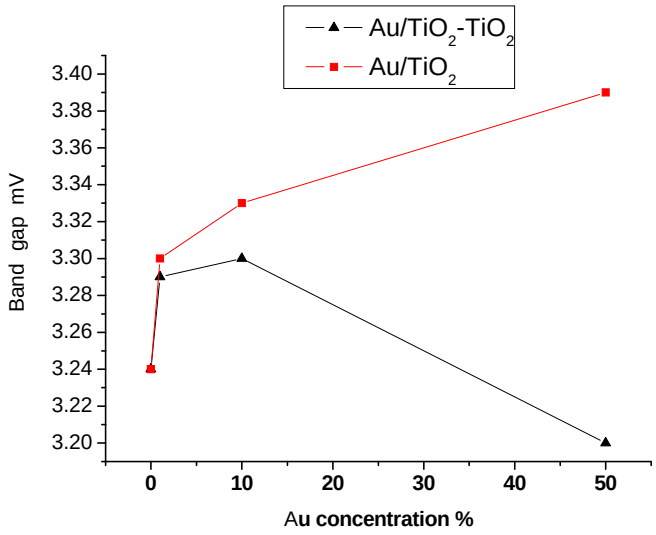

Figure 5-19 Comparison of band gap of Au/TiO_2-TiO_2 two layer composite films with that of the original Au/TiO_2 composite films.

5.7.2 Electrochemical properties of Au/TiO_2 –TiO_2 composite films

Figure 5-20 illustrates the cyclic voltammograms of modified Au/TiO_2–TiO_2 composite films in 0.5M Na_2SO_4 in the dark. Significant anodic current is only observed with 0.1%Au, which can be due to the early oxidation of the small nanoparticles as discussed in Section 5.2. The anodic wave for the 5% Au film has virtually disappeared, and the 50% Au wave is also reduced in size, which could indicate the TiO_2 thin layer efficiently block the dark current(compare Figure 5-3). Similar rectifying behavior as with the standard films is observed, however, the additional blocking layer pushes back the onset of hydrogen evolution from the ca. -300mV vs. SCE seen with the standard films, which means a more negative open circuit potential. The extent of this negative shift decreases with increasing Au content.

Under illumination at 340nm the modified composite films display dramatically increased the photocurrent compared to their counterparts without blocking layer, as shown for 50%Au in Figure 5-21. On this figure, which has an enlarged scale compared to Figure 5-20, it can also be seen that the 50% Au modified film shows both an oxidation peak at ca. 520mV and a reduction peak at ca. 180mV, presumably the reduction of AuO back to metallic Au. This suggests that this 50% Au modified composite is exhibiting the metallic properties of a Au thin film, consistent with that reported in the De Wael *et al.*'s work[17]. As such this could become a method to deposit an ultra thin Au layer similar as the description in Mcfarland's ballistic solar cell [18]. However, the advantage of this new method is that Au particles co-deposited with TiO_2 particles in sol-gel states could help control Au particle size and form a homogeneous Au dispersion.

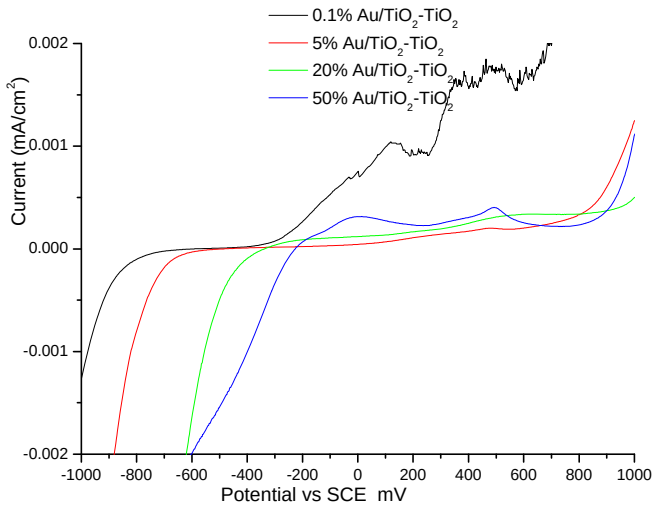

Figure 5-20 Cyclic voltammograms of modified Au/TiO_2-TiO_2 composite films with different Au concentrations in 0.5M Na_2SO_4 in the dark.

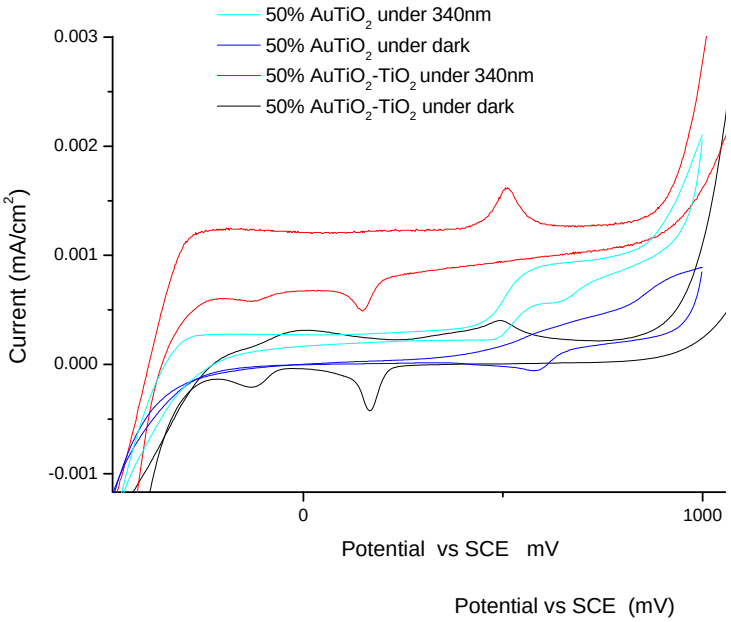

Figure 5-21 Cyclic voltammograms of 50% Au/TiO_2 composite films with and without blocking layers in 0.5M Na_2SO_4 in the dark and under 340 nm irradiation.

5.7.3 Impedance measurements of Au/TiO_2-TiO_2 composite films

Electrochemical impedance spectroscopy was also performed on the modified Au/TiO_2-TiO_2 films (Figure 5-22). Figures 5-23 and 5-24 show comparisons of the polarization resistance and interfacial capacitance obtained from these modified films

with their standard composite counterparts. The blocking layer only significantly effected the interfacial capacitance at very low Au levels with small particle size, where is caused a significant increase. At higher Au levels with big particle size the capacitance is thought to become dominated by the double layer capacitance (Section 5.2), so the blocking layer has less affect. The blocking layer also increased R_p values at all Au levels, this was expected as a pure TiO_2 layer should be more resistive than one doped with Au particles.

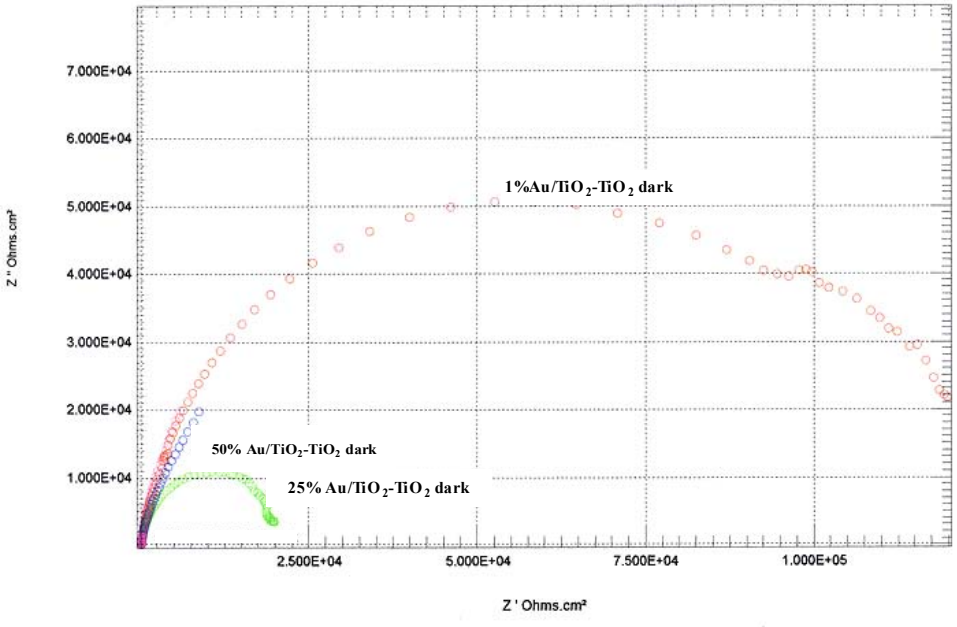

Figure 5-22 Nyquist plots of Au/TiO_2-TiO_2 composite films in 0.5 M Na_2SO_4 in the dark. Note that the semicircle for the pure TiO_2 film was too large to show without over compressing those of the other composites.

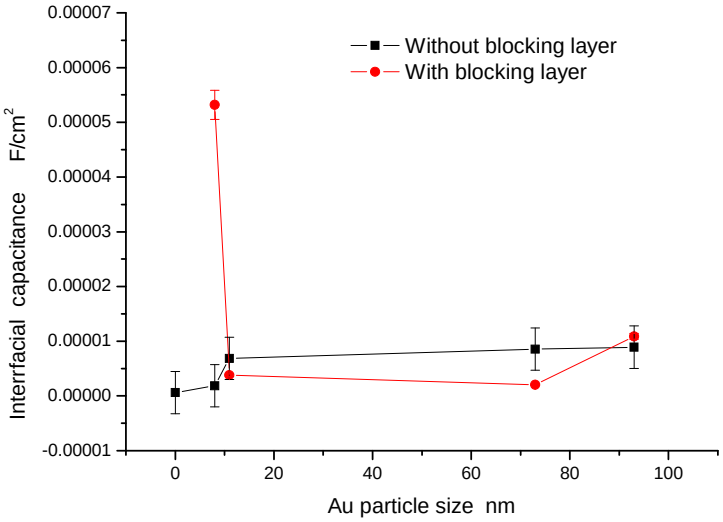

Figure 5-23 Comparison of interfacial capacitance of Au/TiO_2 composite films before and after modified by blocking layer.

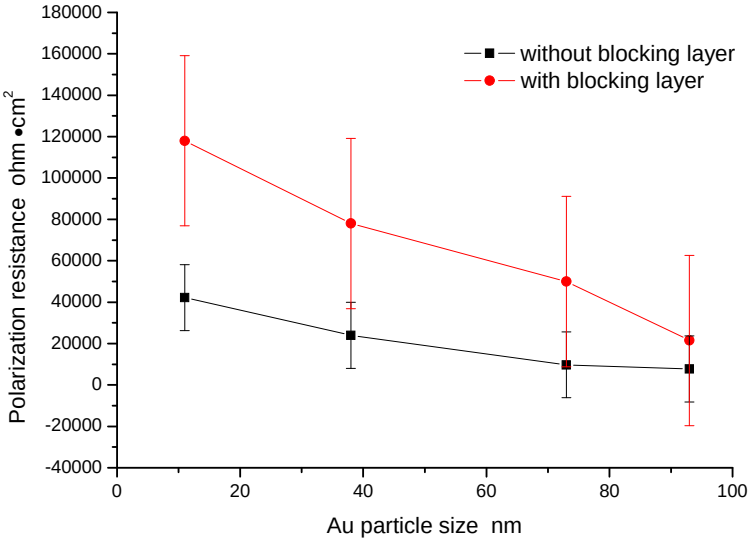

Figure 5-24 Comparison of polarization resistance of Au/TiO_2 composite films before and after modified by blocking layer.

5.7.4 Photocurrent change in Au/TiO_2-TiO_2 composite films

The Au/TiO_2-TiO_2 composite films exhibited different photoelectrochemical performances from the standard composite films. As shown in Figure 5-25, the most important improvement is that the edge for the onset of photocurrent shifted to the visible region, especially in the 50% Au/TiO_2-TiO_2. This change was attributed to the

band gap shift of modified composite films, obtained from the UV-visible spectra and illustrated in Figure 5-19. However, this advantage was lost when the surface of the modified composites was modified by a dye, i.e. dye-sensitization shifted the onset of photocurrent back into the UV region (Figure 5-26). This suggests that the role of Au particles and dye in the visible region have a conflict, perhaps the electrons photon-excited by dye were captured by the Au particles. Only those electrons with high excited energy can get into the conduction band of TiO_2 film as illustrated in Figure 5-27, hence the reduced efficiency after dye-sensitization. However, for 50% Au/TiO_2-TiO_2 composite film, the dye attached on the large Au particles did not enhance the electron injection in the visible region, as the Au particles trapped the electrons. Moreover, the dye attached to the Au particles occupies their active pointers, such as dangling bonds, thereby reducing their activity towards photon-electron conversion.

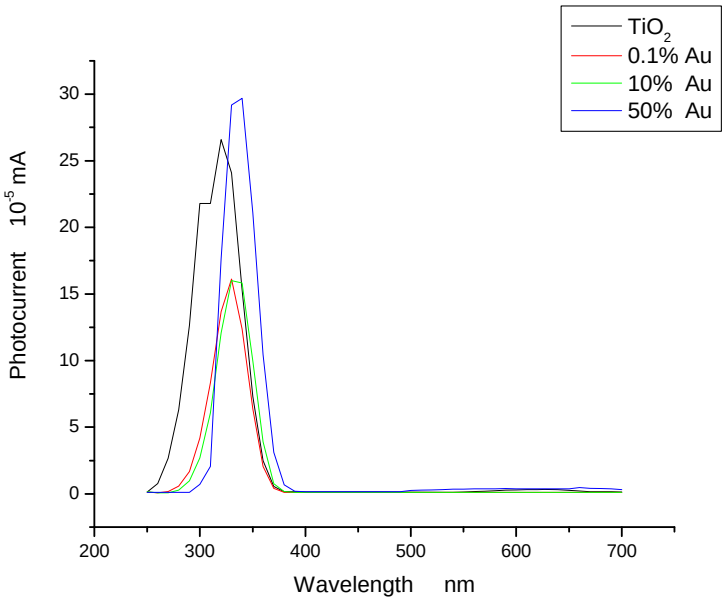

Figure 5-25 Photocurrent of TiO_2 and Au/TiO_2-TiO_2 composite films without dye-sensitization) in 0.5M Na_2SO_4.

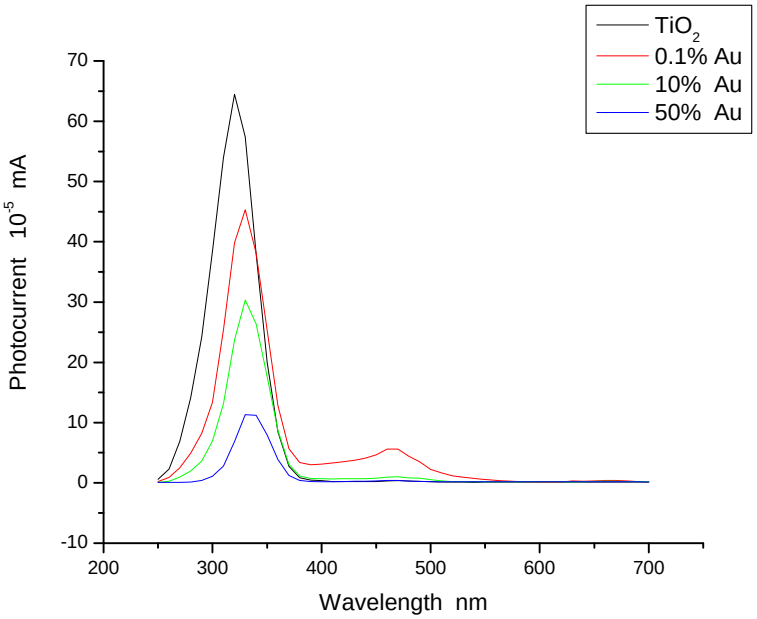

Figure 5-26 Photocurrent of TiO_2 and Au/TiO_2-TiO_2 composite films in 0.5M Na_2SO_4 after dye-sensitization.

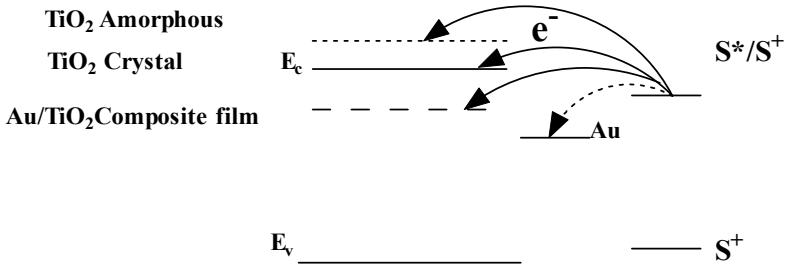

Figure 5-27 Schematic representaition of photo-excited electron transport into TiO_2 films under different situations. Electron injected into the low energy level, such as on Au particles or interface state formed by Au particles is relatively easier. However, injection is difficult into higher energy levels, such as the energy stats in amorphous structures.

Nevertheless, somewhat surprisingly, 0.1% Au/TiO_2-TiO_2 film exhibited a significant improvement of photocurrent in the visible region after dye-sensitization region, much better than the pure TiO_2 case. This could be due to the small size Au particles having more active surface atoms, which could attach more dye molecules thereby enhancing the dye-sensitization. Furthermore, the electrons photon-excited by the dye could be injected into the conduction band of TiO_2 easily through the SPR action. This indicates

that dye-sensitization efficiency of Au/TiO_2 composites is dependent on the quantity and position of the dye attachment.

Overall the difference in the photocurrent response between the modified and unmodified composite films is mainly the location of the onset of photocurrent edge, which shifts towards the visible region when a blocking under layer is used. This difference is thought to mainly come from a decrease in the band gap, which in turn is related to the structure of composite films, as shown in Figure 5-28.

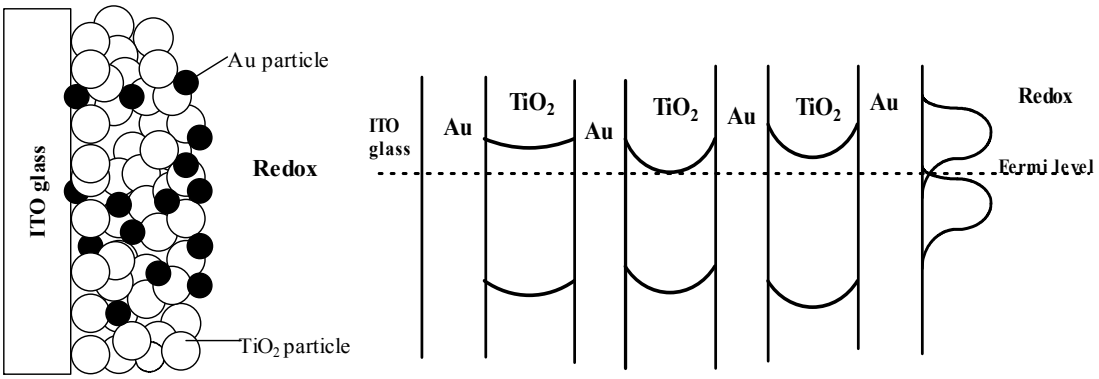

a) Au/TiO_2 composite film

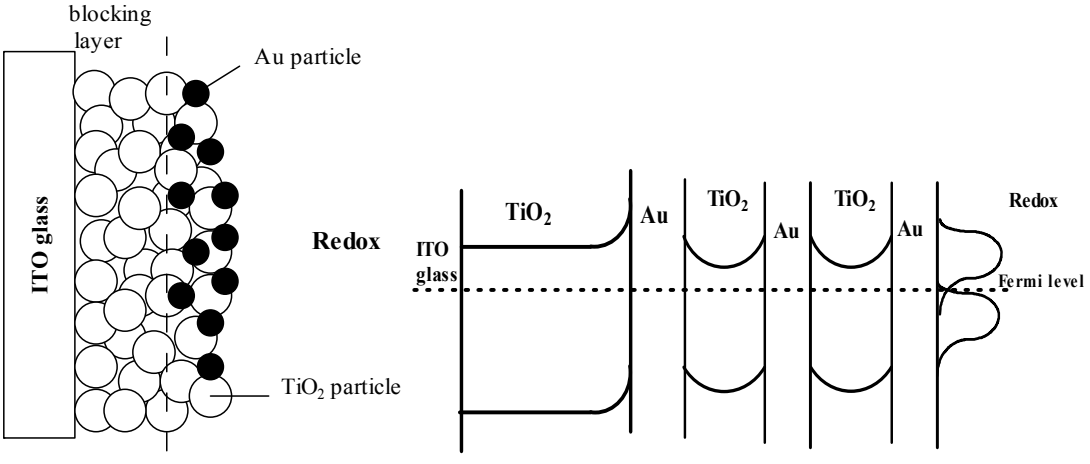

b) Au/TiO_2-TiO_2 composite film

Figure 5-28 Schematic demonstration of the relation ship between the Au particles, TiO_2 particle, electrolyte, and ITO glass in the Au/TiO_2 and Au/TiO_2-TiO_2 composite films.

After excitation the electrons have to make their way to the back contact, this is likely to involve a series of hops between Au particles and the conduction band of the TiO_2 particles; from assuming that the Au particles do not form a continuous path. Figure 5-28a) schematically shows the band structure of unmodified composite film, in which the Au particles are dispersed throughout the TiO_2 film; of course in the real film there will be many Au/TiO_2/Au repeat units between the two surfaces of the composite. It can be seen that a Schottky barrier is formed on both sides of each TiO_2 particle and thus the electron will have to travel "uphill" to overcome the inner of these two barriers and hop into the next Au particle. As suggested by Zhao *et al.*[13], this could be the reason for the reduced photocurrents observed for the composite films compared with pure TiO_2 films. Further reference to Figure 5-28a) reveals that it some Au particles are likely to be in direct contacted with the ITO glass back contact electrode whilst others with be exposed to the solution containing the redox electrolyte. Hence there may be some pathways where the Au particles effectively act as a bridge between the ITO and the redox solution, i.e. provide an easy path for the passage of unwanted dark current back reactions that could further lower the measured photocurrent. Finally, when the composites were characterized in Chapter 4 Section 4.2, at high Au concentrations the metal particles were found to be aggregated together and this caused a reduction in the crystallization of TiO_2 film. Since lattice imperfections can act as bulk recombination sites this also causes a reduction in the photocurrent observed from the UV region. In contrast, modified composite film, with the blocking underlayer will exhibit a different band structure as shown schematically in Figure 5-28b). It is clear that any excited electron generate close to the solution interface would now have less "uphill" Schottky barrier to surmount on its journey to the back contact electrodes; both the original and modified composite films having the

same total thickness. Likewise, the pure TiO_2 in the underlayer is expected to be more crystalline than that in the Au containing upper layer (Chapter 4 Section 4.4), meaning that it will have a lower density of bulk recombination sites. Furthermore, the TiO_2 blocking layer isolates Au nanoparticles from ITO glass, removing any chance of a direct metallic path from the electrolyte to the back contact and thereby greatly reducing the dark current. Together, these effects explain why the modified composite films showed improved photocurrent efficiencies.

5.7.5 Photoluminescence and Raman Spectroscopy of Au/TiO_2-TiO_2 films

Figure 5-29 shows photoluminescence spectra from Au/TiO_2-TiO_2 composite films with different Au concentrations. It is evident that the photoluminescence decreased with increasing Au concentration, also all the PL spectra of composite films are blue-shifted with respect to a pure TiO_2 film. However, the size of the blue-shift does not increase with increasing Au level, on the contrary, it slightly decreases.

In Chapter 4, Section 4.8.3, it was seen that the PL spectra of the non-modified composites consisted of three peaks that were assigned as: Peak A 370~450nm, related to unsaturated surface Ti^{3+}; Peak B 450~550nm, related to unsaturated surface Ti^{4+}; and Peak C 550~650nm, related to SPR. The modified Au/TiO_2-TiO_2 films appear to be dominated by Peak B, i.e. mainly Ti^{4+} species, suggesting fewer surface defects. However, the blue shift seen on the addition of Au could be due to the introduction of Ti^{3+} as was the case with unmodified films at high Au levels. Significant SPR (Peak C) was only seen with the lowest Au level (0.1%), which had the smallest metallic particles and thus expected to have the more efficient SPR processes.

The blue-shift of PL spectra of Au/TiO_2-TiO_2 film may be due to the effect of Au particles on the oxygen vacancies. The oxygen vacancies supply electronic states within the energy gap, so that when an electron is excited from the valence band, it is easier to jump into/out of the oxygen vacancy levels than across the whole band gap. According to Yang's[19] research, Au atoms bind readily at the oxygen vacancy sites of TiO_2 films. When an electron is excited, it can no longer jump into the oxygen vacancy level, but has to jump into a higher level, e.g. the conduction band. Therefore, when the electron relaxes, it releases higher energy photons, i.e. it is blue shifted. However, in the present case the extent of the blue shift is less than would be expected if the lowest energy relaxation was across the band gap (3.2eV corresponds to about 390nm), so it is postulated here that the Au particles only eliminate the lowest any oxygen vacancy states rather than all of them. Furthermore, it may be that the efficiency with which the Au particles can bind through the oxygen vacancy sites decreases as their size increases, hence higher Au levels (large particles) cause a smaller blue shift.

Furthermore, the PL intensity decreased with increasing Au concentration, possibly due to the excited electrons being trapped by the Au particles. Once the electrons are localized at the surface of Au nanoparticles, the absorbed photon energy would be converted into vibration energy of the dipole at the surface of Au particle; i.e. phonon energy, so the composite heats up. Alternatively, the lower observed PL intensity could be due to scattering of either the incoming or out going photons by the Au particles.

The Raman scattering spectra of the modified composite films show the characteristics of the anatase structure in all case (Figure 5-30). This is in contrast to the unmodified composite films where the Au particles reduced the crystallinity, as seen by a reduction in the intensity of the smaller A_{1g} and B_{1g} bands (Chapter 4, Section 4.3). The main effect on the Raman spectra of adding Au to the modified composites appears to be signal enhancement, i.e. the SERS mechanism[20]. The exception was the 50% Au level, which not only caused an enhancement of the Raman bands but as caused a significant blue shift in the location of the strongest (E_g) band, a phenomenon that was earlier explained in terms of a reduction in the crystallite size of the TiO_2 matrix (Chapter 4, Section 4.3). The overall conclusion from the Raman data is that the presence of the blocking layer helps to preserve the anatase structure in the composite films.

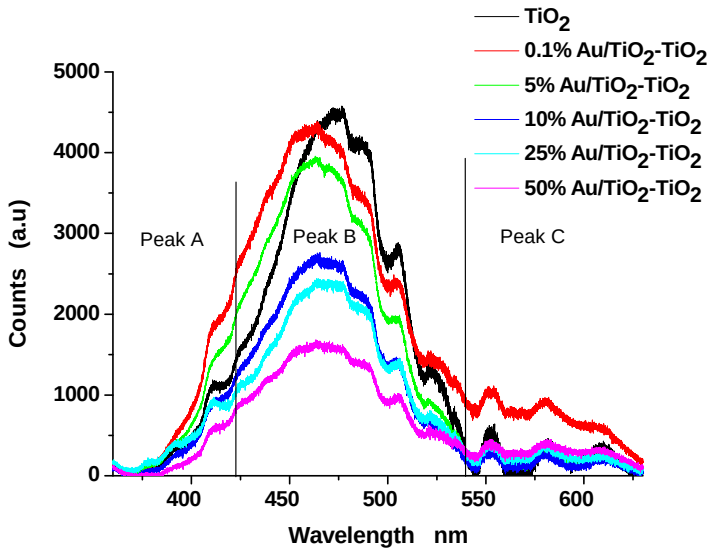

Figure 5-29 Photoluminescence of modified Au/TiO_2-TiO_2 composite films under UV irradiation (325.15nm).

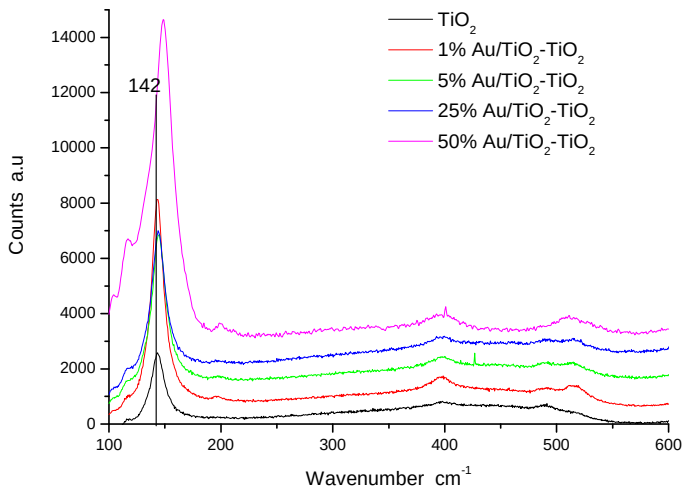

Figure 5-30 Raman scattering spectra of Au/TiO_2-TiO_2 composite film after 500 ^oC sintering (30mW Ar-ion laser at 514nm).

5.8 Summary

Photovoltage and photocurrent investigations were carried out to determine the effects of Au particles on the photon-electron conversion efficiency of TiO_2 films. The photovoltages were determined from the difference in the open-circuit potential in the dark and under irradiation. The results showed that the addition of small (<40nm) Au particles increased the magnitude of the TiO_2 film's photovoltage suggesting a more negative Fermi-levels in the composite films; allowing for more band unbending under illumination. This could be the result of a higher degree of electrons accumulating at the composite/electrolyte interface in the presence of small Au particles. However, the addition of Au particles decreased the UV photocurrent from the TiO_2 films and no photocurrent was found in the visible, that is to say the SPR generated by the Au nanopartilces did not produce any photocurrent. This suggests that the SPR absorption is too weak to inject an electron into the semiconductor's conduction band. A possible reason for the Au particles causing a decrease in the photocurrent observed under UV light is the lower crystallinity of the composite films compared to the pure TiO_2 (See Chapter 4).

The Au/TiO_2 composites also did not perform well in the presence of a dye sensitizer. However, in this study, all the films were deposited as a compact this layer, rather than the porous layer used in Grätzel cell type DSSC. Since the surface area of a compact film is much smaller than a porous one, it absorbs much less dye so there are fewer opportunities for electron injection into the semiconductor's, which partially explains the small magnitude of the visible photocurrent obtained with the Au/TiO_2 composites. Increased metallic character of the Au/TiO_2 composites is also believed to contribute the reduction in conversion efficiency.

For this chapter, the focus was mainly on the electron injection into and the electron transport within the Au/TiO_2 composite films. Investigations found that increasing Au levels caused a reduction in the polarization resistance, the electron lifetime and the electron density within the composite films. Recalling the finding presented in Chapter 4, that the Au particle sizes increased as its concentration increased, indicates that the larger Au particles may have caused the composite films to take on a more metallic character, as opposed to the semiconductor nature of pure TiO_2 films. An increase in metallic character is consistent with the observations of a decrease in the polarization resistance and a reduction in the magnitude of the photovoltage in the presence of large Au particles; e.g. the 25% loading with the largest Au particles showed the lowest polarization resistance and smallest photovoltage.

With respect to why high Au levels dramatically reduced the electron density and electron lifetime this is most likely due to the Au particles forming recombination centers in the TiO_2, as suggested by the appearance of Ti^{3+} states in the XPS and Raman data present in Chapter 4. In the high Au (>10% Au) concentration composite

films, the depression in the photocurrent from the TiO_2 was explained in terms of the large Au particles forming a conductive channel between electrolyte and the back contact electrode, thus by-passing the need for electron transport in the conduction band of the semiconductor. However, at low Au concentrations (1% Au) the electron density and electron lifetime showed improved performance over that of the pure TiO_2 film, which was explained in terms of the size effect of Au nanoparticles.

Overall, the photon-electron conversion efficiencies of the Au composite films were not as good as anticipated at the outset of this research project. To address this issue, efforts were focused on how to decrease the extent of the metallic character induced into the films by the Au particles. The strategy adopted was to add a blocking layer between the Au composite and the back contact electrode, i.e. producing an Au/TiO_2-TiO_2 film structure and changing several properties of the composite films. It was also found that the blocking layer increased the polarization resistance of composite film, especially under irradiation which indicates better semiconductor behavior. Photocurrent investigations in the presence of dye sensitization revealed that the effect of the blocking layer depended on the concentration of Au in the composite film. At very low Au loadings an increase in the photocurrent from the visible region was detected, i.e. the blocking layer help improve the dye-sensitization. This improvement was attributed to the nanosized Au particles aiding energy transfer to the excited electron from the dye sensitization, in a similar manner to how Au is believed to operate in the Surface Enhanced Raman effect. However, at high Au loadings no improved dye sensitization was observed, however, the blocking layer did cause the direct photocurrent from the TiO_2 (i.e. that from promotion across the band gap) to extend slightly into the visible region. This was explained in terms of how the

structure of the modified composite would influence electron transport and illustrated with model shown in Figure 5.28. Furthermore, Raman spectroscopy and PL measurements indicated that the blocking layer helps to preserve the anatase structure in the composite films, possibly allowing a slight reduction in the band gap. This would be consistent with the observed red-shift in the onset of the direct photocurrent.

From the above discussion, the conclusions were drawn as below:

As for Au/TiO_2 composite film, the addition of Au particles also changed the impedance of the composite films. In the absence of Au particles, pure TiO_2 films have a high dielectric constant and electron transport is via trapping/detrapping mechanism; traps are located at just under the conduction band. This mechanism is the typical electron transport mode in metal oxide semiconductors. However, the presence of Au particles formed deep traps in the composite film. Hence, the impedance of composite film was reduced, and the electron lifetime was increased. However, these low resistance metals particles may act as recombination centers, which caused a reduction in the photocurrent.

In photon-electron conversion, compared to pure TiO_2 films, the Au/TiO_2 composite films exhibited an improvement on the photovoltage and at least for the low Au concentrations a negative shift of open-circuit potential. Although these results should have been beneficial to the photon-electron conversion, the Au/TiO_2 composite films exhibited a dampened photocurrent in the UV region and the measured photocurrent in the SPR region was very weak.

The dampened photocurrent in the UV region was attributed to the reduced crystallization of the TiO_2 matrix as the Au concentration increased, possibly due to a widening of the band gap. For the high Au concentration composite films, the large size of the Au particles physically blocking the light from reaching the TiO_2 film was also an important reason for the dampened photocurrent in the UV region. From the electrochemical impedance spectroscopy results it was found that the charge transfer resistance decreased as the Au concentration increased. This was believed to be due to Au particles forming a near continuous metallic pathway from the composite/electrolyte to the back contact electrode.

The Au particles also changed the surface condition of the TiO_2 films. First, the surface of composite film became rougher as more particles were added, which combined with a higher Au level on the surface caused more light scattering and thus resulted in a reduction in light absorption. Secondly, the Au particles also influenced the surface chemistry of the films, since as mentioned above these caused a reduction in the crystallinity of the TiO_2 matrix. This incomplete crystallization of the TiO_2 film resulted in an increased number of surface defects, which trapped most of the photon excited electrons. When a dye was added, the higher level of surface traps also decreased the efficiency of dye sensitization, i.e. less of the photon excited electrons in the dye were efficiently injected into the TiO_2 and transported to the back contact electrode.

In order to improve the properties of Au/TiO_2 film, the composite film was modified by the extra TiO_2 film. The conclusions from the Au/TiO_2-TiO_2 film were listed as below:

The addition of a compacted TiO_2 blocking layer, between the Au/TiO_2 composite film and ITO conductive glass back electrode (labeled as Au/TiO_2-TiO_2 films), such that the Au nanoparticles were confined on the surface of composite films, was also investigated in the work presented in this thesis.

When the blocking layer was included, the first observed change was appearance of an additional absorption peak at the TiO_2's optical absorption edge which apparently shifts the band gap of TiO_2 films to the visible region, i.e. photocurrent showed a red-shift at the band edge. Although the blocking layer reduced the dark current, which arises from direct contact between the back electrode and the electrolyte, the photocurrent in the UV region from the modified composite films was still lower than that of a pure TiO_2 film. This was believed to be due to the Au particles physically blocking the optical absorption by the TiO_2 matrix.

With dye-sensitization treatment, 0.1% Au/TiO_2-TiO_2 composites exhibited photocurrent in the optical absorption region of dye superior to that observed in the absence of Au particles. Although these results were based on compact films the observation is likely to be also relevant to the porous structure films used in most DSSC's. That is low levels of Au particles should be beneficial to DSSC's.

Reference

(1) Kamat, P. V. *Pure Appl. Chem.* **2002**, *74*, 1693-1706.

(2) Memming, R. *Semiconductor Electrochemistry*; WILEY-VCH: Weinheim, **2001.**

(3) Wang, Q.; Moser, J.-E.; Grätzel, M. *J. Phys. Chem. B* **2005**, *109*, 14945-14953.

(4) Morrison, S. R. *Electrochemistry of semiconductors and oxidised metal electrodes*; Plenum: New York, **1980.**

(5) Kumari, S.; Chaudhary, Y. S.; Agnihotry, S. A.; Tripathi, C.; Verma, A.; Chauhan, D.; Shrivastav, R.; Dass, S.; Satsangi, V. R. *International Journal of Hydrogen Energy* **2007**, *32*, 1299-1302.

(6) Loef, R.; Schoonman, J.; Goossens, A. *J. Appl. Phys.* **2007**, *102*, 024512-6.

(7) Jochum, W.; Eder, D.; Kaltenhauser, G.; Kramer, R. *Topics in Catalysis* **2007**, *46*, 49-55.

(8) Linsebigler, A. L.; Lu, G.; Yates, J. T. *Chem. Rev.* **1995**, *95*, 735-758.

(9) Valden, M.; Lai, X.; Goodman, D. W. *Science* **1998**, *281*, 1647-1650.

(10) Franco, G.; Gehring, J.; Peter, L. M.; Ponomarev, E. A.; Uhlendorf, I. *J. Phys. Chem. B* **1999**, *103*, 692-698.

(11) Peter, L. M.; Wijayantha, K. G. U. *Electrochem. Commun.* **1999**, *1*, 576-580.

(12) Schlichthorl, G.; Huang, S. Y.; Sprague, J.; Frank, A. J. *J. Phys. Chem. B* **1997**, *101*, 8141-8155.

(13) Zhao, G.; Kozuka, H.; Yoko, T. *Sol. Energy Mater. Sol. Cells* **1997**, *46*, 219-231.

(14) Wahlstrom, E.; Vestergaard, E. K.; Schaub, R.; Ronnau, A.; Vestergaard, M.; Laegsgaard, E.; Stensgaard, I.; Besenbacher, F. *Science* **2004**, *303*, 511-513.

(15) Hart, J. N.; Menzies, D.; Cheng, Y.-B.; Simon, G. P.; Spiccia, L. *C. R. Chim.* **2006**, *9*, 622-626.

(16) Sugawara, M.; Fujii, T.; Yamazaki, S.; Nakajima, K. *Appl. Phys. Lett.* **1989**, *54*, 1353-1355.

(17) De Wael, K.; Westbroek, P.; Adriaens, A.; Temmerman, E. *Electrochem. Solid-State Lett.* **2005**, *8*, C65-C68.

(18) McFarland, E. W.; Tang, J. *Nature* **2003**, *421*, 616-618.

(19) Yang, J. H.; Henao, J. D.; Raphulu, M. C.; Wang, Y.; Caputo, T.; Groszek, A. J.; Kung, M. C.; Scurrell, M. S.; Miller, J. T.; Kung, H. H. *J. Phys. Chem. B* **2005**, *109*, 10319-10326.

(20) Fleischmann, M.; Tian, Z. Q.; Li, L. J. *J. Electroana. Chem.,* **1987**, *217*, 397-410.

Chapter 6 Conclusion and Future Work

Au nanoparticles are attractive for solar cell applications due to their enhancement of the optical and photocatalytic properties of metal oxide semiconductors. In this study, Au nanoparticles were employed to modify the TiO_2 films used in dye-sensitized solar cells. As the heart of DSSC system, the TiO_2 is sensitized by the dye to improve the photon-electron conversion efficiency in the visible region. However, dye-sensitization is confined by the dye distribution on the surface of TiO_2 film; i.e dye-sensitization is effective only where dye is absorbed in a monolayer. To improve the efficiency of dye-sensitization and photon-electron conversion, some research work focusing on metal particle composite films, such as Au/TiO_2 composite films has been reported. As Au nanoparticles embedded into dielectric media exhibit Surface Plasmon Resonance (SPR) in the visible region, due to a quantum size effect, this unique property was expected to supplement the disadvantage of the lack of photon-electron conversion efficiency in the visible region by the TiO_2 film. In this study the Au/TiO_2 composites films were synthesized by the sol-gel method and the influence of Au nanoparticles on crystalline structure, optical absorption and photon-electron conversion were studied by changing the Au concentration and the composite films' structure.

Conclusions

As the results showed in this study, the influence of Au nanoparticles on photon-electron conversion had some advantages, but also had some disadvantages:

Au/TiO_2 films

- Au/TiO_2 composite films (>5%) exhibited SPR optical absorption features in the visible region. With increased Au concentration its particle size was found to increase and this caused the SPR peak to broaden and red-shift as well as to increase in intensity. From TEM data it was observed that the size distribution of the Au particle was narrow at low Au concentrations (<5%), but broad distributions of particle size were found at high Au levels (>5%), in line with the observed SPR performance.

- Increasing the Au concentration directly influenced the particle size and crystallization of the TiO_2 matrix. The presence of Au particles reduced the crystallization of the TiO_2 so that at high Au levels TiO_2 crystallinity was obviously reduced. This also impacted the band gap structure of the composite film, e.g. increasing Au particle size blue-shifted the absorption band edge. The decrease in crystallization could be due to the synthesis method. The sol-gel synthesis is a co-deposited method, but the crystallizations sequence of Au and TiO_2 are different. Au particles crystallized as-deposited, due to its chemical stability, but TiO_2 crystallization required subsequent heat-treatment. This difference in crystalline structure with increasing Au levels is believed to be the main reason for the change in the band gap as well as changes to the photon-electron conversion efficiency.

- The addition of Au particles also changed the impedance of the composite films. In the absence of Au particles, pure TiO_2 films have a high dielectric constant and electron transport is via trapping/detrapping mechanism; traps are

located at just under the conduction band. This mechanism is the typical electron transport mode in metal oxide semiconductors. However, the presence of Au particles formed deep traps in the composite film. Hence, the impedance of composite film was reduced, and the electron lifetime was increased. However, these low resistance metals particles may act as recombination centers, which caused a reduction in the photocurrent.

- In photon-electron conversion, compared to pure TiO_2 films, the Au/TiO_2 composite films exhibited an improvement on the photovoltage for large Au particle composite and a negative shift of open-circuit potential for the small Au particle composite. Although these results should have been beneficial to the photon-electron conversion, the Au/TiO_2 composite films exhibited a dampened photocurrent in the UV region and the measured photocurrent in the SPR region was very weak. The dampened photocurrent in the UV region was attributed to the reduced crystallization of the TiO_2 matrix as the Au concentration increased, possibly due to a widening of the band gap.

- From the Raman and photoelectron spectroscopy data it was concluded that the insertion of Au nanoparticles increased the concentrations of Ti^{3+} and Ti^{2+} species (as opposed to Ti^{4+}), which are believed to influence the density of surface states as well as the level of oxygen vacancies at the film's surface. Oxygen vacancies are thought to be effective pathways for electron injection in TiO_2, but these are also the positions occupied first by Au atoms inserted into the composite films. The loss of the injection pathways contributes to the lowering of the photocurrents.

- For the high Au concentration composite films, the large size of the Au particles physically blocking the light from reaching the TiO_2 film was also an important reason for the dampened photocurrent in the UV region.

- From the electrochemical impedance spectroscopy results it was found that the charge transfer resistance decreased as the Au concentration increased. This was believed to be due to Au particles forming a near continuous metallic pathway from the composite/electrolyte to the back contact electrode.

- The Au particles also changed the surface condition of the TiO_2 films. First, the surface of composite film became rougher as more particles were added, which combined with a higher Au level on the surface caused more light scattering and thus resulted in a reduction in light absorption. Secondly, the Au particles also influenced the surface chemistry of the films, since as mentioned above these caused a reduction in the crystallinity of the TiO_2 matrix. This incomplete crystallization of the TiO_2 film resulted in an increased number of surface defects, which trapped most of the photon excited electrons. When a dye was added, the higher level of surface traps also decreased the efficiency of dye sensitization, i.e. less of the photon excited electrons in the dye were efficiently injected into the TiO_2 and transported to the back contact electrode.

Au/TiO_2-TiO_2 films

The addition of a compacted TiO_2 blocking layer, between the Au/TiO_2 composite film and ITO conductive glass back electrode (labeled as Au/TiO_2-TiO_2 films), such

that the Au nanoparticles were confined on the surface of composite films, was also investigated in the work presented in this thesis.

- The first change observed when the blocking layer was included was appearance of an additional absorption peak at the TiO_2's optical absorption edge, which apparently shifts the band gap of TiO_2 films to the visible region, i.e. photocurrent showed a red-shift at the band edge. Although the blocking layer reduced the dark current, which arises from direct contact between the back electrode and the electrolyte, the photocurrent in the UV region from the modified composite films was still lower than that of a pure TiO_2 film. This was believed to be due to the Au particles physically blocking the optical absorption by the TiO_2 matrix.

- With dye-sensitization treatment, 0.1% Au/TiO_2-TiO_2 composites exhibited photocurrent in the optical absorption region of dye superior to that observed in the absence of Au particles. Although these results were based on compact films the observation is likely to be also relevant to the porous structure films used in most DSSC's. That is low levels of Au particles should be beneficial to DSSC's.

Overall it was found in this study that the SPR effect did not show any noticeable improvement in the photocurrent efficiency and that the influence of Au nanoparticle concentration is not simply to improve or depressed the photocurrent of the TiO_2 film. Rather its influence is dependent on the size distribution of the Au particles and how it alters the structure of composite film. Future work should concentrate on

understanding the mechanism of charge transfer between the Au nanoparticles and TiO_2 matrix.

Future work

The results presented in the thesis show that the influence of Au particles on the efficiency of the photon-electron conversion at TiO_2 films was not as beneficial as had been hoped for. Nevertheless, there was still enough to encourage further development, especially the improvement in dye sensitization in the 0.1% Au/TiO_2-TiO_2 film, which is clearly one area where further work should be directed. However, there is a need to first find the optimum combination between Au particle size and its distribution at the composite's surface.

Limitations in the instrumentation used in the present experiments prevented clarification of why the SPR from the Au nanoparticles did not lead to any significant photocurrent being observed. An investigation of the SPR performance of Au particles in the liquid could be helpful to explain this question.

For the photon-electron conversion, whether the Au nanoparticles attached to the TiO_2 will affect the electron injection from dye into the conduction of TiO_2 still needs further investigation, as it will affect the efficiency of dye-sensitization.

Dye attachment on Au and TiO_2 particles is another important question that needs further investigation, since if this was clarified the efficiency of dye sensitization could be improved. The answers to these questions would also be helpful in explaining why the photon-electron conversion band edge of the TiO_2 was retarded by the dye-sensitization.